REPORT FOR ABERRATIONS AS FUNCTIONS OF THE SHAPE FACTOR, CONJUGATE FACTOR, AND INDEX OF REFRACTION

by

Vanessa Ayala-Miranda

A Master's Report Submitted to the Faculty of the

COLLEGE OF OPTICAL SCIENCES

In Partial Fulfillment of the Requirements
For the Degree of

MASTER OF SCIENCE

In the Graduate College

THE UNIVERSITY OF ARIZONA

2019

Contents

Acknowledgements

I would like to express great appreciation and thanks to Dr. José Sasián at the College of Optical Sciences at the University of Arizona for his patience, and his valuable suggestions during the construction and writing of this Master's Report. Dr. Sasián provided advice and direction and was always available for discussion and assistance.

I would also like to thank my family, friends, and boyfriend for their unending support and guidance during the highs and lows of the past two and a half years. Their continuous encouragement made this accomplishment possible.

List of Figures

List of Tables

Abstract

In this report, fourth and sixth-order monochromatic aberrations are analyzed against the shape factor, conjugate factor, and the index of refraction. Additionally, these aberrations are also measured at different fields of view and object heights in order to obtain a comprehensive understanding of the behavior of these aberrations.

The wave aberration function is examined in its algebraic and vector forms in order to understand its dependence on the field vectors and aperture vectors. Then, the wave aberration function is related to geometric terms and written in terms of Seidel aberration coefficients up to the fourth-order. In the sixth-order, the monochromatic aberrations are broken down into their intrinsic and extrinsic parts, and their derivations are briefly explained.

The shape factor, conjugate factor, and index of refraction are studied in Chapter 2. Although these terms are simple, their importance to aberration theory is introduced through structural coefficients. These structural coefficients are rearrangements of the Seidel coefficients, and they are written in terms of the shape factor, the conjugate factor, and the index of refraction.

In order to analyze the fourth and sixth-order aberrations, a macro in *Zemax's OpticStudio* is used; this macro calculates the fourth and sixth-order aberrations through Seidel aberration coefficients up to the fourth-order, and calculates the sixth-order coefficients through the various equations that are introduced later in this report. Additionally, the thin lens system that is used throughout this report is modeled in *OpticStudio*.

The thin lens system used in this report has the following basic prescription:

- f/4 thin lens with thickness of 5 mm.
- Stop at the lens.
- Wavelength of 0.58 μm.

The lens material, fields of view, and object heights are changed depending on whether the report changing the shape factor, conjugate factor, or index of refraction. It's important to note that although the lens is considered thin, this description is simply because the thickness is small compared to the focal length. When designing the lens in *OpticStudio*, the lens is not "thin," but has a thickness of 5 mm.

In order to analyze the fourth and sixth-order aberrations as functions of the shape factor, *OpticStudio's* Merit Function editor is set up to change the radii of curvature of the thin lens. A desired shape factor is set as the target, and the system is optimized in order to fit the criteria. Then, the fourth and sixth-order aberrations are calculated through the macro and recorded.

In order to analyze the fourth and sixth-order aberrations as functions of the conjugate factor, an object is set at a specific distance away from the lens for a specific transverse magnification that results in the desired conjugate factor. In *OpticStudio,* the distance from the object to the lens is set as variable, and the desired magnification is set as the target. The thin lens system is optimized, and the specification magnification target is hit. Knowing this magnification results in an easy calculation of the conjugate factor. Again, the macro is used and the fourth and sixth-order aberrations are calculated and recorded.

Finally, in order to analyze the fourth and sixth-order aberrations as functions of the index of refraction, all that is changed is the index of refraction of the thin biconvex lens. The

crucial detail that is necessary for this portion is that the Abbe number be set to zero so that *OpticStudio* does not make assumptions on ray behavior. The index of refraction is then manually changed and the fourth and sixth-order aberrations are calculated and recorded through the macro.

Chapter 1

Introduction

Aberrations in an optical system are departures from ideal behavior. These deviations have been analyzed and classified by the properties and behaviors they exhibit. This report will focus on discussions of the fourth and sixth-order monochromatic aberrations of spherical aberration, coma aberration, astigmatism, field curvature, and distortion. This discussion will begin with an introduction to wavefront deformations, where the wave theory of aberrations is pioneered by H. H. Hopkins [7]. Then, this report proceeds into a discussion of these aberrations geometrically.

In Section 1.1.1 the wavefront aberration function consists of zeroth, second, fourth, and sixth-order terms. By breaking down zeroth and second-order terms in the wavefront aberration function, and relating them to Gaussian and Newtonian optics, this report explains why these terms are usually ignored in aberration analysis. The fourth-order terms in the wavefront aberration function are explained in two separate topics: the Seidel coefficients and pupil aberrations.

Next, in Section 1.2 the sixth-order terms in the wavefront aberration function are heavily discussed. Sixth-order aberrations consist of an intrinsic and extrinsic term, both of which require further understanding geometrically as well as analytically. Sixth-order aberrations are

typically less prominent than fourth-order aberrations in simple lens systems, however understanding sixth-order aberrations is necessary in having a more complete understanding of aberration theory. Additionally, sixth-order aberrations are analyzed in a thin lens system later in this report.

1.1 Theory of Sixth-Order Aberrations

1.1.1 The Wave Aberration Function

This report begins with an explanation of the wave aberration function for an axially symmetric system. The aberration function, $W(\vec{H},\vec{p})$ is a function of the normalized field vector and the aperture vector, $\vec{H}$ and $\vec{p}$ respectively. Before delving any further, it is incredibly crucial to note that a reference must be defined. In this study, the aberration function is built around a reference sphere that is centered at the ideal image plane. This is in direct relation to Gaussian and Newtonian optics upon which first-order rays travel in accordance to the collinear transformation.

The aberration function gives the geometrical deformation of the wavefront at the exit pupil of the system. That is, the aberration function gives an optical path, in this case the optical path given is the distance between the reference sphere and the actual wavefront of the system as measured along a particular ray. This ray is defined by the tip of the field and aperture vectors.

The field vector is located at the object plane of the system, while the aperture vector is located at the exit pupil plane of the system. These two vectors are necessary to define a ray, and subsequently, the aberration function, as stated above. Figure 1.1 gives an example of how the field and aperture vectors are defined in their separate planes, along with a view down the optical axis.

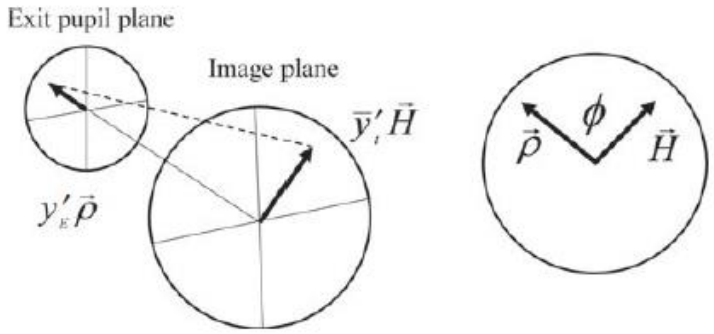

Figure 1.1 [2] The exit and image planes with the aperture and field vectors respectively. These are scaled by the marginal ray height, y', at the exit pupil, and by the chief ray height, $\bar{y}'$, at the image plane. On the right, these are pictured looking down the optical axis, along with the angle in between them, ϕ.

Written to the sixth-order approximation, the wave aberration function[1] is,

$$\begin{aligned} W(\vec{H},\vec{\rho}) = {} & W_{000} + W_{200}(\vec{H}\cdot\vec{H}) + W_{111}(\vec{H}\cdot\vec{\rho}) + W_{020}(\vec{\rho}\cdot\vec{\rho}) + W_{040}(\vec{\rho}\cdot\vec{\rho})^2 \\ & + W_{131}(\vec{H}\cdot\vec{\rho})(\vec{\rho}\cdot\vec{\rho}) + W_{222}(\vec{H}\cdot\vec{\rho})^2 + W_{220}(\vec{H}\cdot\vec{H})(\vec{\rho}\cdot\vec{\rho}) \\ & + W_{311}(\vec{H}\cdot\vec{H})(\vec{H}\cdot\vec{\rho}) + W_{400}(\vec{H}\cdot\vec{H})^2 + W_{240}(\vec{H}\cdot\vec{H})(\vec{\rho}\cdot\vec{\rho})^2 \\ & + W_{331}(\vec{H}\cdot\vec{H})(\vec{H}\cdot\vec{\rho})(\vec{\rho}\cdot\vec{\rho}) + W_{422}(\vec{H}\cdot\vec{H})(\vec{H}\cdot\vec{\rho})^2 + W_{420}(\vec{H}\cdot\vec{H})^2(\vec{\rho}\cdot\vec{\rho}) \\ & + W_{511}(\vec{H}\cdot\vec{H})^2(\vec{H}\cdot\vec{\rho}) + W_{600}(\vec{H}\cdot\vec{H})^3 + W_{060}(\vec{\rho}\cdot\vec{\rho})^3 + W_{151}(\vec{H}\cdot\vec{\rho})(\vec{\rho}\cdot\vec{\rho})^2 \\ & + W_{242}(\vec{H}\cdot\vec{\rho})^2(\vec{\rho}\cdot\vec{\rho}) + W_{333}(\vec{H}\cdot\vec{\rho})^3. \end{aligned} \tag{1.1}$$

where each term represents a different aberration term. The sum of all the terms is the total wavefront deformation.

It is very quickly noted that there are various dot products, $\vec{H}\cdot\vec{H}$, $\vec{\rho}\cdot\vec{\rho}$, and $\vec{H}\cdot\vec{\rho}$. These dot products are necessary in order to ensure that the wave aberration function is a scalar

[1] The wave aberration function is given in *Introduction to aberrations in optical imaging systems* (p. 71) by J. Sasián [3].
[2] Reprinted [adapted] from *Introduction to aberrations in optical imaging systems* (p. 71) by J. Sasián [3].

value. The angle between these values is simply ϕ. Since the defined system is axially symmetric a rotation about the optical axis does not change the values of the field and aperture vectors. That is, the dot products are invariant with rotation about the optical axis.

The wave aberration function [3] can also be written as a simple sum given by,

$$W(\vec{H},\vec{\rho}) = \sum_{j,m,n} W_{k,l,m}(\vec{H}\cdot\vec{H})^{j}(\vec{H}\cdot\vec{\rho})^{m}(\vec{\rho}\cdot\vec{\rho})^{n} \tag{1.2}$$

where the sub-indices, j,m,n represent integers k,l,m with values $k = 2j + m,\ \ l = 2n + m$. The index m is the same for both sets of indices. Equation (1.2) is not a sum by strict definition since going numerically through $j,m,$ and n will not yield a wave aberration function that makes sense. Simply, equation (1.2) is written in this way to relate the sub-indices of $W_{k,l,m}$ to the powers of the dot products. Additionally, it's important to realize that equations (1.1) and (1.2) are equal. Equation (1.1) is simply an expansion to the sixth-order of the terms given by equation (1.2).

In Table 1.1 each wavefront aberration is broken down into its vector and algebraic form. Recall that the field and aperture vectors are normalized. When these both are unity, this results in the wavefront coefficients representing the maximum amplitude of the aberration in units of waves. Upon inspection of Table 1.1 it can be seen why it may be convenient to refer to the wave aberration coefficients in terms of a sum. For example, in analyzing the coma wave aberration coefficient, W_{131}, it can be seen that $k = 1$, $l = 3$, and $m = 1$.

Next, the values for the sub-indices must be calculated using the relationships between both groups of indices. The equations of k and l can be rearranged as follows:

$$k = 2j + m \rightarrow 2j = k - m,$$
$$l = 2n + m \rightarrow 2n = l - m.$$

Aberration name	Vector form	Algebraic form	j	m	n
Zero order					
Uniform piston	W_{000}	W_{000}	0	0	0
Second order					
Quadratic piston	$W_{200}(\vec{H}\cdot\vec{H})$	$W_{200}H^2$	1	0	0
Magnification	$W_{111}(\vec{H}\cdot\vec{\rho})$	$W_{111}H\rho\cos(\phi)$	0	1	0
Focus	$W_{020}(\vec{\rho}\cdot\vec{\rho})$	$W_{020}\rho^2$	0	0	1
Fourth order					
Spherical aberration	$W_{040}(\vec{\rho}\cdot\vec{\rho})^2$	$W_{040}\rho^4$	0	0	2
Coma	$W_{131}(\vec{H}\cdot\vec{\rho})(\vec{\rho}\cdot\vec{\rho})$	$W_{131}H\rho^3\cos(\phi)$	0	1	1
Astigmatism	$W_{222}(\vec{H}\cdot\vec{\rho})^2$	$W_{222}H^2\rho^2\cos^2(\phi)$	0	2	0
Field curvature	$W_{220}(\vec{H}\cdot\vec{H})(\vec{\rho}\cdot\vec{\rho})$	$W_{220}H^2\rho^2$	1	0	1
Distortion	$W_{311}(\vec{H}\cdot\vec{H})(\vec{H}\cdot\vec{\rho})$	$W_{311}H^3\rho\cos(\phi)$	1	1	0
Quartic piston	$W_{400}(\vec{H}\cdot\vec{H})^2$	$W_{400}H^4$	2	0	0
Sixth order					
Oblique spherical aberration	$W_{240}(\vec{H}\cdot\vec{H})(\vec{\rho}\cdot\vec{\rho})^2$	$W_{240}H^2\rho^4$	1	0	2
Coma	$W_{331}(\vec{H}\cdot\vec{H})(\vec{H}\cdot\vec{\rho})(\vec{\rho}\cdot\vec{\rho})$	$W_{331}H^3\rho^3\cos(\phi)$	1	1	1
Astigmatism	$W_{422}(\vec{H}\cdot\vec{H})(\vec{H}\cdot\vec{\rho})^2$	$W_{422}H^4\rho^2\cos^2(\phi)$	1	2	0
Field curvature	$W_{420}(\vec{H}\cdot\vec{H})^2(\vec{\rho}\cdot\vec{\rho})$	$W_{420}H^4\rho^2$	2	0	1
Distortion	$W_{511}(\vec{H}\cdot\vec{H})^2(\vec{H}\cdot\vec{\rho})$	$W_{511}H^5\rho\cos(\phi)$	2	1	0
Piston	$W_{600}(\vec{H}\cdot\vec{H})^3$	$W_{600}H^6$	3	0	0
Spherical aberration	$W_{060}(\vec{\rho}\cdot\vec{\rho})^3$	$W_{060}\rho^6$	0	0	3
Un-named	$W_{151}(\vec{H}\cdot\vec{\rho})(\vec{\rho}\cdot\vec{\rho})^2$	$W_{151}H\rho^5\cos(\phi)$	0	1	2
Un-named	$W_{242}(\vec{H}\cdot\vec{\rho})^2(\vec{\rho}\cdot\vec{\rho})$	$W_{242}H^2\rho^4\cos^2(\phi)$	0	2	1
Un-named	$W_{333}(\vec{H}\cdot\vec{\rho})^3$	$W_{333}H^3\rho^3\cos^3(\phi)$	0	3	0

Table 1.1[3] Wavefront aberrations in vector and algebraic form

[3] Reprinted [adapted] from *Introduction to aberrations in optical imaging systems* (p. 72) by J. Sasián [3].

Then, by substituting in the values for k, l and m the results are,

$$j = \frac{k-m}{2} = \frac{1-1}{2} = 0,$$

$$n = \frac{l-m}{2} = \frac{3-1}{2} = 1.$$

Finally, the wave aberration function given by equation (1.2) for a system with coma is,

$$\begin{aligned} W(\vec{H},\vec{\rho}) &= \sum_{j,m,n} W_{k,l,m}(\vec{H}\cdot\vec{H})^j(\vec{H}\cdot\vec{\rho})^m(\vec{\rho}\cdot\vec{\rho})^n \\ &= \sum_{0,1,1} W_{131}(\vec{H}\cdot\vec{H})^0(\vec{H}\cdot\vec{\rho})^1(\vec{\rho}\cdot\vec{\rho})^1 \\ &= W_{131}(\vec{H}\cdot\vec{\rho})(\vec{\rho}\cdot\vec{\rho}) \\ &= W_{131}(H\rho\cos\phi)(\rho^2) \\ &= W_{131}H\rho^3\cos\phi. \end{aligned} \tag{1.3}$$

In equation (1.3), coma aberration has been written in both its vector and algebraic forms by using the sum notation in equation (1.2). This can be done for every aberration. This form of writing the aberration function in terms of dot products is introduced by R.V. Shack [6].

1.1.2 Aberrations of the Zeroth and Second-Order

The wave aberration function [3] written to the second-order is,

$$W(\vec{H},\vec{\rho}) = W_{000} + W_{200}(\vec{H}\cdot\vec{H}) + W_{111}(\vec{H}\cdot\vec{\rho}) + W_{020}(\vec{\rho}\cdot\vec{\rho}). \quad (1.4)$$

There are four separate aberrations in this shortened aberration function. The goal of this section is to examine each of these terms individually and explain why this report does not consider them in later calculations.

The first term, W_{000} is the zeroth-order piston term. This term simply shifts the wavefront, advancing or delaying it, and has no effect on image quality. Thus, it is not considered a true aberration and is ignored.

To the same argument, there is a second-order piston term, $W_{200}(\vec{H}\cdot\vec{H})$, that is called quadratic piston. This term solely relies on the field of view, and like the zeroth-order piston term, it has no effect on the image quality. Although this report will ignore this term, if the reference is changed with respect to the object point and the exit pupil, this quadratic piston term

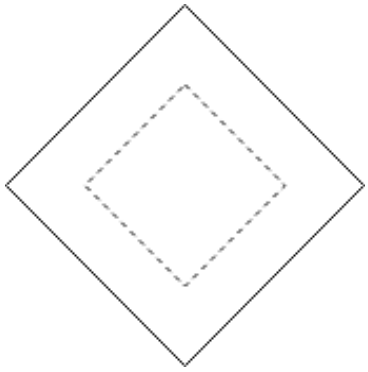

Figure 1.2 An example of change of magnification where the solid line represents the ideal image, and the dashed line represents the change in magnification of the image.

becomes useful in determining a relationship between the change of focus and the longitudinal change of focus.

The $W_{111}(\vec{H}\cdot\vec{\rho})$ term is a quadratic term known as the change of magnification. It is linear as a function of both the field of view and the aperture. This term represents a departure from the ideal size of the image. An example of change of magnification of an image can be seen in Figure 1.2. Although this report is just considering monochromatic aberrations, there is a chromatic change of magnification term that must be considered when the system has multiple wavelength. The chromatic change of magnification is mentioned just for completion.

The last term, $W_{020}(\vec{\rho}\cdot\vec{\rho})$ is known as change of focus, and it is a quadratic term as a function of the aperture. It is independent of the field of view. This term is also known as defocus. What this term represents is a departure in focus from the nominal ideal image plane. An example of this is shown in Figure 1.3. Like chromatic change of magnification, there is a chromatic second-order term called chromatic change of focus. Again, this term will be ignored since the focus is on monochromatic aberrations.

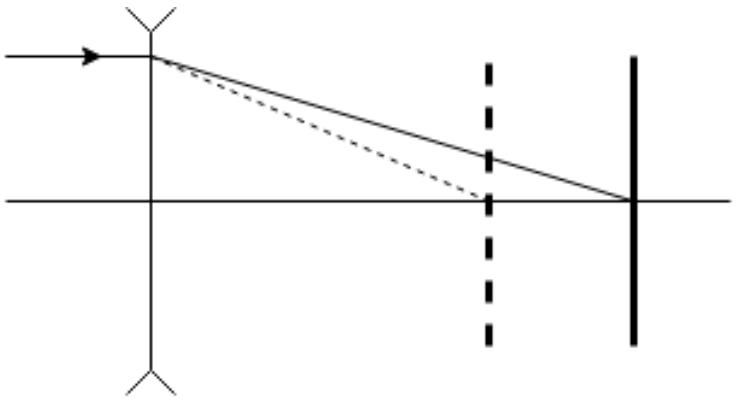

Figure 1.3 An example of defocus where the solid lines represent the ray and the location of the nominal image plane. The dashed line represents the actual location of the image plane

The value of the zeroth and second-order wave aberrations depends on the choice of reference. As stated previously in Section 1.1.1, the reference has been chosen to be a reference sphere centered at the ideal image plane in order to relate to Gaussian and Newtonian optics definitions. As a result, the change in magnification and defocus are zero. That is, $W_{111} = W_{020} = 0$ because the longitudinal change in position and the transverse size of an image are accounted for in Newtonian and Gaussian equations.

1.1.3 The Seidel Aberration Coefficients of Fourth-Order Terms

In Table 1.1 each aberration is written in a vector and algebraic form. However, the vector and algebraic forms aren't particularly convenient forms to use in geometric calculations. By tracing paraxial marginal and chief rays through the system, paraxial quantities can be derived and used to rewrite the wave aberration function in geometrical terms. In fact, these can be written in terms of the Seidel sums, of which the fourth-order sums can be seen in Table 1.2. As stated in Section 1.1.2, second-order terms are not considered. Sixth-order terms will be discussed later. Additionally, this report will not include the derivation of these sums; the usage of these sums in calculations is the more relevant topic.

The fourth-order wave aberration coefficients are spherical aberration, coma aberration, astigmatism, field curvature, distortion, and quartic piston, each listed respectively in Table 1.2.

In Table 1.2, each aberration is written as a Seidel sum. In a system, each surface has an individual contribution towards the Seidel sum and therefore towards the total amount of

Aberration	Seidel Sum
$W_{040} = \frac{1}{8} S_{\mathrm{I}}$	$S_{\mathrm{I}} = -\sum A^2 y \Delta\left(\frac{u}{n}\right)$
$W_{131} = \frac{1}{2} S_{\mathrm{II}}$	$S_{\mathrm{II}} = -\sum A \bar{A} y \Delta\left(\frac{u}{n}\right)$
$W_{222} = \frac{1}{2} S_{\mathrm{III}}$	$S_{\mathrm{III}} = -\sum \bar{A}^2 y \Delta\left(\frac{u}{n}\right)$
$W_{220} = \frac{1}{4} S_{\mathrm{IV}}$	$S_{\mathrm{IV}} = -\sum \Psi^2 P - \sum \bar{A}^2 y \Delta\left(\frac{u}{n}\right)$
$W_{311} = \frac{1}{2} S_{\mathrm{V}}$	$S_{\mathrm{V}} = -\sum \frac{\bar{A}}{A}\left[\Psi^2 P + \bar{A}^2 y \Delta\left(\frac{u}{n}\right)\right],$
	$S_{\mathrm{V}} = -\sum \bar{A}\left[\bar{A}^2 \Delta\left(\frac{1}{n^2}\right) y - (\Psi + \bar{A} y)\bar{y} P\right]$
$W_{400} = \frac{1}{8} S_{\mathrm{VI}}$	$S_{\mathrm{VI}} = -\sum \bar{A}^2 \bar{y} \Delta\left(\frac{\bar{u}}{n}\right)$

Table 1.2[4] Fourth-order wave aberration coefficients in terms of the Seidel sums.

[4] Reprinted [adapted] from *Theory of sixth-order wave aberrations* (p. D72) by J. Sasián [5].

aberration. For example, a single lens has two surfaces, surface 1 and surface 2. Then, in calculating spherical aberration, the Seidel sum term would be,

$$S_I = -\sum_{i=1}^{2}\left(A^2 y \Delta\left(\frac{u}{n}\right)\right)_i$$
$$= -A_1^2 y_1 \Delta\left(\frac{u_1}{n_1}\right) - A_2^2 y_2 \Delta\left(\frac{u_2}{n_2}\right),$$

where each surface has contributed its own term to the Seidel sum.

The first-order quantities that constitute the fourth-order wave aberration coefficients from Table 1.2 are found in Table 1.3. The quantity $\Delta(u/n)$ refers to the calculation of the term after and before refraction. That is, $\Delta(u/n) = u'/n' - u/n$ where the primed terms indicate the value of the terms after refraction, and the unprimed terms indicate the value of the terms before refraction.

As will be seen later, this report uses the equations from Table 1.2 in order to do calculations on the aberrations of the thin lens system.

Quantity	Formula
Refraction-invariant marginal ray	$A = ni = nu + nyc$
Refraction- invariant chief ray	$\bar{A} = n\bar{i} = n\bar{u} + n\bar{y}c$
Lagrange invariant	$\Psi = n\bar{u}y - nu\bar{y} = \bar{A}y - A\bar{y}$
Surface curvature	$c = \frac{1}{r}$
Petzval sum term	$P = c \cdot \Delta\left(\frac{1}{n}\right)$

Table 1.3[5] Quantities derived in paraxial ray tracing used in calculating Seidel sums.

[5] Reprinted [adapted] from *Theory of sixth-order wave aberrations* (p. D72) by J. Sasián [5].

1.1.4 Fourth-Order Pupil Aberrations

Although this report does not use pupil aberration equations for the calculation of fourth-order aberrations, this discussion is necessary in understanding sixth-order extrinsic aberrations.

This report has previously used a system comprising of the nominal image and object. However, in consideration of pupil aberrations, the system is now comprised of the entrance and exit pupil. As a result, if the system consists of multiple components, the exit pupil of a component becomes the entrance pupil of the next component; these pupils are mismatched. Additionally, the marginal ray and chief ray of the object/image system now interchange roles; the marginal ray becomes the chief ray and the chief ray become the marginal ray in the entrance/exit pupil system.

With the entrance/exit pupil system then a new problem arises. Now, image aberrations change when the object is axially moved. However, this problem is simply solved upon realizing that an object shift is equal to a stop shift in the pupil system.

With this knowledge in mind, a pupil aberration function can be constructed to fourth-order. The function[6] is,

$$\begin{aligned}\bar{W}(\vec{H},\vec{\rho}) = {} & \bar{W}_{000} + \bar{W}_{200}(\vec{\rho}\cdot\vec{\rho}) + \bar{W}_{111}(\vec{H}\cdot\vec{\rho}) + \bar{W}_{020}(\vec{H}\cdot\vec{H}) + \bar{W}_{040}(\vec{H}\cdot\vec{H})^2 \\ & + \bar{W}_{131}(\vec{H}\cdot\vec{H})(\vec{H}\cdot\vec{\rho}) + \bar{W}_{222}(\vec{H}\cdot\vec{\rho})^2 + \bar{W}_{220}(\vec{H}\cdot\vec{H})(\vec{\rho}\cdot\vec{\rho}) \\ & + \bar{W}_{311}(\vec{\rho}\cdot\vec{\rho})(\vec{H}\cdot\vec{\rho}) + \bar{W}_{400}(\vec{\rho}\cdot\vec{\rho})^2 .\end{aligned} \tag{1.5}$$

The barred terms indicate aberrations of the pupil planes.

[6] The pupil aberration function is written in *Introduction to aberrations in optical imaging systems* (p. 162) by J. Sasián [3].

When comparing equations (1.1) and (1.5) up to fourth-order, it is very clear of the change in system – that is, $\vec{H}$ has essentially replaced $\vec{p}$ and vice versa in our equations. Of course, this makes more sense when laid out in a figure. In Figure 1.4 the object plane, the image plane, the entrance pupil plane, and the exit pupil plane are represented. As per previous definitions, the field vector is located in the object plane and the aperture vector is located in the exit pupil plane. In the object/image system, the calculation of aberrations begins in the object plane, where $\vec{H}$ is located. However, in the entrance/exit pupil system, the pupil aberration calculation begins in the entrance pupil plane, where $\vec{\rho}$ is located. This is essentially the "switch" between $\vec{H}$ and $\vec{\rho}$ that occurs in equations (1.1) and (1.5).

Relationships between aberrations in the object/image system and entrance/exit pupil systems can be derived. When changing from an object/image to an entrance/exit pupil system the following changes must be made:

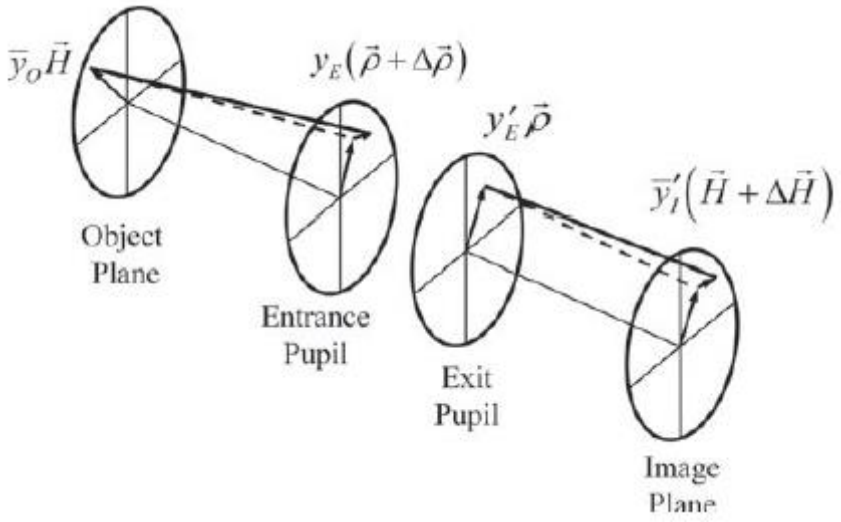

Figure 1.4[7] An optical system where the object/image plane system is used. The object and image planes, as well as the entrance and exit pupil planes are optically conjugated.

[7] Reprinted [adapted] from *Introduction to aberrations in optical imaging systems* (p. 163) by J. Sasián [3].

$$\Psi = -\overline{\Psi}$$

$$y \rightarrow \bar{y}$$

$$A \rightarrow \bar{A}.$$

By algebraic manipulation, and with the changes to the terms just mentioned, the results in Table 1.4 are derived. In Table 1.4 the term $\bar{W}_{220}$ refers to the sagittal pupil field curvature and the term W_{220} refers to the sagittal image field curvature.

Name	Identity between Pupil and Image Aberration Coefficients
Pupil spherical aberration	$\bar{W}_{040} = W_{400}$
Pupil coma	$\bar{W}_{131} = W_{311} + \frac{1}{2}\Psi \cdot \Delta\{\bar{u}^2\}$
Pupil astigmatism	$\bar{W}_{222} = W_{222} + \frac{1}{2}\Psi \cdot \Delta\{u\bar{u}\}$
Pupil sagittal field curvature	$\bar{W}_{220} = W_{220} + \frac{1}{4}\Psi \cdot \Delta\{u\bar{u}\}$
Pupil distortion	$\bar{W}_{311} = W_{131} + \frac{1}{2}\Psi \cdot \Delta\{u^2\}$
Pupil piston	$\bar{W}_{400} = W_{040}$

Table 1.4[8] Relationship between fourth-order pupil and image aberration coefficients.

[8] Reprinted [adapted] from *Theory of sixth-order wave aberrations* (p. D72) by J. Sasián [5].

1.2 Sixth-Order Aberrations

1.2.1 The Sixth-Order Aberration Function[9]

In truncating equation (1.1), so to just focus on sixth-order aberrations, the sixth-order aberration function is,

$$\begin{aligned} W(\vec{H},\vec{\rho}) = {} & W_{240}(\vec{H}\cdot\vec{H})(\vec{\rho}\cdot\vec{\rho})^2 + W_{331}(\vec{H}\cdot\vec{H})(\vec{H}\cdot\vec{\rho})(\vec{\rho}\cdot\vec{\rho}) \\ & + W_{422}(\vec{H}\cdot\vec{H})(\vec{H}\cdot\vec{\rho})^2 + W_{420}(\vec{H}\cdot\vec{H})^2(\vec{\rho}\cdot\vec{\rho}) \\ & + W_{511}(\vec{H}\cdot\vec{H})^2(\vec{H}\cdot\vec{\rho}) + W_{600}(\vec{H}\cdot\vec{H})^3 + W_{060}(\vec{\rho}\cdot\vec{\rho})^3 \\ & + W_{151}(\vec{H}\cdot\vec{\rho})(\vec{\rho}\cdot\vec{\rho})^2 + W_{242}(\vec{H}\cdot\vec{\rho})^2(\vec{\rho}\cdot\vec{\rho}) + W_{333}(\vec{H}\cdot\vec{\rho})^3. \end{aligned} \tag{1.6}$$

There are ten sixth-order aberrations. Six of these ten are improvements of their fourth-order counterparts where they now have an additional quadratic dependence on the field. The other four are new wavefront aberrations, however one is referred to as sixth-order spherical aberration. These new shapes can be seen in Figure 1.5.

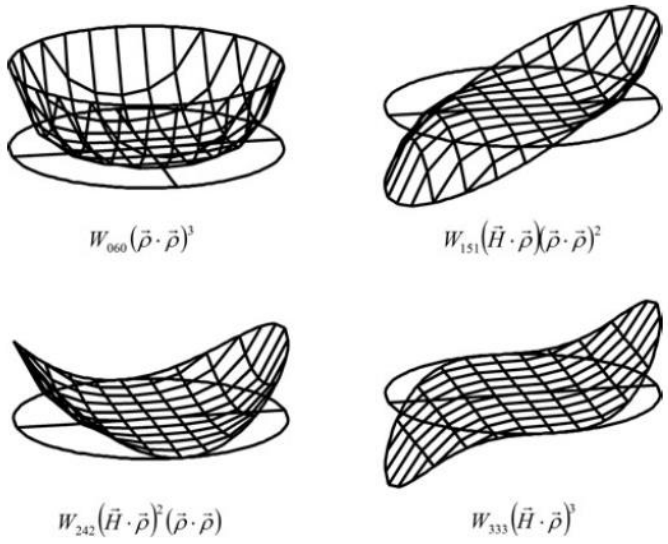

Figure 1.5[10] Wavefront deformations of new aberrations in the sixth-order.

[9] The study on sixth-order aberrations is taken from *Introduction to aberrations in optical imaging systems* (p. 187-199) by J. Sasián [3] and *Theory of sixth-order wave aberrations* by J. Sasián [5].
[10] Reprinted [adapted] from *Introduction to aberrations in optical imaging systems* (p. 188) by J. Sasián [3].

In the study of sixth-order aberrations there are two parts that consist of the total aberration: the intrinsic part and the extrinsic part. Up until now, this study has focused on the intrinsic part. This intrinsic aberration is the aberration that is contributed by the surfaces and by the system itself when an incoming beam has no aberration. However, in the sixth-order study, extrinsic aberrations must be considered.

1.2.2 Extrinsic Aberrations

Extrinsic, or induced, aberrations arise in an optical surface when there is aberration before that surface. These extrinsic aberrations result from distortion from the entrance and exit pupils. In the explanation[11] for extrinsic aberrations used in this report, second-order aberrations are ignored, and the reference sphere is centered at the ideal Gaussian image point.

Consider two optical systems, *A* and *B.* These systems have aberration functions to the sixth-order, written below,

$$W_A(\vec{H},\vec{\rho}) = W_A^{(4)}(\vec{H},\vec{\rho}) + W_A^{(6)}(\vec{H},\vec{\rho})$$
$$W_B(\vec{H},\vec{\rho}) = W_B^{(4)}(\vec{H},\vec{\rho}) + W_B^{(6)}(\vec{H},\vec{\rho})$$

where the aberration function consists of fourth and sixth-order terms. These aberration functions are written with the aperture vector located at the exit pupil. However, it's crucial to note that the exit pupil of system *A* is the entrance pupil of system *B.*

In combining these two systems into one system, *C*, the combined aberration function is,

$$W_C(\vec{H},\vec{\rho}) = W_A(\vec{H},\vec{\rho}) + W_B(\vec{H},\vec{\rho}+\Delta\vec{\rho}'). \tag{1.7}$$

In equation (1.7) the term $W_A(\vec{H},\vec{\rho})$ is expected from the combined system—it's the contribution from system *A*. However, system *B*'s contribution to the aberration function has been written with an additional $\Delta\vec{\rho}'$ added to its $\vec{\rho}$ dependence. This $\Delta\vec{\rho}'$ term is the exit pupil distortion caused by system *A* that effects system *B*. This term is crucial in the combined

[11] The mathematical methods used in the explanation for extrinsic aberrations comes from a combination of techniques used in *Introduction to aberrations in optical imaging systems* (p.188-189) [3] and *Theory of sixth-order wave aberrations* (p.D74-D75) [5] both by J. Sasián.

aberration function since the exit pupil of system *A* is the entrance pupil of system *B.* Although this report will not be going strictly into the calculations, it's important to note that the exit pupil distortion can be written as,

$$\Delta\vec{\rho}' = \frac{1}{\Psi}\nabla_H \bar{W}_A(\vec{H},\vec{\rho}) + O^{(5)}, \tag{1.8}$$

where the pupil aberrations of system *A* are being used. The fifth-order terms, $O^{(5)}$ will be ignored in this analysis.

So, what is the extrinsic aberration of system *B*? Figure 1.6 can be used as a visual aide in order to determine the answer. Figure 1.6 is a visual representation of system *A*'s exit pupil. However, recall that system *A*'s exit pupil is also system *B*'s entrance pupil. As a result, also recall that system B then has an extrinsic aberration term caused by the exit pupil distortion from system *A.* However, let it be clear that the extrinsic term is a result of the *fourth-order* exit pupil distortion by system *A*. Then, the sixth-order extrinsic term for system *B* is,

$$W_B^{(6E)}(\vec{H},\vec{\rho}) = W_B^{(4)}(\vec{H},\vec{\rho}+\Delta\vec{\rho}') - W_B^{(4)}(\vec{H},\vec{\rho}). \tag{1.9}$$

Now, proceeding with the knowledge of the behavior of extrinsic terms, equation (1.7) can be expanded as follows:

$$\begin{aligned} W_C(\vec{H},\vec{\rho}) &= W_A^{(4)}(\vec{H}.\vec{\rho}) + W_A^{(6)}(\vec{H},\vec{\rho}) + W_B^{(4)}(\vec{H},\vec{\rho}) + W_B^{(6)}(\vec{H},\vec{\rho}) \\ &= W_A^{(4)}(\vec{H}.\vec{\rho}) + W_A^{(6)}(\vec{H},\vec{\rho}) + W_B^{(4)}(\vec{H},\vec{\rho}) + W_B^{(6I)}(\vec{H},\vec{\rho}) + W_B^{(6E)}(\vec{H},\vec{\rho}). \end{aligned} \tag{1.10}$$

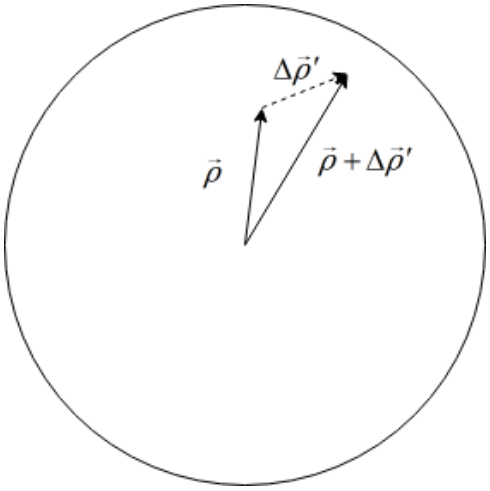

Figure 1.6 An example of system *A*'s exit pupil and system *B*'s entrance pupil with the addition of $\vec{\rho}$ and $\Delta\vec{\rho}$.

What if instead of focusing on system *A* and system *B*'s respective exit and entrance pupils, the focus lies on the exit pupil of the combined system *C*? That is, the induced aberrations of system *A*'s exit pupil are not considered until its effects in combined system *C*'s exit pupil. In short, the extrinsic terms will be calculated by locating the aperture vector at the exit pupil of system *C.* Then, equation (1.8) is no longer valid and a different equation must be written. Now,

$$\Delta\vec{\rho} = -\frac{1}{\Psi}\nabla_H \bar{W}_B(\vec{H},\vec{\rho}) + O^{(5)}$$

and the pupil aberrations of system *B* are being used. Then, the aberration function on system *C* can be written as,

$$W_C(\vec{H},\vec{\rho}) = W_A^{(4)}(\vec{H},\vec{\rho}+\Delta\vec{\rho}') + W_A^{(6I)}(\vec{H},\vec{\rho}) + W_B{}^{(4)}(\vec{H},\vec{\rho}) + W_B{}^{(6I)}(\vec{H},\vec{\rho}).$$

So, the extrinsic term $W_B^{(6E)}(\vec{H},\vec{\rho})$ from equation (1.9) is no longer valid in its current form. The equation must be rewritten by replacing $\vec{\rho}$ with $\vec{\rho}+\Delta\vec{\rho}$ in $W_A^{(4)}(\vec{H},\vec{\rho})$ so that the result is,

$$W_B^{(6E)}(\vec{H},\vec{\rho}) = W_A^{(4)}(\vec{H},\vec{\rho}+\Delta\vec{\rho}) - W_A^{(4)}(\vec{H},\vec{\rho}).$$

In summary, there are two techniques that were outlined above for calculating the extrinsic terms of a combined system *A* and *B*. The first was by locating the aperture vector at the entrance pupil of the combined system, and the second was locating the aperture vector at the exit pupil of the combined system. Table 1.5 lists the extrinsic aberration equations for sixth-order aberrations with respect to the different locations of the aperture vector.

With Aperture Vector $\vec{\rho}$ at Entrance Pupil	With Aperture Vector $\vec{\rho}$ at Exit Pupil
$W^-_{060E} = \frac{1}{\Psi}\{4W^B_{040}\bar{W}^A_{311}\}$	$W^+_{060E} = -\frac{1}{\Psi}\{4W^A_{040}\bar{W}^B_{311}\}$
$W^-_{151E} = \left\{\frac{1}{\Psi}\,3W^B_{131}\bar{W}^A_{311} + 8W^B_{040}\bar{W}^A_{220} + 8W^B_{040}\bar{W}^A_{222}\right\}$	$W^+_{151E} = -\frac{1}{\Psi}\{3W^A_{131}\bar{W}^B_{311} + 8W^A_{040}\bar{W}^B_{220} + 8W^A_{040}\bar{W}^B_{222}\}$
$W^-_{242E} = \frac{1}{\Psi}\{2W^B_{222}\bar{W}^A_{311} + 4W^B_{131}\bar{W}^A_{220} + 6W^B_{131}\bar{W}^A_{222} + 8W^B_{040}\bar{W}^A_{131}\}$	$W^+_{242E} = -\frac{1}{\Psi}\{2W^A_{222}\bar{W}^B_{311} + 4W^A_{131}\bar{W}^B_{220} + 6W^A_{131}\bar{W}^B_{222} + 8W^A_{040}\bar{W}^B_{131}\}$
$W^-_{333E} = \frac{1}{\Psi}\{4W^B_{131}\bar{W}^A_{131} + 4W^B_{222}\bar{W}^A_{222}\}$	$W^+_{333E} = -\frac{1}{\Psi}\{4W^A_{131}\bar{W}^B_{131} + 4W^A_{222}\bar{W}^B_{222}\}$
$W^-_{240E} = \frac{1}{\Psi}\{2W^B_{131}\bar{W}^A_{220} + 2W^B_{220}\bar{W}^A_{311} + 4W^B_{040}\bar{W}^A_{131}\}$	$W^+_{240E} = -\frac{1}{\Psi}\{2W^A_{131}\bar{W}^B_{220} + 2W^A_{220}\bar{W}^B_{311} + 4W^A_{040}\bar{W}^B_{131}\}$
$W^-_{331E} = \frac{1}{\Psi}\{5W^B_{131}\bar{W}^A_{131} + 4W^B_{220}\bar{W}^A_{220} + 4W^B_{220}\bar{W}^A_{222} + 4W^B_{222}\bar{W}^A_{220} + W^B_{311}\bar{W}^A_{311} + 16W^B_{040}\bar{W}^A_{040}\}$	$W^+_{331E} = -\frac{1}{\Psi}\{5W^A_{131}\bar{W}^B_{131} + 4W^A_{220}\bar{W}^B_{220} + 4W^A_{220}\bar{W}^B_{222} + 4W^A_{222}\bar{W}^B_{220} + W^A_{311}\bar{W}^B_{311} + 16W^A_{040}\bar{W}^B_{040}\}$
$W^-_{422E} = \frac{1}{\Psi}\{2W^B_{311}\bar{W}^A_{222} + 4W^B_{220}\bar{W}^A_{131} + 6W^B_{222}\bar{W}^A_{131} + 8W^B_{131}\bar{W}^A_{040}\}$	$W^+_{422E} = -\frac{1}{\Psi}\{2W^A_{311}\bar{W}^B_{222} + 4W^A_{220}\bar{W}^B_{131} + 6W^A_{222}\bar{W}^B_{131} + 8W^A_{131}\bar{W}^B_{040}\}$
$W^-_{420E} = \frac{1}{\Psi}\{2W^B_{220}\bar{W}^A_{131} + 2W^B_{311}\bar{W}^A_{220} + 4W^B_{131}\bar{W}^A_{040}\}$	$W^+_{420E} = -\frac{1}{\Psi}\{2W^A_{220}\bar{W}^B_{131} + 2W^A_{311}\bar{W}^B_{220} + 4W^A_{131}\bar{W}^B_{040}\}$
$W^-_{511E} = \frac{1}{\Psi}\{3W^B_{311}\bar{W}^A_{131} + 8W^B_{220}\bar{W}^A_{040} + 8W^B_{222}\bar{W}^A_{040}\}$	$W^+_{511E} = -\frac{1}{\Psi}\{3W^A_{311}\bar{W}^B_{131} + 8W^A_{220}\bar{W}^B_{040} + 8W^A_{222}\bar{W}^B_{040}\}$
$W^-_{600E} = \frac{1}{\Psi}\{4W^B_{311}\bar{W}^A_{040}\}$	$W^+_{600E} = -\frac{1}{\Psi}\{4W^A_{311}\bar{W}^B_{040}\}$
Added terms when the center of the reference sphere is located at the intersection of the chief ray with the Gaussian image plane	
$\Delta W^-_{331E} = -W^B_{311}\Delta^A\{u^2\}/2$	$\Delta W^+_{331E} = +W^A_{311}\Delta^B\{u^2\}/2$
$\Delta W^-_{422E} = -W^B_{311}\Delta^A\{u\bar{u}\}$	$\Delta W^+_{422E} = +W^A_{311}\Delta^B\{u\bar{u}\}$
$\Delta W^-_{420E} = -W^B_{311}\Delta^A\{u\bar{u}\}/2$	$\Delta W^+_{420E} = +W^A_{311}\Delta^B\{u\bar{u}\}/2$
$\Delta W^-_{511E} = -3W^B_{311}\Delta^A\{\bar{u}^2\}/2$	$\Delta W^+_{511E} = +3W^A_{311}\Delta^B\{\bar{u}^2\}/2$

Table 1.5[12] Extrinsic aberrations of combination of systems *A* and *B*.

[12] Reprinted [adapted] from *Theory of sixth-order wave aberrations* (p. D75) by J. Sasián [5].

1.2.3 Intrinsic Aberrations

Intrinsic aberrations are extensions of their fourth-order aberration counterparts. They are aberrations contributed simply by the surfaces of the system; its assumed that the incoming light beam will has no aberrations. However, in calculation of intrinsic aberrations it is incredibly crucial to be aware of changes to the wavefront propagation and changes to the aperture location. The equations for the intrinsic aberrations will be built upon these ideas.

In order to begin understanding intrinsic aberrations, an explanation on intrinsic sixth-order spherical aberration must be given. The equation for intrinsic sixth-order spherical aberration[13] is written as,

$$W_{060I} = W_{040}\left[\frac{1}{2}\frac{y^2}{r^2} - \frac{1}{2}A\left(\frac{u'}{n'} + \frac{u}{n}\right) + 2\frac{y}{r}u'\right] - \frac{8}{\mathcal{H}}W_{040}W_{040}\frac{\bar{y}}{y} \tag{1.11}$$

where the entire term must be applied to every surface of the system. The first order terms in this equation can be found in Table 1.3. The sixth-order intrinsic term for spherical aberration is proportional to fourth-order spherical aberration.

Notice that if the stop is at the surface, the second term in equation (1.11) completely disappears since $\bar{y} = 0$. This term arises from shifting the stop to a different location; the wavefront propagates from an old pupil plane to a new pupil plane and there is a new wavefront change, $\Delta_Z W(\vec{H},\vec{\rho})$ which is given by:

$$\Delta_Z W(\vec{H},\vec{\rho}) = -\frac{1}{2}\frac{\bar{y}}{y}\frac{1}{\mathcal{H}}\nabla_\rho W(\vec{H},\vec{\rho})\cdot\nabla_\rho W(\vec{H},\vec{\rho}). \tag{1.12}$$

[13] The equation for intrinsic sixth-order spherical aberration is from *Introduction to aberrations in optical imaging systems* (p. 190) by J. Sasián [3].

So, in the presence of fourth-order spherical aberration the wavefront change is:

$$\Delta_Z W(\vec{H},\vec{\rho}) = -\frac{1}{2}\frac{\bar{y}}{y}\frac{1}{Ж}\nabla_\rho\left(W_{040}(\vec{\rho}\cdot\vec{\rho})^2\right)\cdot\nabla_\rho\left(W_{040}(\vec{\rho}\cdot\vec{\rho})^2\right)$$

$$= -\frac{1}{2}\frac{\bar{y}}{y}\frac{1}{Ж}4W_{040}\rho^3\cdot 4W_{040}\rho^3$$

$$= -\frac{16}{2}\frac{\bar{y}}{y}\frac{1}{Ж}W_{040}W_{040}$$

$$= -\frac{8}{Ж}\frac{\bar{y}}{y}W_{040}W_{040}$$

which is exactly the second term in equation (1.11). This wavefront deformation can be calculated for each aberration, and the results can be seen in Table 1.6[14].

The next step in calculating intrinsic aberration terms is shifting the stop to the center of curvature, which results in $\bar{A}=0$. This results in a sixth-order aberration function given by,

$$\begin{aligned} W_{CC}(\vec{H},\vec{\rho}) = {} & W_{040}(\vec{\rho}\cdot\vec{\rho})^2 + W_{220P}(\vec{H}\cdot\vec{H})(\vec{\rho}\cdot\vec{\rho}) + W_{240CC}(\vec{H}\cdot\vec{H})(\vec{\rho}\cdot\vec{\rho})^2 \\ & + W_{331CC}(\vec{H}\cdot\vec{H})(\vec{H}\cdot\vec{\rho})(\vec{\rho}\cdot\vec{\rho}) + W_{422CC}(\vec{H}\cdot\vec{H})(\vec{H}\cdot\vec{\rho})^2 \\ & + W_{420CC}(\vec{H}\cdot\vec{H})^2(\vec{\rho}\cdot\vec{\rho}) + W_{060CC}(\vec{\rho}\cdot\vec{\rho})^3 + W_{151CC}(\vec{H}\cdot\vec{\rho})(\vec{\rho}\cdot\vec{\rho})^2 \\ & + W_{242CC}(\vec{H}\cdot\vec{\rho})^2(\vec{\rho}\cdot\vec{\rho}) \end{aligned}$$

where fourth-order terms with a $\bar{A}$ term are zero. Then, the intrinsic sixth-order aberration coefficients, when the stop has been moved to the center of curvature, are given in Table 1.7[15].. This report will not go into the details necessary to derive these terms, however the derivation can be found in *Theory of sixth-order aberrations* by José Sasián, pages D.91-D.95.

[14] Reprinted [adapted] from "*Sixth-order aberrations"* (p. 13) by J. Sasián [4]
[15] Reprinted [adapted] from *Introduction to aberrations in optical imaging systems* (p. 192-193) by J. Sasián [3].

Table 1. **Wavefront deformation change upon propagation.**
$\Delta_z W(\vec{H},\vec{\rho}) = \frac{1}{2}\frac{\bar{y}}{y}\frac{1}{\Psi}\nabla_\rho W(\vec{H},\vec{\rho})\cdot\nabla_\rho W(\vec{H},\vec{\rho})$
$\Delta W_{060} = \frac{1}{2}\frac{\bar{y}}{y}\frac{1}{\Psi}\{16W_{040}W_{040}\}$
$\Delta W_{151} = \frac{1}{2}\frac{\bar{y}}{y}\frac{1}{\Psi}\{24W_{040}W_{131}\}$
$\Delta W_{242} = \frac{1}{2}\frac{\bar{y}}{y}\frac{1}{\Psi}\{16W_{040}W_{222} + 8W_{131}W_{131}\}$
$\Delta W_{240} = \frac{1}{2}\frac{\bar{y}}{y}\frac{1}{\Psi}\{16W_{040}W_{220} + W_{131}W_{131}\}$
$\Delta W_{333} = \frac{1}{2}\frac{\bar{y}}{y}\frac{1}{\Psi}\{8W_{131}W_{222}\}$
$\Delta W_{331} = \frac{1}{2}\frac{\bar{y}}{y}\frac{1}{\Psi}\{8W_{040}W_{311} + 4W_{131}W_{222} + 12W_{131}W_{220}\}$
$\Delta W_{422} = \frac{1}{2}\frac{\bar{y}}{y}\frac{1}{\Psi}\{4W_{131}W_{311} + 4W_{222}W_{222} + 8W_{222}W_{220}\}$
$\Delta W_{420} = \frac{1}{2}\frac{\bar{y}}{y}\frac{1}{\Psi}\{4W_{220}W_{220} + 2W_{311}W_{131}\}$
$\Delta W_{511} = \frac{1}{2}\frac{\bar{y}}{y}\frac{1}{\Psi}\{4W_{222}W_{311} + 4W_{220}W_{311}\}$
$\Delta W_{600} = \frac{1}{2}\frac{\bar{y}}{y}\frac{1}{\Psi}\{W_{311}W_{311}\}$

Table 1.6[14] Wavefront deformation change for sixth-order aberration terms.

The last step to achieving a complete sixth-order aberration coefficient equation for the intrinsic terms is stop shifting back to the surface. While in fourth-order theory a stop shift is performed by substituting the aperture vector $\vec{\rho}$ for a stop shift vector $\vec{\rho}_{shift}$ given by,

$$W_{220P} = -\frac{1}{4}\mathcal{K}^2 P$$

$$W_{040} = -\frac{1}{8}A^2\Delta\left(\frac{u}{n}\right)y$$

$$W_{060CC} = W_{040}\left[\frac{1}{2}\frac{y^2}{r^2} - \frac{1}{2}A\left(\frac{u'}{n'} + \frac{u}{n}\right) + 2\frac{y}{r}u'\right] + \frac{8}{Ay}W_{040}W_{040} - \frac{\overline{A}}{A}\frac{8}{\mathcal{K}}W_{040}W_{040}$$

$$W_{240CC} = +\frac{1}{16}\frac{A}{r}\mathcal{K}^2\Delta\left\{\frac{u}{n^2}\right\} + \frac{1}{8}\frac{1}{r}\mathcal{K}^2\Delta\left\{\frac{u^2}{n}\right\} + \frac{1}{4}\frac{y^2}{r^2}W_{220P} + \frac{y}{r}u'W_{220P} - \frac{1}{4}\frac{u}{r}\mathcal{K}^2\Delta\left\{\frac{u}{n}\right\} - \frac{8}{\mathcal{K}}\left(\frac{\overline{A}}{A}\right)W_{040}W_{220P}$$

$$W_{420CC} = \frac{3}{16}\frac{1}{r^3}\mathcal{K}^4\Delta\left\{\frac{1}{n}\right\}\frac{1}{A^2} - \frac{2}{\mathcal{K}}\left(\frac{\overline{A}}{A}\right)W_{220P}W_{220P}$$

$$W_{331CC} = -2W_{220P}u'\left(\overline{u}' - \frac{\overline{A}}{A}u'\right)$$

$$W_{422CC} = -W_{220P}\left(\overline{u}' - \frac{\overline{A}}{A}u'\right)^2$$

$$W_{151CC} = -4W_{040}u'\left(\overline{u}' - \frac{\overline{A}}{A}u'\right)$$

$$W_{242CC} = -2W_{040}\left(\overline{u}' - \frac{\overline{A}}{A}u'\right)^2$$

Table 1.7[15] Sixth-order aberrations with stop at center of curvature.

$$\vec{\rho}_{shift} = \vec{\rho} + \frac{\overline{A}}{A}\vec{H},$$

the same cannot be done for the sixth-order. In sixth-order theory, if the stop is shifted then the exit pupil changes locations. Additionally, with a stop shift there is an accompanied wavefront propagation. These two results of stop shifting require more mathematical rigor.

Upon stop shifting, the wavefront equation for the center of curvature is altered as follows,

$$W_{shift}(\vec{H},\vec{\rho}) = \left[W_{CC}(\vec{H},\vec{\rho}) - \frac{1}{2}\frac{\bar{A}}{A}\frac{1}{\not{K}}\nabla_{\rho}W_{CC}(\vec{H},\vec{\rho})\cdot\nabla_{\rho}W_{CC}(\vec{H},\vec{\rho}) \right]_{\vec{\rho}+\frac{\bar{A}}{A}\vec{H}} .$$

Upon substitution of $W_{CC}(\vec{H},\vec{\rho})$ and evaluation at $\vec{\rho}_{shift}$, equations for intrinsic aberrations of a spherical surface are obtained. These equations can be found in Table 1.8[16].

[16] Reprinted [adapted] from *Introduction to aberrations in optical imaging systems* (p. 194) by J. Sasián [3].

$$W_{060I} = W_{060I}$$

$$W_{151I} = 6\left(\frac{\overline{A}}{A}\right) W_{060I} + W_{151CC}$$

$$W_{242I} = 12\left(\frac{\overline{A}}{A}\right)^2 W_{060I} + 4\left(\frac{\overline{A}}{A}\right) W_{151CC} + W_{242CC}$$

$$W_{333I} = 8\left(\frac{\overline{A}}{A}\right)^3 W_{060I} + 4\left(\frac{\overline{A}}{A}\right)^2 W_{151CC} + 2\left(\frac{\overline{A}}{A}\right) W_{242CC}$$

$$W_{240I} = 3\left(\frac{\overline{A}}{A}\right)^2 W_{060I} + \left(\frac{\overline{A}}{A}\right) W_{151CC} + W_{240CC}$$

$$W_{331I} = 12\left(\frac{\overline{A}}{A}\right)^3 W_{060I} + 6\left(\frac{\overline{A}}{A}\right)^2 W_{151CC} + 4\left(\frac{\overline{A}}{A}\right) W_{240CC} + 2\left(\frac{\overline{A}}{A}\right) W_{242CC} + W_{331CC}$$

$$W_{422I} = 12\left(\frac{\overline{A}}{A}\right)^4 W_{060I} + 8\left(\frac{\overline{A}}{A}\right)^3 W_{151CC} + 4\left(\frac{\overline{A}}{A}\right)^2 W_{240CC} + 5\left(\frac{\overline{A}}{A}\right)^2 W_{242CC} + 2\left(\frac{\overline{A}}{A}\right) W_{331CC} + W_{422CC}$$

$$W_{420I} = 3\left(\frac{\overline{A}}{A}\right)^4 W_{060I} + 2\left(\frac{\overline{A}}{A}\right)^3 W_{151CC} + 2\left(\frac{\overline{A}}{A}\right)^2 W_{240CC} + \left(\frac{\overline{A}}{A}\right)^2 W_{242CC} + \left(\frac{\overline{A}}{A}\right) W_{331CC} + W_{420CC}$$

$$W_{511I} = 6\left(\frac{\overline{A}}{A}\right)^5 W_{060I} + 5\left(\frac{\overline{A}}{A}\right)^4 W_{151CC} + 4\left(\frac{\overline{A}}{A}\right)^3 W_{240CC} + 4\left(\frac{\overline{A}}{A}\right)^3 W_{242CC} + 3\left(\frac{\overline{A}}{A}\right)^2 W_{331CC} + 2\left(\frac{\overline{A}}{A}\right) W_{422CC} + 2\left(\frac{\overline{A}}{A}\right) W_{420CC}$$

$$W_{600I} = \overline{W}_{060I}$$

Table 1.8[16] Intrinsic aberration coefficients of the sixth-order for a spherical surface.

Chapter 2

Section 2.1 will focus on the discussion of three system properties: the shape factor, the conjugate factor, and the index of refraction. These three properties play interesting roles in the aberration function of Seidel sums, and introducing these allows a new coefficient, the structural coefficient, to be defined and used in geometrical aberration analysis.

The shape factor is a ratio of surface curvatures that describes the shape of a lens. Manipulation of the shape factor results in lens bending and subsequent marginal and chief ray angle changes. Understanding of the shape factor leads to interesting results in aberration control.

The conjugate factor is a ratio of marginal ray angles that when applied to a thin lens is related to the transverse magnification of a system. Moving an object across different distances from the lens results in changes to marginal ray angles. This can result in aberration for rays that deviate from paraxial definitions because of these object location changes.

Finally, the index of refraction is a material property that describes ray propagation through media. Different materials cause different ray angles across refracting surfaces which of course result in aberrations.

These properties can all be strictly related to aberrations through structural coefficients, which will be discussed in Section 2.2.

2.1 Lens Properties

2.1.1 The Shape Factor

The shape factor of a thin lens specifies the shape of the lens[17], as it is governed by the curvatures of the two surfaces. The shape factor is then written as,

$$X = \frac{c_1 + c_2}{c_1 - c_2} \tag{2.1}$$

where c_1 and c_2 are the curvatures of the first and second surface. If the thin lens is convex-plano, the shape factor is $X = 1.0$. If the thin lens is plano-convex, then the shape factor is $X = -1.0$. And, if the curvatures of the lens are equal but opposite, such as in an equi-concave, or equi-convex lens, the shape factor is $X = 0.0$.

The shape factor is not defined for equal curvatures. This is explored in the math below where $c_2 = c_1$:

$$X = \frac{c_1 + c_1}{c_1 - c_1}$$

$$= \frac{2c_1}{0}.$$

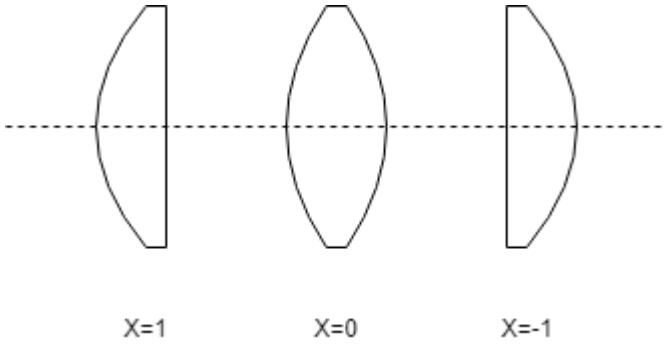

Figure 2.1 Examples of lens shape with three specific shape factors.

[17] The theory of the shape factor comes from *Fundamental Optical Design* (p. 139-140) by. M. Kidger [1].

This is clearly undefined.

The shape factor can also be written in terms of the radius of the surfaces using the simple relation $R = \frac{1}{c}$. The equation then becomes:

$$\begin{aligned} X &= \frac{1/r_1 + 1/r_2}{1/r_1 - 1/r_2} \\ &= \frac{(r_2 + r_1)/r_1 r_2}{(r_2 - r_1)/r_1 r_2} \\ &= \frac{r_1 + r_2}{r_1 r_2} \cdot \frac{r_1 r_2}{r_2 - r_1} \\ &= \frac{r_1 + r_2}{r_2 - r_1} \\ &= -\frac{r_1 + r_2}{r_1 - r_2}. \end{aligned} \tag{2.2}$$

The shape factor is a very powerful design parameter, especially when involved in aberration control. While maintain paraxial approximations and while holding the power of the lens constant, as the shape factor changes then paraxial chief and marginal ray paths through the lens do not change.

2.1.2 The Conjugate Factor

The conjugate factor[18] is another system design parameter that describes marginal ray angles of the system and is related to the transverse magnification of a thin lens. It is defined as,

$$Y = \frac{\omega' + \omega}{\omega' - \omega} = \frac{n'u' + nu}{n'u' - nu} \tag{2.3}$$

where n' and n are the indices of refraction and u' and u are the marginal ray after and before a surface, respectively.

If the system is a thin lens in air, the conjugate factor can be simplified further. Since the object and image space have the same refractive index $n' = n \cong 1$, the equation becomes,

$$Y = \frac{u' + u}{u' - u} \tag{2.4}$$

This equation can be simplified even further by using the equation for magnification given below:

$$m = \frac{nu}{n'u'} = \frac{u}{u'}. \tag{2.5}$$

Rearranging equation (2.5) such that $u' = mu'$ we can write,

$$Y = \frac{u' + mu'}{u' - mu'}$$

$$= \frac{m+1}{m-1}. \tag{2.6}$$

[18] The theory for the conjugate factor comes from *Fundamental Optical Design* (p. 140-141) by M. Kidger [1].

2.1.3 The Index of Refraction

The index of refraction plays a crucial role in aberration theory. The index of refraction of a material dictates by how much a ray of light is bent upon entering and exiting materials of different refractive indices. The basic rule for how much a ray of light is bent is given by Snell's Law,

$$n\sin(I) = n'\sin(I') \tag{2.7}$$

where n and n' are the indices of refraction of the material surrounding the refracting surface, and where I and I' are the angles of ray incidence and refraction.

As stated previously, aberrations are a result of a geometrical deformation in the wavefront. These deviations are described as separate types of aberrations, listed previously in Table 1.2, to the fourth-order in terms of Seidel sums, and in Table 1.5, Table 1.7, and Table 1.8 to the sixth-order.

The geometrical calculation of these aberrations breaks down to several first-order quantities which are found in Table 1.3. Among all these listed tables, the index of refraction term pops up frequently. Frequently, the index of refraction is divided through entire aberration equations so that the result is an optical path. But, the index of refraction also pops up in the calculation of first-order quantities as well as in structural aberration coefficients which will be discussed in the next section.

2.2 Aberrations as Functions of the Shape Factor, Conjugate Factor, and Index of Refraction

2.2.1 Structural Coefficients of Fourth-Order Aberrations

The Seidel sums of section 1.1.3 can be restructured in terms of the optical power of each component, the marginal ray height at the principle plane, y_p, the Lagrange invariant, and new terms called the structural coefficients. Table 2.1 lists the Seidel sums rewritten in terms of the variables just mentioned. Table 2.1 also includes Seidel sums C_L and C_T which are the sums for chromatic change of focus and chromatic change of magnification, which this report will not discuss.

Pupils located at principal planes
$S_I = \frac{1}{4} y_P^4 \Phi^3 \sigma_I$
$S_{II} = \frac{1}{2} \mathcal{H} y_P^2 \Phi^2 \sigma_{II}$
$S_{III} = \mathcal{H}^2 \Phi \sigma_{III}$
$S_{IV} = \mathcal{H}^2 \Phi \sigma_{IV}$
$S_V = \frac{2\mathcal{H}^3 \sigma_V}{y_P^2}$
$C_L = y_P^2 \Phi \sigma_L$
$C_T = 2\mathcal{H} \sigma_T$

Table 2.1[19] Seidel sums in terms of the marginal ray height at the principle planes, the Lagrange invariant, the power, and the structural coefficients of fourth-order aberration terms.

[19] Reprinted [adapted] from *Introduction to aberrations in optical imaging systems* (p. 148) by J. Sasián [3].

The reasoning for rewriting the Seidel sums in terms of structural coefficients begins to become more evident when looking at Table 2.2. The structural aberration coefficients relating to the monochromatic fourth-order aberrations are written in terms of the indices of refraction and the conjugate factor of the lens – both physical properties of the system that were described in Section 2.1.

The structural aberration coefficients in Table 2.2 are for individual surfaces. That is, if a system consists of a simple lens with two surfaces, the structural coefficients would need to be calculated for each surface, and each surface would contribute an individual term to the Seidel sum. The conjugate factor term used would then be the one defined in equation (2.3).

Now, as mentioned before, the optical system used in this report is a thin lens in air, with the stop at the lens. Conveniently, the structural aberration coefficients can be simplified further

Structural aberration coefficients

$$\sigma_I = -\frac{1}{2}\left[\frac{n'+n}{n'-n} - Y\right]^2\left[\frac{n'^2-n^2}{n^2n'^2}\cdot Y - \frac{n'^2+n^2}{n^2n'^2}\right]$$

$$\sigma_{II} = -\frac{1}{2}\left[\frac{n'+n}{n'-n} - Y\right]\left[\frac{n'^2-n^2}{n^2n'^2}\cdot Y - \frac{n'^2+n^2}{n^2n'^2}\right]$$

$$\sigma_{III} = -\frac{1}{2}\left[\frac{n'^2-n^2}{n^2n'^2}\cdot Y - \frac{n'^2+n^2}{n^2n'^2}\right]$$

$$\sigma_{IV} = \frac{1}{nn'}$$

$$\sigma_V = \frac{n'^2-n^2}{n^2n'^2}$$

$$\sigma_L = \frac{1}{2}\left[Y - \frac{n'+n}{n'-n}\right]\cdot\Delta\left(\frac{\delta n}{n}\right)$$

$$\sigma_T = \Delta\left(\frac{\delta n}{n}\right)$$

Table 2.2[20] Structural aberration coefficients of a single surface, with the stop at the surface.

[20] Reprinted [adapted] from *Introduction to aberrations in optical imaging systems* (p. 150) by J. Sasián [3].

for a thin lens in air. Table 2.3 lists the structural aberration coefficients of a thin lens, along with simplified first-order identities for this system. Note that the conjugate factor used is the one which this report has defined as equation (2.6).

First-order identities

$$\Phi = (n-1)\cdot(c_1 - c_2) = (n-1)\cdot\left(\frac{1}{r_1} - \frac{1}{r_2}\right)$$

$$X = \frac{c_1 + c_2}{c_1 - c_2} = -\frac{r_1 + r_2}{r_1 - r_2} \qquad Y = \frac{\omega' + \omega}{\omega' - \omega} = \frac{1+m}{1-m}$$

$$c_1 = \frac{1}{2}\frac{\Phi}{n-1}(X+1) \qquad c_2 = \frac{1}{2}\frac{\Phi}{n-1}(X-1)$$

$$\omega = nu = -\frac{1}{2}(Y-1)(\Phi\cdot y_P) \qquad \omega' = n'u' = -\frac{1}{2}(Y+1)(\Phi\cdot y_P)$$

Structural aberration coefficients

$$\sigma_I = AX^2 - BXY + CY^2 + D \qquad A = \frac{n+2}{n(n-1)^2}$$

$$\sigma_{II} = EX - FY \qquad B = \frac{4(n+1)}{n(n-1)}$$

$$\sigma_{III} = 1 \qquad C = \frac{3n+2}{n}$$

$$\sigma_{IV} = \frac{1}{n} \qquad D = \frac{n^2}{(n-1)^2}$$

$$\sigma_V = 0 \qquad E = \frac{n+1}{n(n-1)}$$

$$\sigma_L = \frac{1}{\nu} \qquad F = \frac{2n+1}{n}$$

$$\sigma_T = 0 \qquad \nu = \frac{n_F - n_C}{n_d - 1}$$

Table 2.3[21] First-order identities and structural aberration coefficients of fourth-order aberrations for a thin lens in air, with the stop at the lens.

[21] Reprinted [adapted] from *Introduction to aberrations in optical imaging systems* (p. 151) by J. Sasián [3].

Chapter 3

This chapter focuses on the fourth and sixth-order monochromatic aberrations as functions of the shape factor.

The first section describes the f/4 BK7 thin lens used in this report. This section also describes the methods used to control and change the shape factor as well as how the fourth and sixth-order monochromatic aberrations are calculated. *Zemax's OpticStudio* is used very heavily in this section. The lens design, shape factor manipulation, and aberration calculation are all done within *OpticStudio*.

In the second section, plots of the fourth and sixth-order aberrations as functions of the shape factor are shown. These plots are analyzed with regards to the fields of view chosen, and they are compared against Seidel aberration equations written in terms of structural coefficients. Additionally, the fourth and sixth-order aberrations are compared with each other.

In the last section, certain shape factors have been chosen, and their respective thin lens layouts and wave fans have been plotted using *OpticStudio*. The reason for this is to understand the deviation of the rays from the nominal image plane by comparing the wave fans and the lens layouts.

3.1 Introduction to the Thin Lens System

3.1.1 Description of the System and its Dependence on the Shape Factor

This section will begin with an overview as to the optical system used, as well as to the methodologies used in changing the shape factor and in recording the fourth and sixth-order monochromatic aberrations.

The optical system used in this report is a thin lens in air, with the stop located at the lens. Below are the thin lens system properties:

- Stop at the lens.
- Lens made of BK7 with a thickness of 5 mm.
- f/4 lens with an effective focal length of 100 mm.
- Wavelength of 0.58 μm and fields of view of 0, 10, and 30 degrees.

It's important to note that this lens is described as a "thin" simply because its thickness is small compared to the focal length. However, this lens does have a thickness. An example of the basic

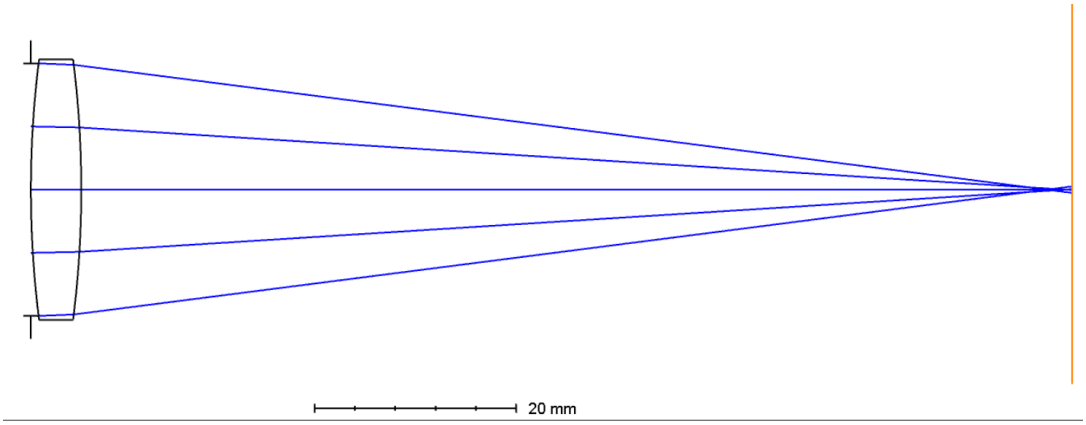

Figure 3.1 Thin lens f/4 BK7 system with stop at the lens, a focal length of 100 mm, and a shape factor of $X = 0$.

layout and prescription of this thin lens with a shape factor of $X = 0$ can be seen in Figure 3.1 and Table 3.1.

Table 3.1 shows the lens prescription above put into place for a thin lens with shape factor $X = 0$. The stop (surface 1) is located at the thin lens. Again, the lens is thin (5mm thick) in comparison with the defined effective focal length of the system.

The system is f/4, which can be determined by use of the following equation:

$$f/\# = \frac{f}{D_{EP}} = \frac{100}{25} = 4.$$

Thus, a thin lens with a shape factor of $X = 0$ and with the desired system properties has been laid out and defined.

Next, the technique used to quickly bend a lens into the desired shape will be described through an example. Take a desired shape factor of $X = 2$. First, remember the equation of the shape factor given by,

$$X = \frac{c_1 + c_2}{c_1 - c_2}. \tag{2.1}$$

	Surface Type		Comment	Radius	Thickness		Material	Coating	Clear Semi-Dia	
0	OBJECT	Standard		Infinity	Infinity				Infinity	
1	STOP	Standard		Infinity	0.000				12.500	U
2		Standard		102.501	5.000		BK7		12.638	
3		Standard		-102.501	98.338	M			12.881	
4	IMAGE	Standard		Infinity	-				19.238	

Table 3.1 Prescription for f/4 BK7 thin lens system with lens at the stop, a focal length of 100 mm, and a shape factor of $X = 0$.

By changing the curvature of the surfaces, the shape factor is changed. Keeping this in mind, use *OpticStudio's* Merit Function editor as an aide to quickly solve for curvatures necessary to achieve the desired shape factor.

Let the radii of the surfaces (surfaces 2 and 3 in Table 3.1) be variables in the "Lens Data" editor in *OpticStudio*. Now, let the Merit Function editor read the curvatures of the surfaces, as in rows 1 and 2 of Table 3.2 where surfaces 2 and 3 (column 2) refer to surfaces 2 and 3 of Table 3.1. The third row of Table 3.2 adds these curvatures, and the fourth row takes the difference of these values. The fifth row then divides the sum and difference, which is exactly equation (2.1).

If a desired target and a weight is set in row 5 of Table 3.2, and then the system is optimized through *OpticStudio's* optimization tool, the radii of curvatures of the surfaces of the thin lens will be changed to achieve the desired shape factor. However, it's important to keep in mind that the effective focal length must remain the same for each change in the shape factor, as is seen in row 7 of Table 3.2.

Now, it is necessary to describe the methodology used for the calculation of the fourth and sixth-order aberration coefficients. Luckily, a macro available for download in *OpticStudio*,

	Type	Surf						Target	Weight	Value	% Contrib
1	CVVA	2						0.000	0.000	0.028	0.000
2	CVVA	3						0.000	0.000	9.447E-03	0.000
3	SUMM	1	2					0.000	0.000	0.038	0.000
4	DIFF	1	2					0.000	0.000	0.019	0.000
5	DIVI	3	4					2.000	20.000	2.000	0.206
6	BLNK										
7	EFFL		1					100.0...	50.000	100.000	99.794

Table 3.2 Merit function editor for thin lens f/4 BK7 system with stop at the lens, a focal length of 100 mm, and a shape factor of $X = 0$.

titled, "*Book Wave Coefficients"* [22] calculates fourth and sixth-order aberration coefficients through the use of Seidel aberration coefficients listed in Table 1.2, and through the various equations listed in Section 1.2.

After changing the shape factor of the thin lens, the fourth and sixth-order aberrations were calculated through the macro and recorded.

[22] Details on the macro used can be found in *Introduction to aberrations in optical imaging systems* (p. 247-257) by J. Sasián [3].

3.2 Aberrations as Functions of the Shape Factor

3.2.1 Spherical Aberration as a Function of the Shape Factor

Figure 3.2 shows the amount of spherical aberration (in waves) to the fourth and sixth-orders as a function of the shape factor. This is for a field of 0 degrees – as spherical aberration has no field dependence changing the field will not change the amount of spherical aberration. As expected, the fourth-order aberration is much larger than the sixth-order, however at shape factors of about $-5 \le X \le -2$, the amount of sixth-order aberration is significant.

Let's revisit the equations for fourth and sixth-order spherical aberration. Fourth-order spherical aberration, in terms of structural coefficients is given by,

$$\begin{aligned} W_{040} &= \frac{1}{8} S_I \\ &= \frac{1}{8}\left(\frac{1}{4} y_p^4 \Phi^3 \sigma_I\right) \\ &= \frac{1}{32} y_p^2 \Phi^3 \left[-\frac{1}{2}\left(\frac{n'+n}{n'-n} - Y\right)^2 \left(\frac{n'^2 - n^2}{n^2 n'^2} \cdot Y - \frac{n'^2 + n^2}{n^2 n'^2}\right)\right]. \end{aligned} \tag{2.8}$$

The structural coefficient is taken from Table 2.2 and equation (2.8) is to be applied to every surface.

Equation (2.8) can be simplified to an equation for a thin lens, and is given below,

$$W_{040,thin} = \frac{1}{32} y_p^4 \Phi^3 \left(AX^2 - BXY + CY^2 + D\right), \tag{2.9}$$

where the $A, B, C,$ and D terms are dependent on the index of refraction and can be found in Table 2.3. Equations (2.8) and (2.9) are both necessary in understanding how spherical aberration depends on the shape factor, since the lens, although considered thin, is not thin when designed in *OpticStudio*.

In equations (2.8) we see no explicit shape factor dependence. However, in equation (2.9) we see a quadratic and linear shape factor term. This dependence on the shape factor seems to describe the shape of our fourth-order curve. We can also see that the sixth-order curve does not share the same shape as the fourth-order curve.

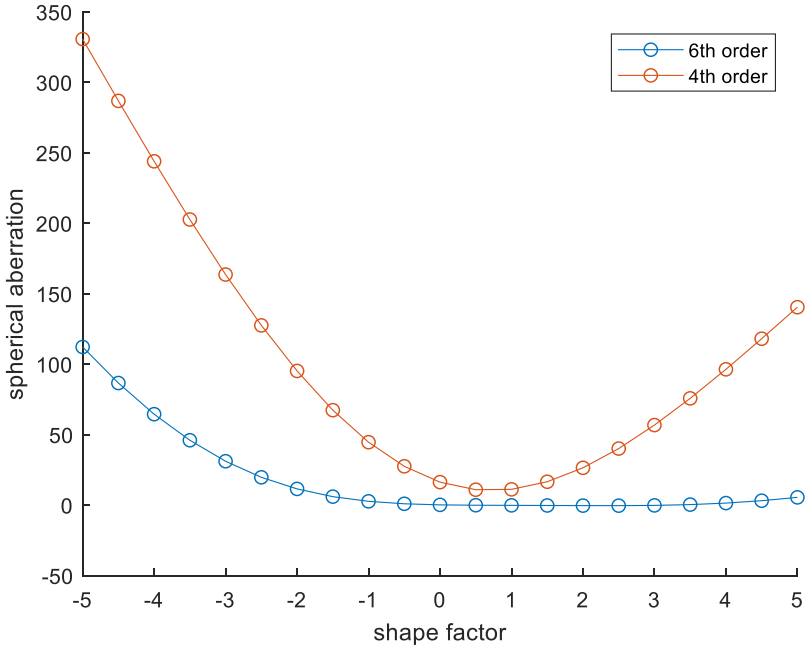

Figure 3.2 Fourth and sixth-order spherical aberration for f/4 BK7 thin lens with focal length of 100 mm and at 10 degrees as a function of the shape factor.

3.2.2 Coma Aberration as a Function of the Shape Factor

Figure 3.3 and Figure 3.4 show the amount of fourth and sixth-order coma aberration as a function of the shape factor. The thin lens system in Figure 3.3 is set to have a field of 10 degrees, and the system in Figure 3.4 has a field of 30 degrees. Measuring the amount of coma across these two fields is important because coma aberration changes as a function of the field, unlike spherical aberration. Additionally, at a field of 0 degrees there is no coma.

The dependence on the field can be seen in,

$$W_{131} H\rho^3 \cos(\phi),$$
$$W_{331} H^3\rho^3 \cos(\phi)$$

which are the algebraic forms of fourth and sixth-order coma respectively. The dependence on the field to the fourth-order is linear, and cubic to the sixth-order.

Now, the fourth-order coma aberration coefficient in terms of structural coefficients is,

$$\begin{aligned} W_{131} &= \frac{1}{2} S_{II} \\ &= \frac{1}{2}\left(\frac{1}{2} \text{Ж} y_p^2 \Phi^2 \sigma_{II}\right) \\ &= \frac{1}{4} \text{Ж} y_p^2 \Phi^2 \left[-\frac{1}{2}\left(\frac{n'+n}{n'-n} - Y\right)\left(\frac{n'^2 - n^2}{n^2 n'^2}\cdot Y - \frac{n'^2 + n^2}{n^2 n'^2}\right)\right] \end{aligned} \tag{2.10}$$

where this equation is applied to every surface. Equation (2.10) can be simplified for a thin lens and is given by,

$$W_{131,thin} = \frac{1}{4} \mathcal{H} y_p^2 \Phi^2 \left(EX - FY \right). \tag{2.11}$$

where E and F are terms dependent on the index of refraction and can be found in Table 2.3.

In equation (2.10) there is no visible dependence on the shape factor. However, in equation (2.11) there is a linear dependence on the shape factor to the fourth-order. In Figure 3.3 and Figure 3.4, for small values of the shape factor, coma's dependence is linear. However, when the magnitude of the shape factor increases, the dependence appears to be cubic.

There is a reasonable explanation to this deviation from the first-order paraxial calculations. And to put it simply, that reason is that these equations are *paraxial* approximations. In Figure 3.5 the thin f/4 BK7 lens has a focal length of 100 mm, a field of view of 10 degrees and a shape factor of $X = -1$. In Figure 3.6 the same thin f/4 BK7 lens with a focal length of 100 mm and a field of view of 10 degrees is shown, but now it has a shape factor of $X = -5$. The lens in Figure 3.6 is bending the rays at a much larger angle than the lens in Figure 3.5, so much so that this ray trace cannot be considered paraxial. As a result, the amount of coma aberration that is being measured is not linear for shape factors where the lens is being bent by a large amount.

In Figure 3.3 and Figure 3.4 the shape factor greatly affects the amount of coma astigmatism. A shape factor of $X = 1$ lends the system to the least amount of coma aberration.

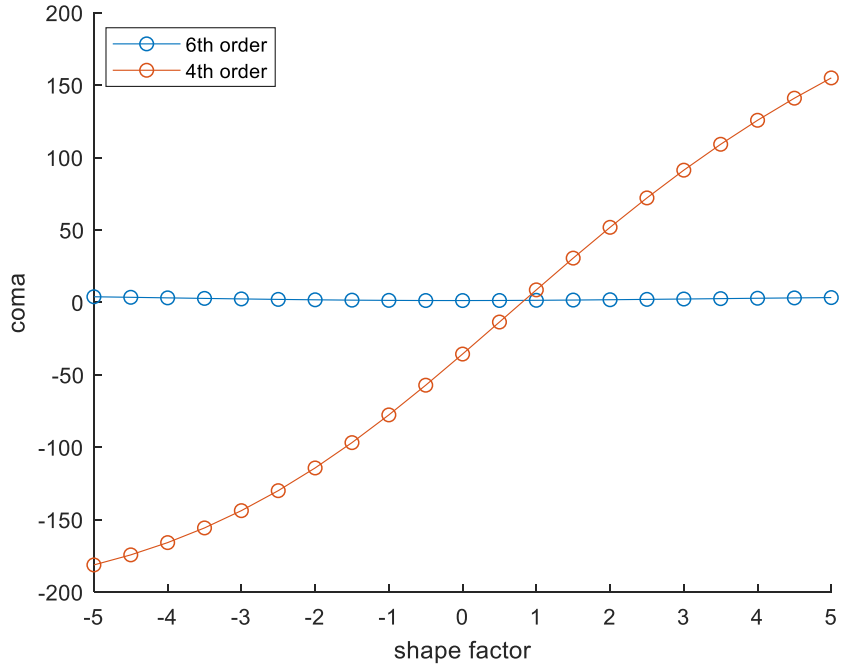

Figure 3.3 Fourth and sixth-order coma aberration for f/4 BK7 thin lens with focal length of 100 mm at 10 degrees as a function of the shape factor.

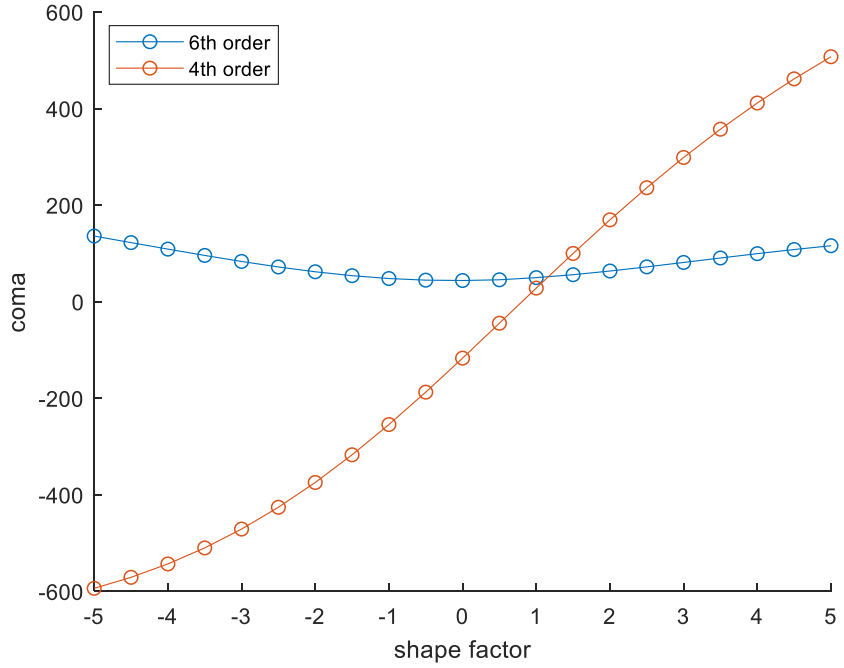

Figure 3.4 Fourth and sixth-order coma aberration for f/4 BK7 thin lens with focal length of 100 mm at 30 degrees as a function of the shape factor.

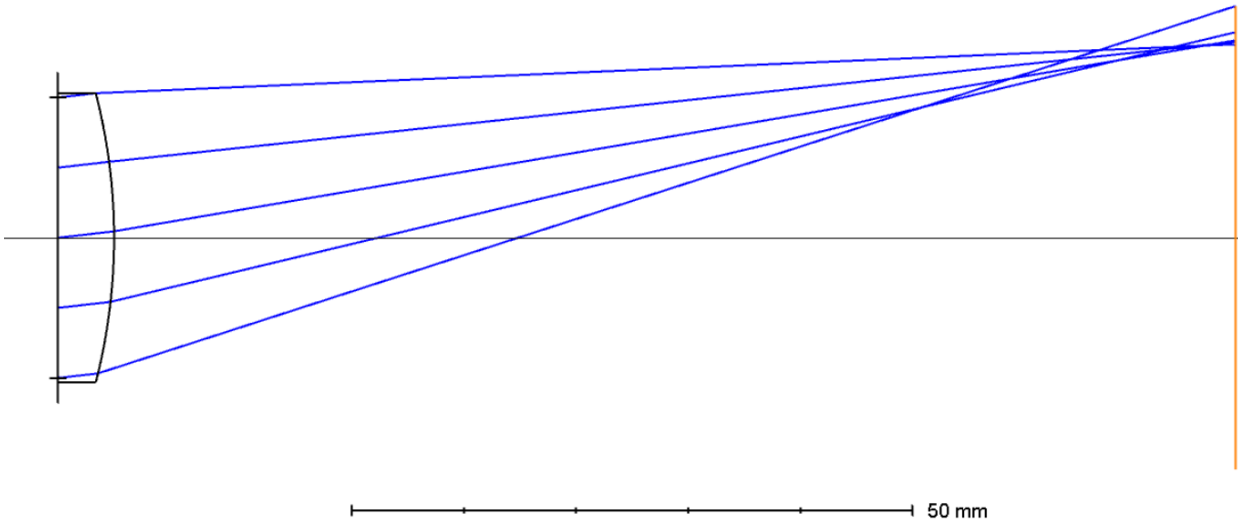

Figure 3.5 Thin f/4 BK7 lens with a focal length of 100 mm, field of view of 10 degrees and a shape factor of -1.

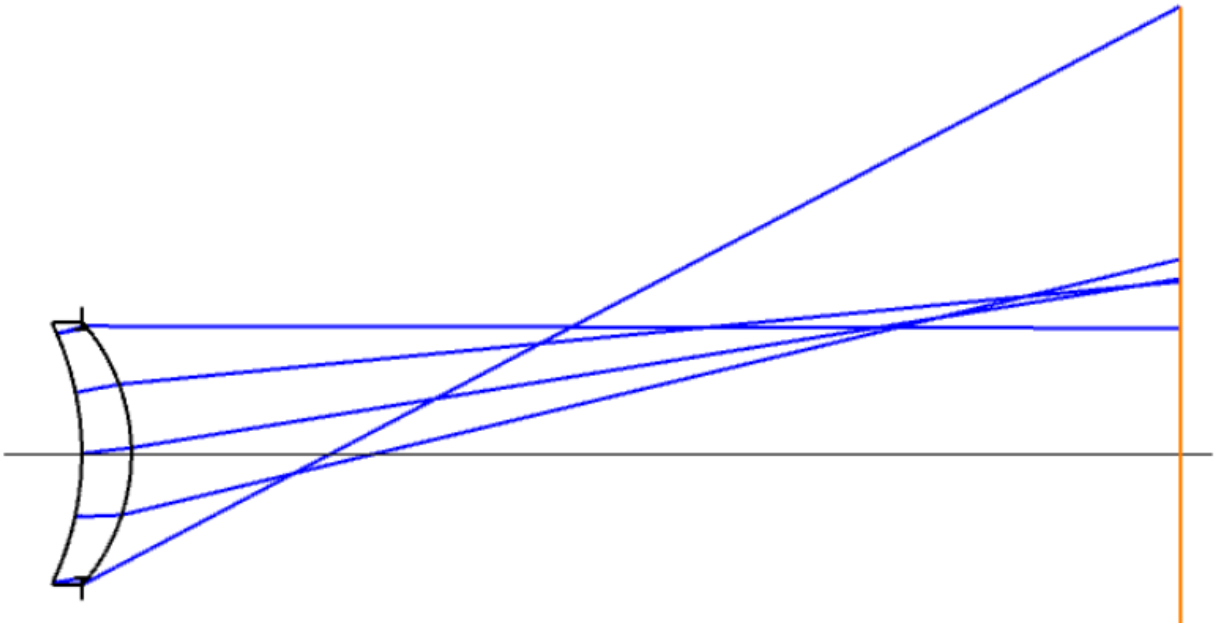

Figure 3.6 Thin f/4 BK7 lens with a focal length of 100 mm, field of view of 10 degrees and a shape factor of -5.

In comparing Figure 3.3 and Figure 3.4, by simply changing the field of view from 10 degrees to 30 degrees almost triples the amount of coma aberration in the fourth-order. Even the sixth-order coma aberration appears to be incredibly significant; at a shape factor of $X = -5$ the amount of coma astigmatism is about 150 mm.

3.2.3 Astigmatism as a Function of the Shape Factor

Figure 3.7 and Figure 3.8 show the amount of fourth and sixth-order astigmatism aberration as a function of the shape factor. The thin lens system in Figure 3.7 is set to have a field of 10 degrees, and the system in Figure 3.8 has a field of 30 degrees. Measuring the amount of astigmatism across these two fields is important because coma aberration changes as a function of the field. Additionally, at a field of 0 degrees there is no astigmatism.

Astigmatism's dependence on the field can be seen in its algebraic to the fourth and sixth-order:

$$W_{222}H^2\rho^2\cos^2(\phi),$$
$$W_{422}H^4\rho^2\cos^2(\phi).$$

Astigmatism's dependence on the field is quadratic to the fourth-order, and quartic to the sixth-order.

Now, the fourth-order astigmatism coefficient in terms of structural coefficients is,

$$\begin{aligned} W_{222} &= \frac{1}{2}S_{III} \\ &= \frac{1}{2}\left(\not{K}^2\Phi\sigma_{III}\right) \\ &= \frac{1}{2}\not{K}^2\Phi\left[-\frac{1}{2}\left(\frac{n'^2-n^2}{n^2n'^2}\cdot Y-\frac{n'^2+n^2}{n^2}n'^2\right)\right] \end{aligned} \tag{2.12}$$

where equation (2.12) must be applied to each individual surface. Equation (2.12) can be simplified for a thin lens and the simplification is seen below:

$$W_{222,thin} = \frac{1}{2}\mathcal{A}K^2\Phi(1)$$

$$= \frac{1}{2}\mathcal{A}K^2\Phi. \tag{2.13}$$

We can see in equations (2.12) and (2.13) that there is no visible shape factor term. As such, astigmatism should not depend on the shape factor. Unfortunately, Figure 3.7 and Figure 3.8 say otherwise.

In Figure 3.7 the fourth-order curve appears to have a quadratic or quartic dependence on the shape factor that approaches a maximum astigmatism value around $X = 2.5$. The sixth-order astigmatism curve can be considered negligible when compared to the fourth-order; the fourth-order terms dominate the sixth-order terms.

In Figure 3.8, where the field has been increased from 10 degrees to 30 degrees, the fourth and sixth-order terms are much more significant, as was expected with the field dependence on astigmatism. Even the sixth-order terms in Figure 3.8 contribute significantly to the total amount of astigmatism. Again, there is a quadratic or quartic dependence on the shape factor and the sixth-order astigmatism curve does not follow the shape of the fourth-order astigmatism curve.

In comparing Figure 3.7 and Figure 3.8, the fourth-order astigmatism curves have an identical shape. In fact, the fourth-order terms from Figure 3.8 are approximately 10.72 times those from Figure 3.7. And, the sixth-order terms from Figure 3.8 are approximately 114.92 times those from Figure 3.7 – in fact, $10.72^2 \approx 114.92$.

It’s crucial to state that the results of Figure 3.7 and Figure 3.8 are incorrect. Equations (2.12) and (2.13) state that there should be no dependence on the shape factor for fourth-order astigmatism, and that is what the results should have shown. These incorrect results could potentially stem from the thickness of the lens being too large, or large fields that result in rays no longer being paraxial. Regardless, Figure 3.7 and Figure 3.8 do not obey equations (2.12) and (2.13) and are therefore not correct.

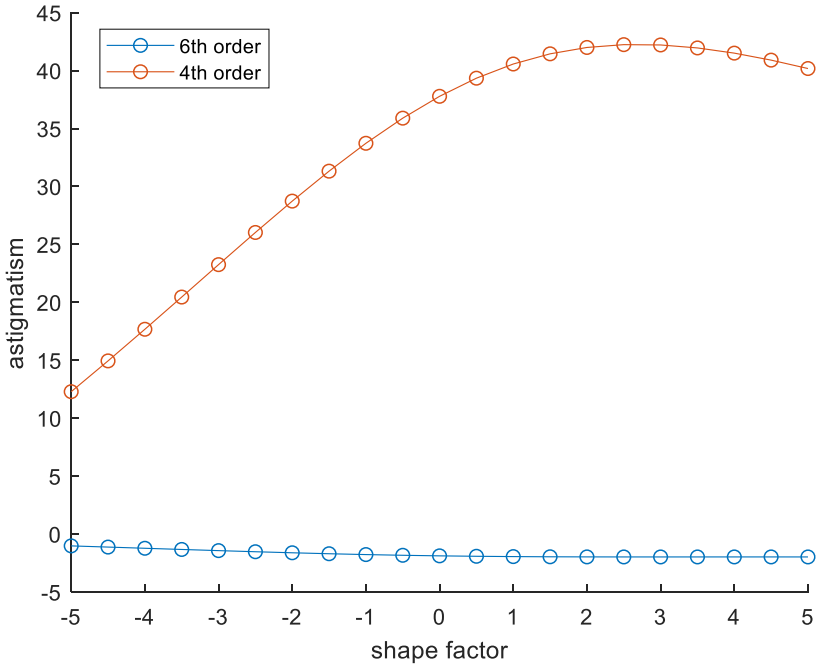

Figure 3.7 Fourth and sixth-order astigmatism aberration for f/4 BK7 thin lens with focal length of 100 mm at 10 degrees as a function of the shape factor.

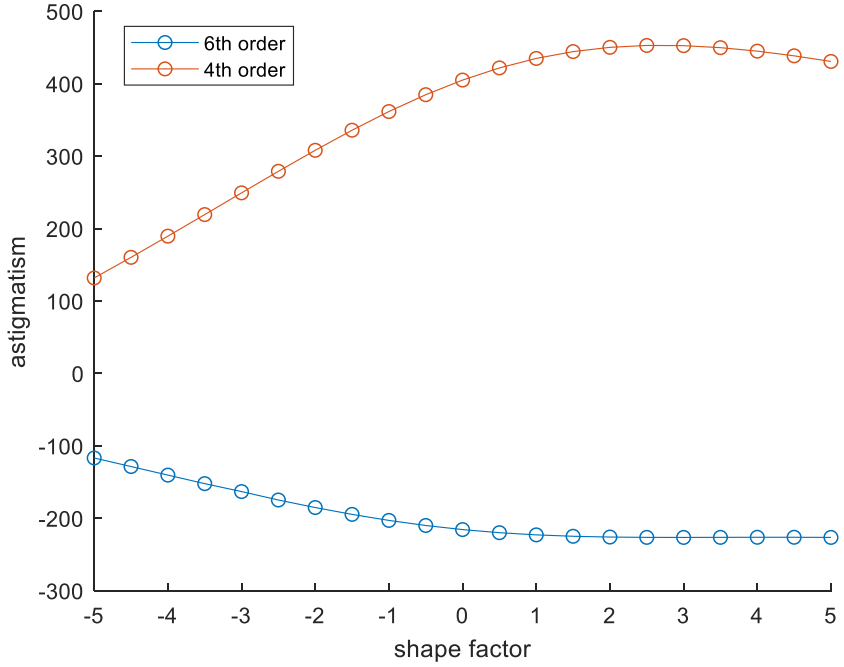

Figure 3.8 Fourth and sixth-order astigmatism aberration for f/4 BK7 thin lens with focal length of 100 mm at 30 degrees as a function of the shape factor.

3.2.4 Field Curvature as a Function of the Shape Factor

Figure 3.9 and Figure 3.10 show the amount of fourth and sixth-order field curvature as a function of the shape factor. The thin lens system in Figure 3.9 is set to have a field of 10 degrees, and the system in Figure 3.10 has a field of 30 degrees. As with coma and astigmatism aberration, measuring the amount of field curvature across different fields is important because field curvature is a function of the field. As such, when the field is 0 degrees, there is no field curvature.

Field curvature's dependence on the field can be seen in the fourth and sixth-order forms below:

$$W_{220}H^2\rho^2,$$
$$W_{420}H^4\rho^2\cos^2(\phi).$$

Field curvature has the same field dependence as that of astigmatism aberration; there is a quadratic dependence on the fourth-order field curvature terms and a quartic dependence on the sixth order field curvature terms.

Now, the fourth-order field curvature coefficient in terms of the structural coefficients is:

$$\begin{aligned} W_{220} &= \frac{1}{2}S_{IV} \\ &= \frac{1}{2}\left(\mathcal{H}^2\Phi\sigma_{IV}\right) \\ &= \frac{1}{2}\mathcal{H}^2\Phi\left(\frac{1}{n'n}\right). \end{aligned} \tag{2.14}$$

Equation (2.14) must be applied to every surface. Again, this equation can be simplified for a thin lens as seen below:

$$W_{220,thin} = \frac{1}{2} \not{K}^2 \Phi \left(\frac{1}{n} \right). \tag{2.15}$$

Equations (2.14) and (2.15) have no dependence on the shape factor. Unfortunately, Figure 3.9 and Figure 3.10 show otherwise.

In Figure 3.9 the fourth-order curve appears to be quadratic. The sixth-order terms are close to zero and negligible when compared to the fourth-order terms. In Figure 3.10 the fourth-order curve appears to have the same quadratic dependence as the curve from Figure 3.9. However, the sixth-order curve is no longer negligible; the sixth-order terms are largely negative.

In comparing Figure 3.9 and Figure 3.10, the fourth-order terms in Figure 3.10 are approximately 10.72 times those of Figure 3.9, and the sixth-order terms of Figure 3.10 are approximately 114.94 times those of Figure 3.9. Interestingly, these are the same multiples as were shown in the graphs for astigmatism in Section 3.2.3. Additionally, notice that the shapes of the curves in Figure 3.9 and Figure 3.10 are the same as Figure 3.7 and Figure 3.8, which are the graphs for astigmatism. These relationships between the field curvature and astigmatism can be attributed to the fact that equation (2.13) and equation (2.15) have the same Lagrange invariant and power terms.

Like the results for astigmatism, Figure 3.9 and Figure 3.10 are incorrect. Equations (2.14) and (2.15) state that there should be no dependence on the shape factor for fourth-order field curvature, and that is what the results should have shown. These incorrect results could potentially stem from the thickness of the lens being too large, or large fields that result in rays no longer being paraxial. Regardless, Figure 3.9 and Figure 3.10 do not obey equations (2.14) and (2.15) and are therefore not correct.

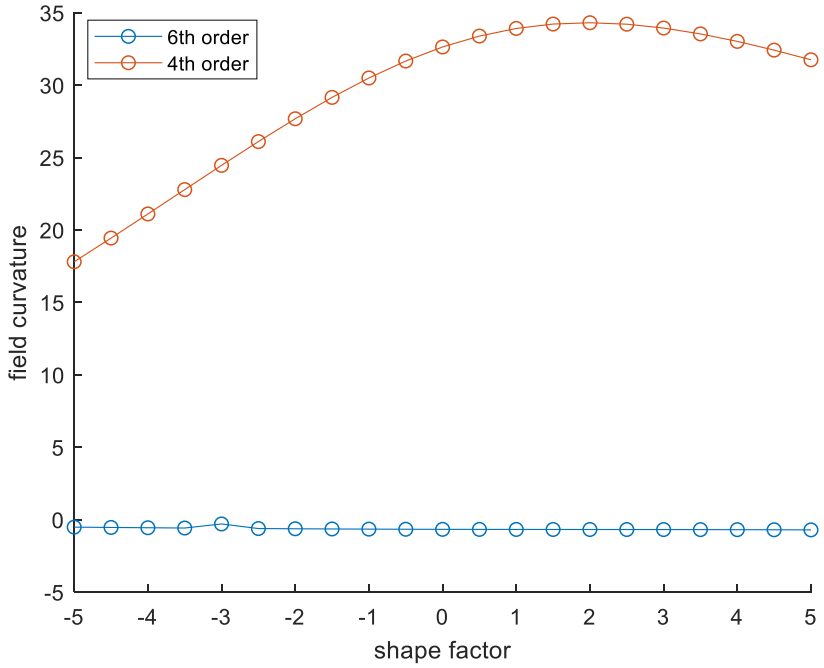

Figure 3.9 Fourth and sixth-order field curvature for f/4 BK7 thin lens with focal length of 100 mm at 10 degrees as a function of the shape factor.

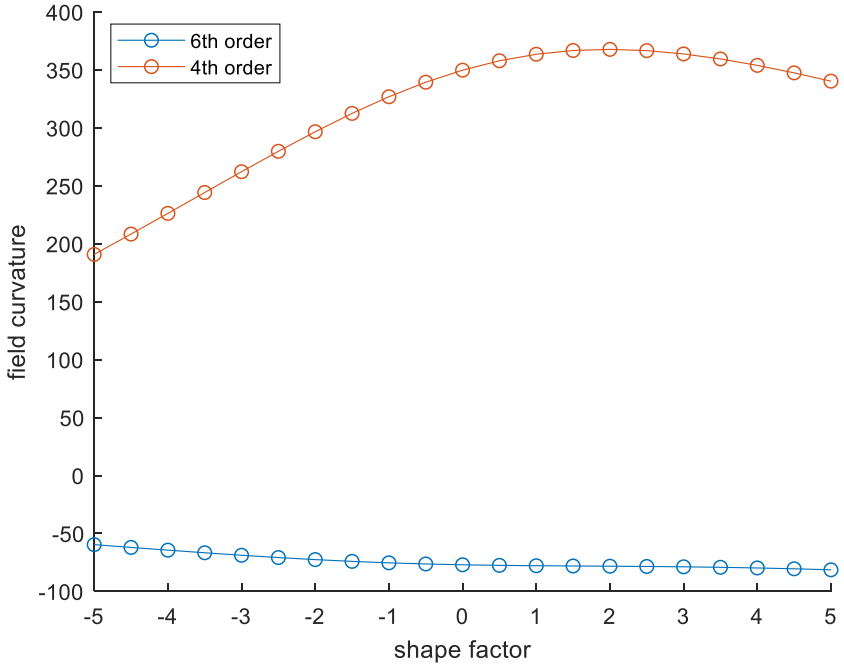

Figure 3.10 Fourth and sixth-order field curvature for f/4 BK7 thin lens with focal length of 100 mm at 30 degrees as a function of the shape factor.

3.2.5 Distortion as a Function of the Shape Factor

Figure 3.11and Figure 3.12 show the amount of fourth and sixth-order distortion as a function of the shape factor. The thin lens system in Figure 3.11 is set to have a field of 10 degrees, and the system in Figure 3.12 has a field of 30 degrees. As with coma, astigmatism, and field curvature, measuring the amount of distortion across different fields is important since distortion is a function of the field. As such, when the field is 0 degrees there is no distortion.

Distortion's dependence on the field can be seen in its algebraic forms written below for the fourth and sixth-orders:

$$W_{311}H^3\rho\cos(\phi),$$
$$W_{511}H^5\rho\cos(\phi).$$

The fourth-order distortion term has a cubic field dependence, and in the sixth-order it has a quintic field dependence.

Now, the fourth-order distortion coefficient in terms of the structural coefficients is:

$$\begin{aligned} W_{311} &= \frac{1}{2}S_V \\ &= \frac{1}{2}\left(\frac{2\mathcal{H}^3\sigma_V}{y_p^2}\right) \\ &= \frac{\mathcal{H}^3}{y_p^2}\left(\frac{n'^2-n^2}{n^2n'^2}\right). \end{aligned} \tag{2.16}$$

This equation needs to applied to every surface in order to get the total contribution. Again, this equation can be simplified for a thin lens. The result is,

$$W_{311,thin} = \frac{\mathcal{K}^3}{y_p^2} \cdot 0$$
$$= 0. \qquad (2.17)$$

In equations (2.16) and (2.17) there is no shape factor dependence, with equation (2.17) going so far as to starting that a thin lens supplies no distortion. Unfortunately, in Figure 3.11 and Figure 3.12 distortion is varying with the shape factor.

In Figure 3.11 the fourth-order distortion curve appears to be negative and linear from $-3 \leq X \leq 4$. The sixth-order distortion curve also appears to be linear, however the slope is much smaller, and the line is positive. The sixth-order distortion also appears to be negligible when compared to the fourth-order distortion.

In Figure 3.12 the fourth and sixth-order curves appear to be more cubic than linear. The amount of distortion measured at a field of 30 degrees is much greater than that measured at a field of 10 degrees. At 30 degrees the sixth-other distortion is no longer negligible and is quite significant.

In comparing Figure 3.11 and Figure 3.12 the general shape of the fourth and sixth-order curves is extremely similar – however, the cubic dependence on the shape factor is made more evident with the increase in field.

It's important to state that the results of Figure 3.11 and Figure 3.12 are incorrect. Equations (2.16) and (2.17) state that there should be no dependence on the shape factor for fourth-order distortion, and that is what the results should have shown. These incorrect results could potentially stem from the thickness of the lens being too large, or large fields that result in

rays no longer being paraxial. Regardless, Figure 3.11 and Figure 3.12 do not obey equations (2.16) and (2.17) and are therefore not correct.

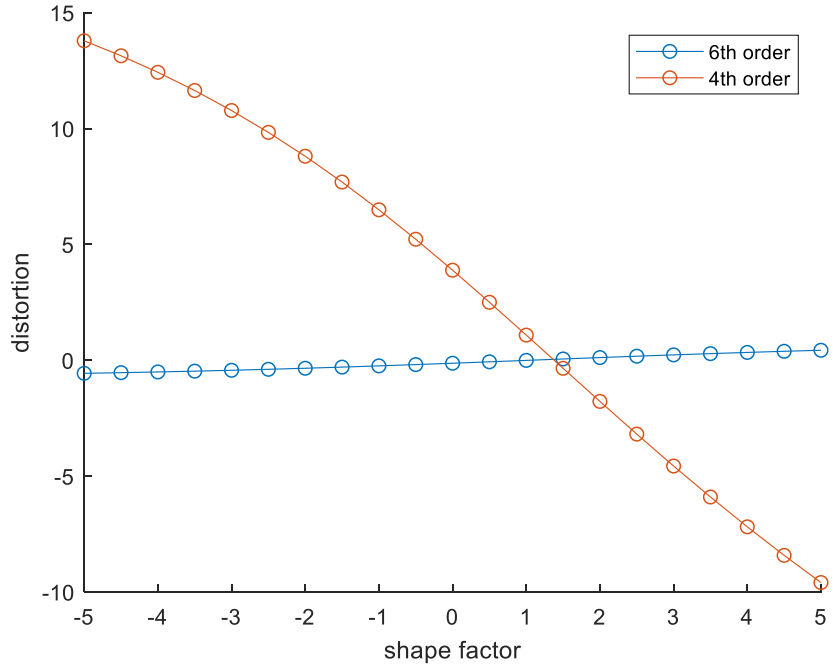

Figure 3.11 Fourth and sixth-order distortion for f/4 BK7 thin lens with focal length of 100 mm at 10 degrees as a function of the shape factor.

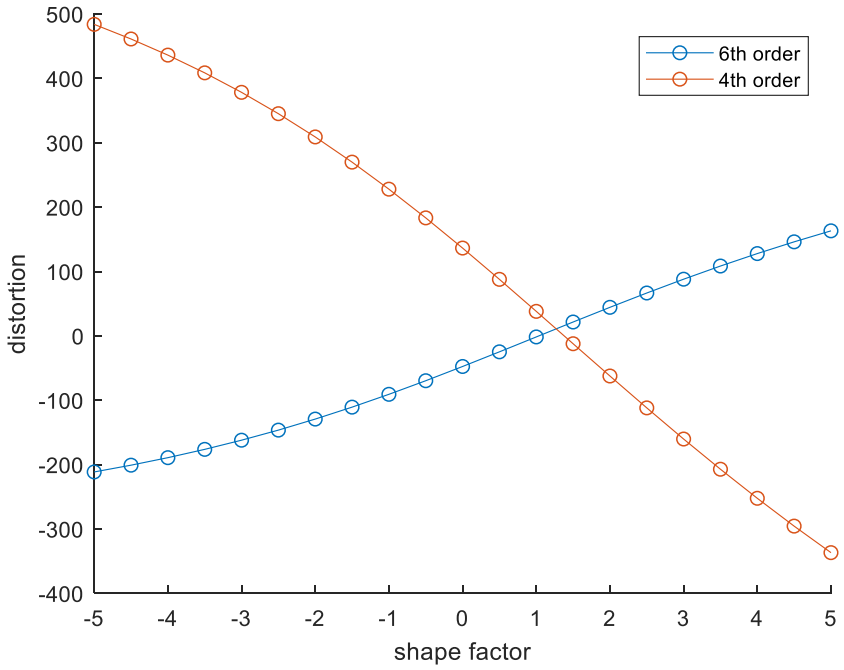

Figure 3.12 Fourth and sixth-order distortion for f/4 BK7 thin lens with focal length of 100 mm at 30 degrees as a function of the shape factor.

3.3 *OpticStudio* Analysis of the Shape Factor

3.3.1 Lens Layouts and Wave Fans

Figure 3.13, Figure 3.15, and Figure 3.17 show the thin lens layouts with shape factors of $X = 0, 2.5$, and $X = 5$, and for fields of 0, 10, and 30 degrees. As the shape factor increases in these figures, the rays appear to spread out further from an ideal point. This is also true as the field of view increases.

Figure 3.14, Figure 3.16, and Figure 3.18 show the wave fans of the respective lenses from Figure 3.13, Figure 3.15, and Figure 3.17. These wave fans include the 0, 10, and 30-degree fields. As the shape factor increases across these lenses, the scale on the wave fan plots increases rapidly. Additionally, as predicted by the thin lens layouts, the 30-degree fields contribute to the most aberration.

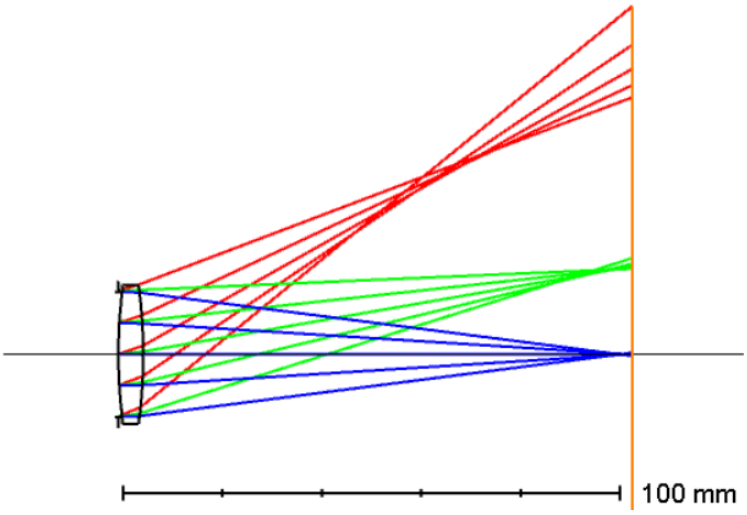

Figure 3.13 Lens layout for f/4 BK7 thin lens with focal length of 100 mm at 0, 10, and 30 degree fields and a shape factor of $X = 0$.

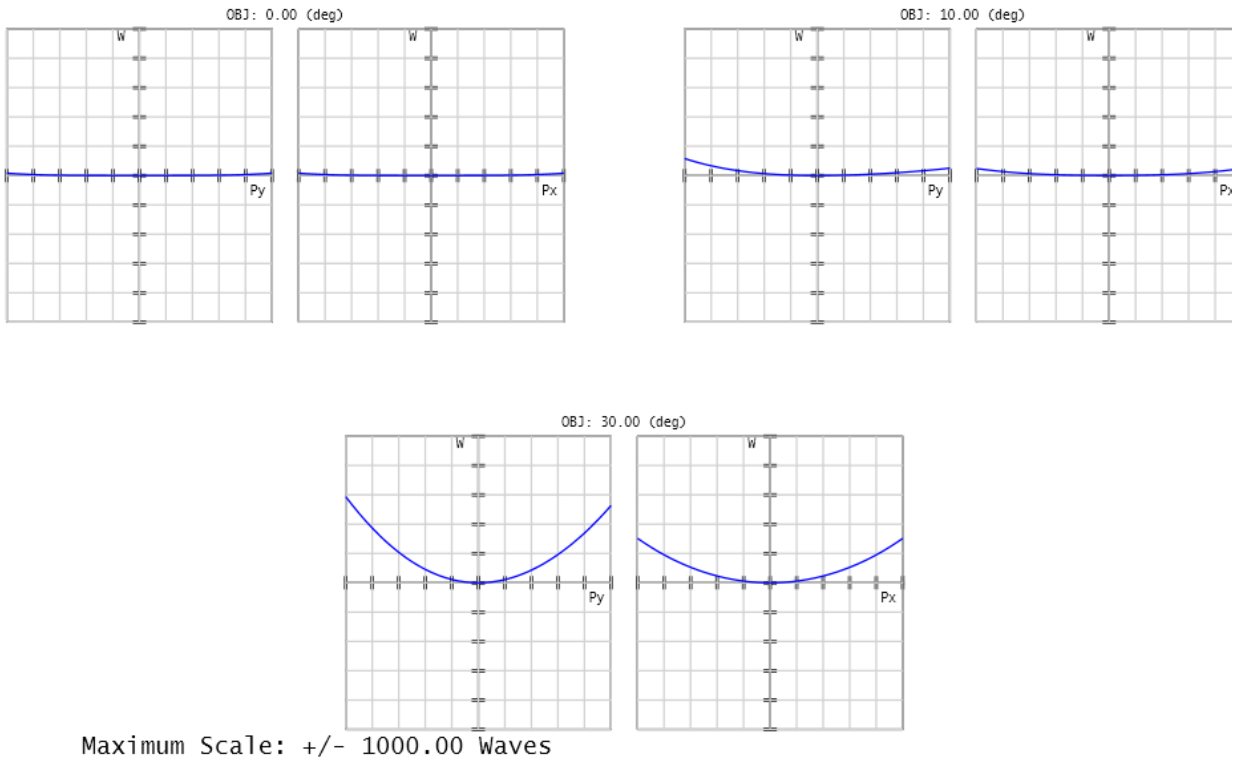

Figure 3.14 Wave fans for f/4 BK7 thin lens with focal length of 100 mm at 0, 10, and 30 degrees fields and a shape factor of $X = 0$.

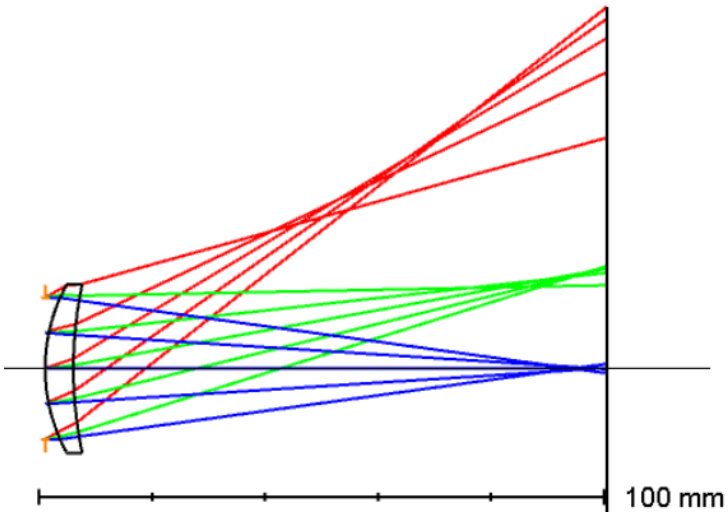

Figure 3.15 Lens layout for f/4 BK7 thin lens with focal length of 100 mm at 0, 10, and 30 degree fields and with a shape factor of $X = 2.5$.

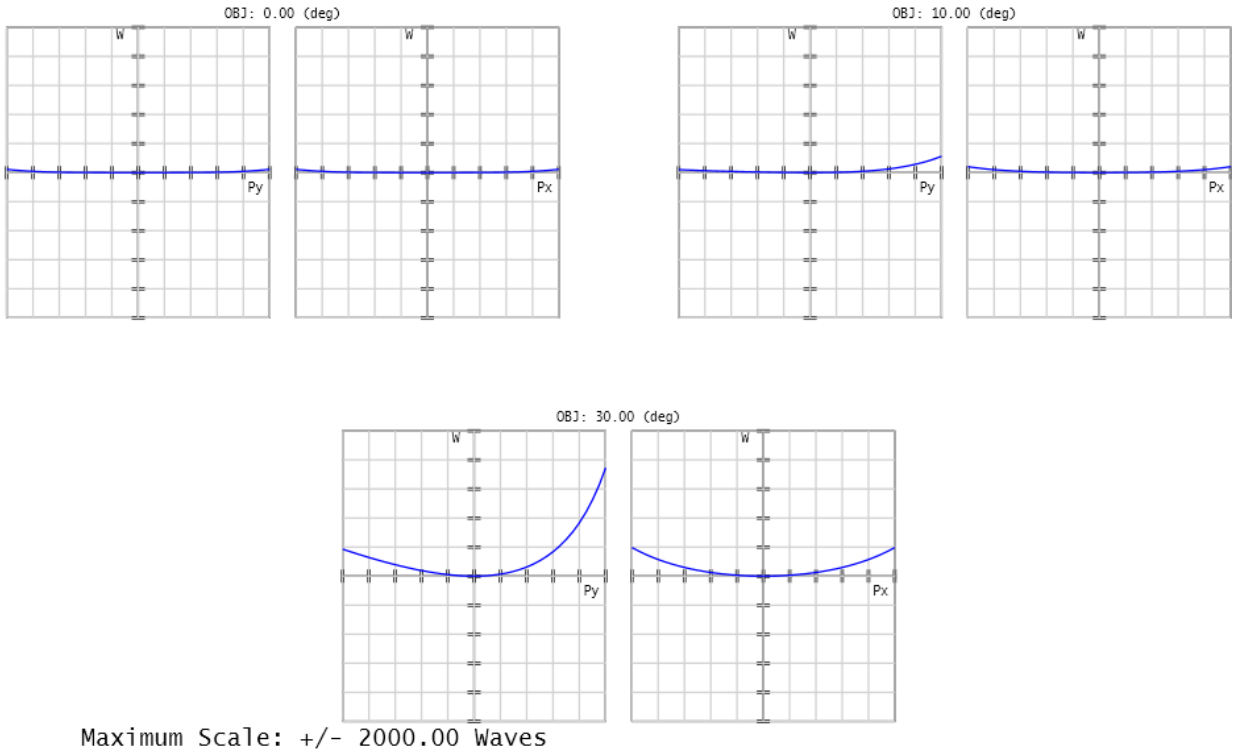

Figure 3.16 Wave fans for f/4 BK7 thin lens with focal length of 100 mm at 0, 10, and 30 degrees fields and a shape factor of $X = 2.5$.

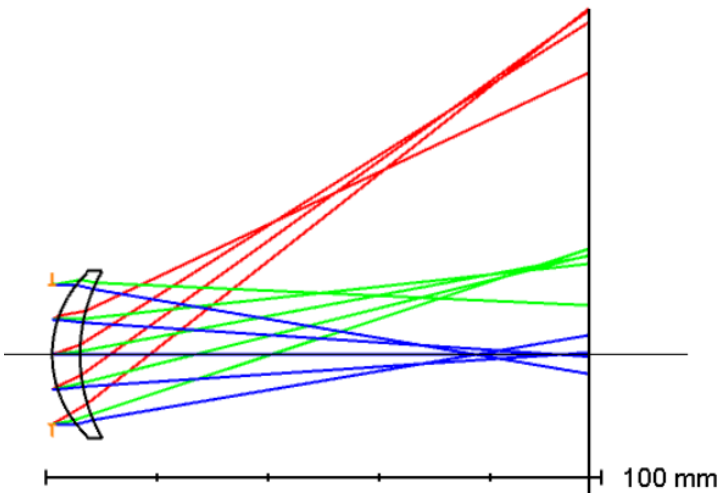

Figure 3.17 Lens layout for f/4 BK7 thin lens with focal length of 100 mm at 0, 10, and 30 degree fields and with a shape factor of $X = 5$.

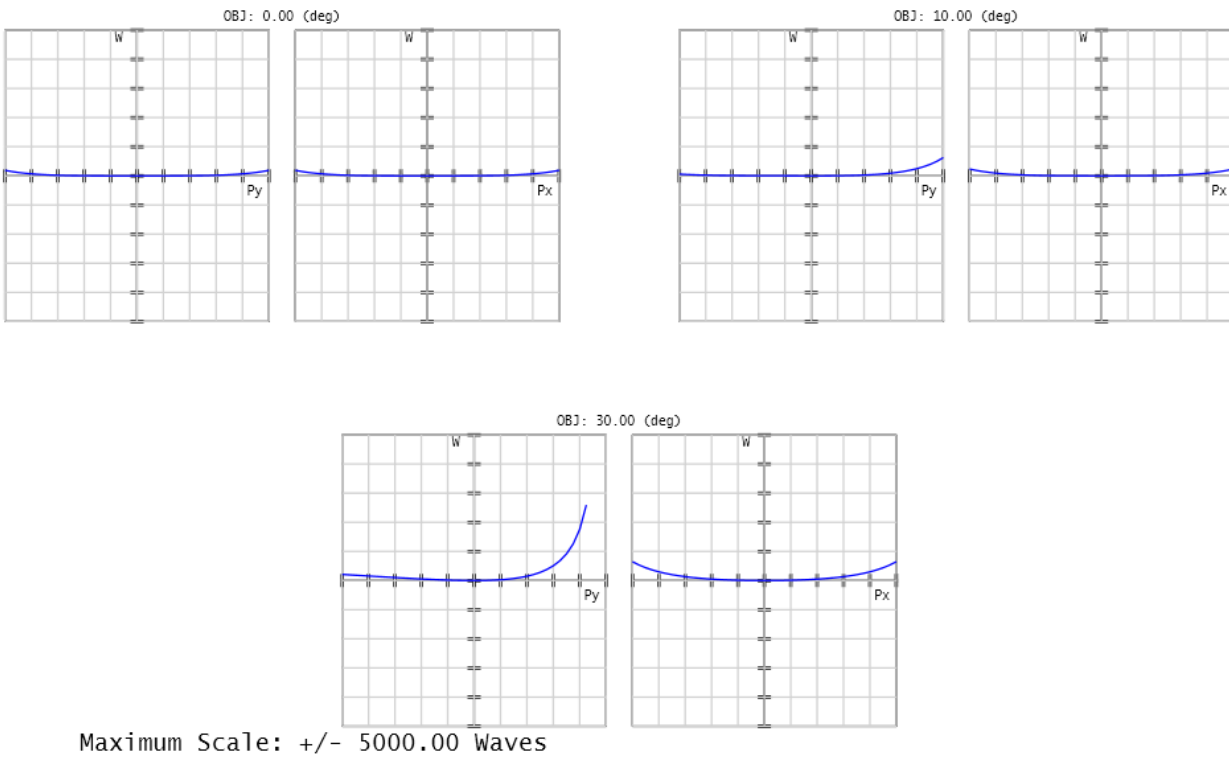

Figure 3.18 Wave fans for f/4 BK7 thin lens with focal length of 100 mm at 0, 10, and 30 degrees fields and a shape factor of $X = 5$.

Figure 3.19 and Figure 3.21 show the thin lens layouts for lens with shape factors of $X = -2.5$, and $X = -5$, and for fields of 0, 10, and 30 degrees. As the magnitude of the shape factor increases in these figures, the rays appear to spread out further from an ideal point. This is also true as the field of view increases.

Figure 3.20 and Figure 3.22 show the wave fans of the respective lenses from Figure 3.19 and Figure 3.21. These wave fans include the 0, 10, and 30-degree fields. As the magnitude of the shape factor increases across these lenses, the scale on the wave fans does not change, however the shape of the wave fans changes.

As expected, across all the wave fans, at 0 degrees there is only spherical aberration. Additionally, as was explained in Section 3.2.1 and as can be seen in the thin lens layouts, at large fields the rays travel far from the optical axis. This interferes with the definition of paraxial rays, where paraxial rays are those close to the optical axis. Many of the approximations made in aberration theory become inaccurate and fail to completely define the scope of all rays.

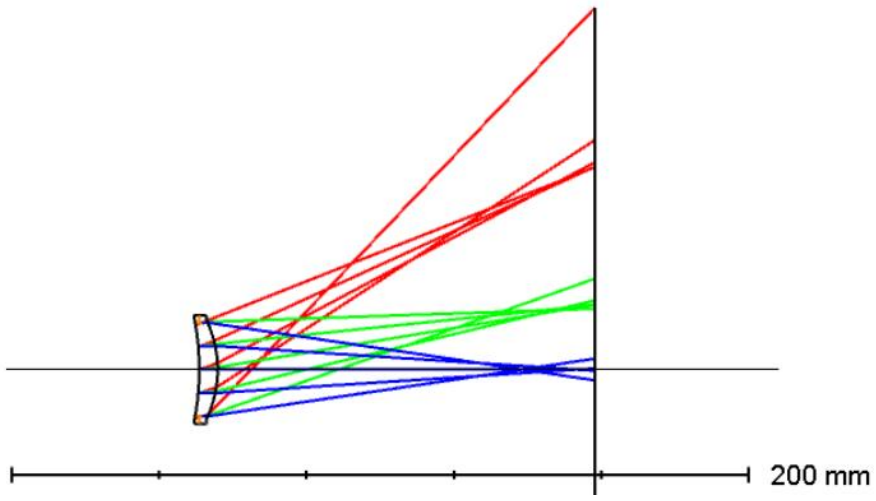

Figure 3.19 Lens layout for f/4 BK7 thin lens with focal length of 100 mm at 0, 10, and 30 degree fields and with a shape factor of $X = -2.5$.

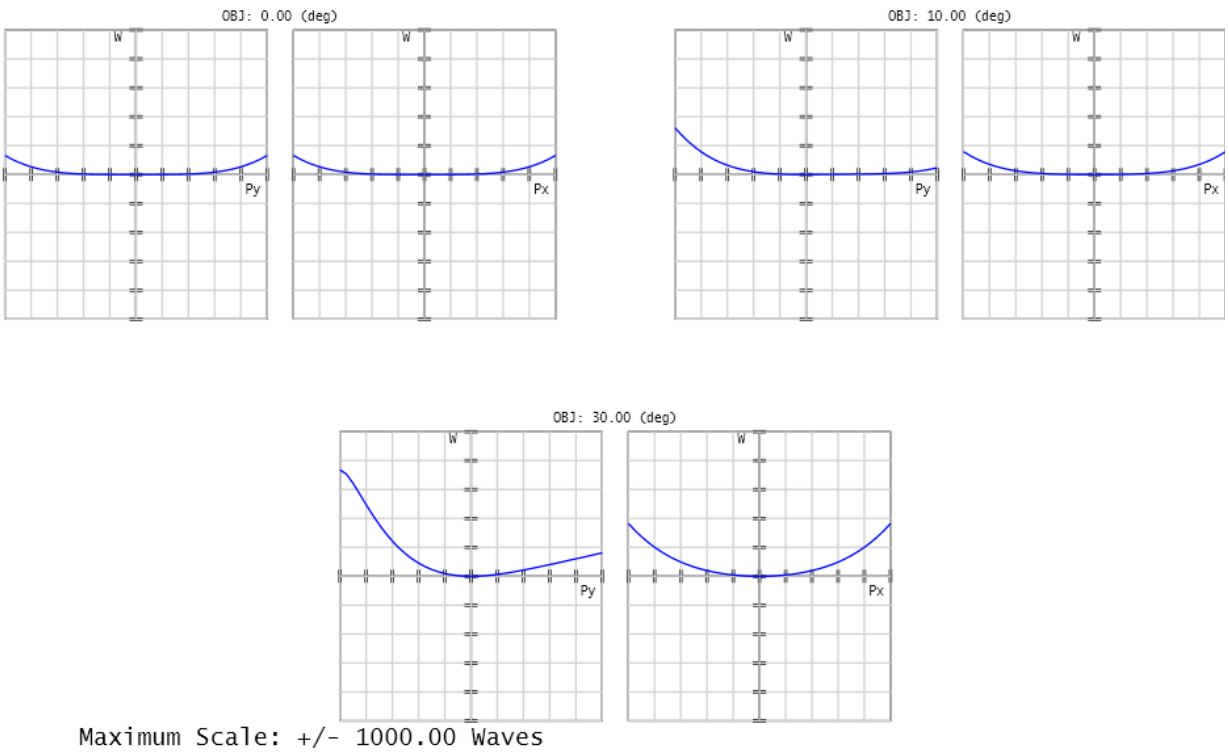

Figure 3.20 Wave fans for f/4 BK7 thin lens with focal length of 100 mm at 0, 10, and 30 degrees fields and a shape factor of $X = -2.5$.

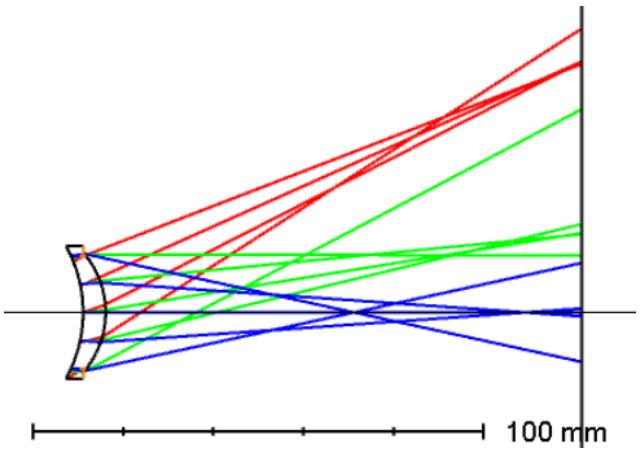

Figure 3.21 Lens layout for f/4 BK7 thin lens with focal length of 100 mm at 0, 10, and 30 degree fields and with a shape factor of $X = -5$.

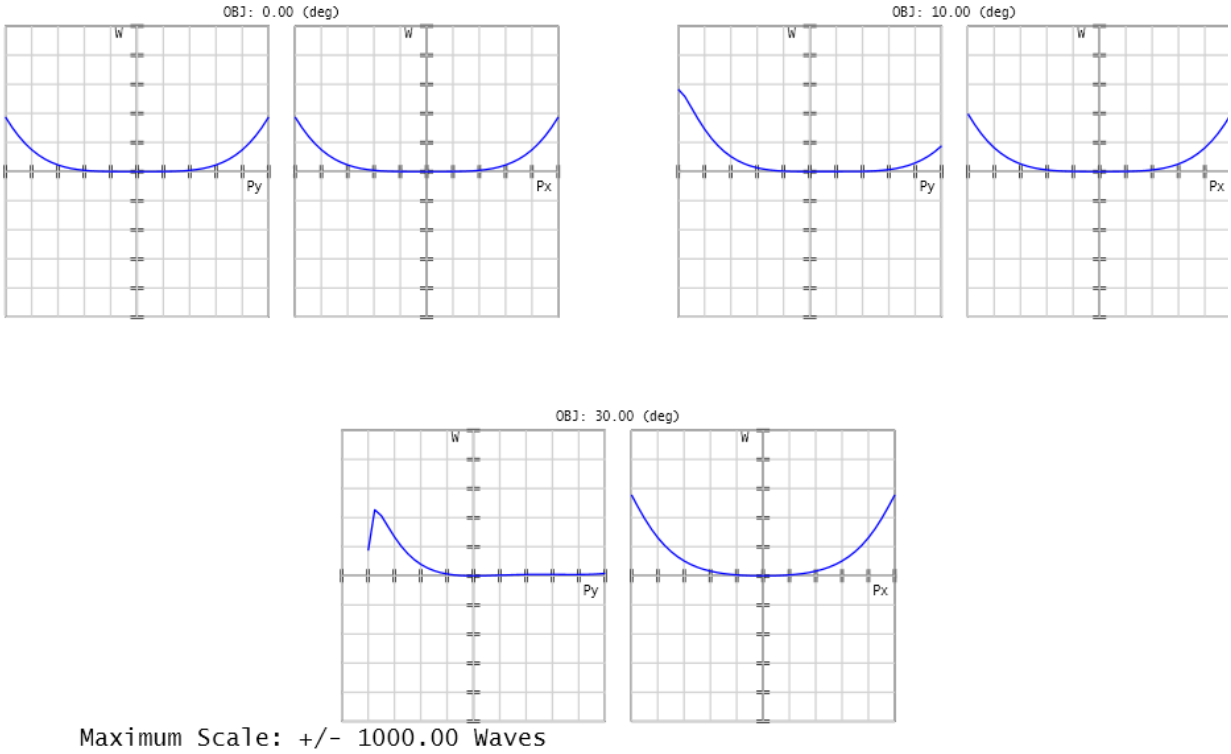

Figure 3.22 Wave fans for f/4 BK7 thin lens with focal length of 100 mm at 0, 10, and 30 degrees fields and a shape factor of $X = -5$.

Chapter 4

This chapter focuses on the fourth and sixth-order monochromatic aberrations as functions of the conjugate factor.

The first section describes the f/4 BK7 thin lens used in this report. This section also describes the methods used to control and change the conjugate factor. The fourth and sixth-order monochromatic aberrations are calculated by the methods outlined in Section 3.1. Again, the lens design and aberration calculation are all done within *OpticStudio*, as well as the conjugate factor manipulation.

In the second section, plots of the fourth and sixth-order aberrations as functions of the conjugate factor are shown. These plots are analyzed with regards to the object heights chosen, and they are compared against Seidel aberration equations written in terms of structural coefficients. Additionally, the fourth and sixth-order aberrations are compared with each other.

In the last section, certain conjugate factors have been chosen, and their respective thin lens layouts and wave fans have been plotted using *OpticStudio*. The reason for this is to understand the deviation of the rays from the nominal image plane by comparing the wave fans and the lens layouts, as was done in Section 3.3.

4.1 Introduction to the Thin Lens System for a Changing Conjugate Factor

4.1.1 Description of the System and its Dependence on the Conjugate Factor

This chapter uses the same initial thin lens system with $X = 0$ that was described in Section 3.1.1. Again, it's important to note that while the thin lens is considered "thin" because its thickness is small compared to its focal length, when designed in *OpticStudio* the lens is not thin. Its prescription is rewritten below:

- Stop at the lens.
- Lens made of BK7 with a thickness of 5 mm.
- f/4 lens with an effective focal length of 100 mm.
- Wavelength of 0.58 μm and fields of view of 0, 10, and 30 degrees.

In Chapter 3 the lens system had an object placed at infinity so that the rays coming in would be parallel to the optical axis. However, in this chapter an object is placed at a known distance from the lens. This distance is selected with the lens design in mind to achieve a certain magnification and subsequent conjugate factor.

From Section 2.1.2, the equation for the conjugate factor was given by,

$$Y = \frac{\omega' + \omega}{\omega' - \omega} = \frac{n'u' + nu}{n'u' - nu} \tag{2.3}$$

which was then simplified for a thin lens in the following equation,

$$Y = \frac{m+1}{m-1}. \tag{2.6}$$

Equation (2.6) can be rearranged so that,

$$m = \frac{-1-Y}{1-Y}. \tag{2.18}$$

So, by specifying a conjugate factor in equation (2.18) a magnification is calculated.

In Figure 4.1 the lens layout is shown; the object height is defined as 10 mm which allows for an object distance other than infinity to be set. Note that the distance from the object to the lens is set as variable. Additionally, the lens is biconvex with the stop at the lens. The lens is 5 mm thick and can be considered thin since this thickness is significantly less than the effective focal length. Figure 4.3 displays the cross section of the lens description from Figure 4.1.

	Surface Type		Coı	Radius	Thickness		Material	Coı	Clear Semi-Di	
0	OBJECT	Standard		Infinity	165.007	V			10.000	
1	STOP	Standard		Infinity	0.000				12.500	U
2		Standard		102.844	5.000		BK7		12.500	P
3		Standard		-102.844	248.340	M			12.764	
4	IMAGE	Standard		Infinity	-				15.668	

Figure 4.1 Prescription for f/4 BK7 thin lens system with stop at the lens and a focal length of 100 mm. The object height is 10 mm, and the distance from the object to the lens results in a magnification of -1.5.

	Type		Wave					Target	Weight	Value	% Contrib
1	PMAG		1					-1.500	20.000	-1.500	100.000
2	BLNK										
3	EFFL		1					100.000	0.000	100.000	0.000

Figure 4.2 Merit function editor for f/4 BK7 thin lens system with stop at the lens and a focal length of 100 mm.

In using the technique from equation (2.18), a value of $Y = -0.2$ was selected for the design shown in Figure 4.1 and Figure 4.3. In plugging $Y = -0.2$ into equation (2.18), the result is $m = -1.5$. Figure 4.2 shows the Merit Function editor in *OpticStudio*. The first row, "PMAG" gives the paraxial magnification of the system. By setting a target of -1.5 and optimizing, the distance from the object to the lens is changed to fit this magnification value. So, the value of the conjugate factor can be controlled by optimizing the lens system to fit a certain magnification.

For simplicity, the conjugate factors used result in only real images, not virtual. So, the conjugate factors have been restricted to values $-0.8 \le Y \le 0.8$.

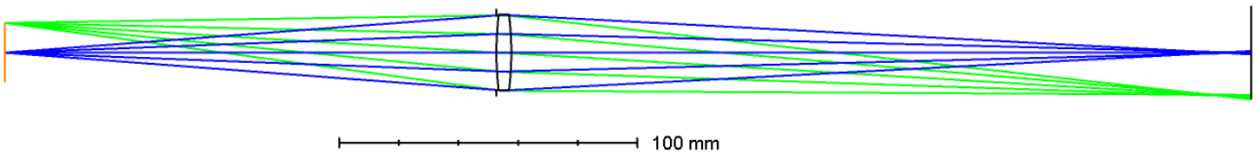

Figure 4.3 Lens layout for f/4 BK7 thin lens system with stop at the lens and a focal length of 100 mm. The object height is 10 mm and the distance from the object to the lens results in a magnification of -1.5.

4.2 Aberrations as Functions of the Conjugate Factor

4.2.1 Spherical Aberration as a Function of the Conjugate Factor

Figure 4.4 shows the fourth and sixth-order spherical aberration for the lens system defined in Section 3.1.1. The object height used is 10 mm. It's important to realize that changing the object height will have no effect on the fourth and sixth-order spherical aberration, for the same reasons that spherical aberration remains the same throughout the field.

Looking again at the equations defined in Section 3.2, for a system of surfaces the fourth-order spherical aberration is given by,

$$W_{040} = \frac{1}{32} y_p^2 \Phi^3 \left[-\frac{1}{2}\left(\frac{n'+n}{n'-n} - Y \right)^2 \left(\frac{n'^2 - n^2}{n^2 n'^2} \cdot Y - \frac{n'^2 + n^2}{n^2 n'^2} \right) \right]. \tag{2.8}$$

Equation (2.8) must be applied to every surface. The equation for fourth-order spherical aberration of a thin lens is given by,

$$W_{040,thin} = \frac{1}{32} y_p^4 \Phi^3 \left(AX^2 - BXY + CY^2 + D \right), \tag{2.9}$$

In equation (2.8) there a linear and quadratic dependence on the conjugate factor. In equation (2.9) the dependence on the conjugate factor is the same and can be seen more clearly.

The fourth-order curve in Figure 4.4 appears to have the quadratic dependence on the conjugate factor from equations (2.8) and (2.9). The sixth-order spherical aberration curve hovers near zero despite the changing conjugate factor. As such, the sixth-order spherical aberration is negligible, especially when compared to the fourth-order spherical aberration.

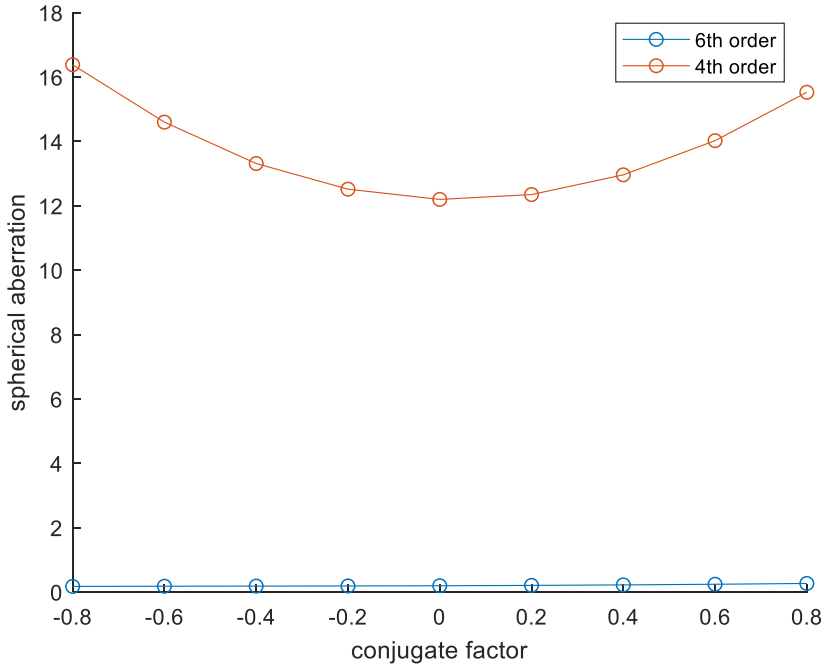

Figure 4.4 Fourth and sixth-order spherical aberration for f/4 BK7 thin lens with focal length of 100 mm and object height of 10 mm as a function of the conjugate factor.

4.2.2 Coma Aberration as a Function of the Conjugate Factor

Figure 4.5 and Figure 4.6 show the fourth and sixth-order coma aberration for the lens system defined in Section 4.1.1. The object heights used are 10 mm and 30 mm respectively. For a system of surfaces, the equation defined in Section 3.2.1 for the fourth-order coma aberration is given by,

$$W_{131} = \frac{1}{4}\mathcal{H}y_p^2\Phi^2\left[-\frac{1}{2}\left(\frac{n'+n}{n'-n}-Y\right)\left(\frac{n'^2-n^2}{n^2n'^2}\cdot Y-\frac{n'^2+n^2}{n^2n'^2}\right)\right]. \tag{2.10}$$

Equation (2.10) must be applied to every surface. The thin lens version of this equation is given by,

$$W_{131,thin} = \frac{1}{4}\mathcal{H}y_p^2\Phi^2\left(EX-FY\right). \tag{2.11}$$

Equation (2.10) has a linear and quadratic conjugate factor term, where the quadratic term appears when the equation is expanded. However, equation (2.11) contains just a linear dependence on the conjugate factor.

In Figure 4.5 the fourth-order coma aberration curve is not linear; the fourth-order coma aberration appears to be quadratic and is therefore following equation (2.10)'s dependence on the conjugate factor. The sixth-order coma aberration curve appears linear—the amount of coma is so close to zero that it is negligible when compared to the fourth-order coma values.

In Figure 4.6 the fourth-order curves are also quadratic. This curve appears to be the same shape as the fourth-order coma aberration curve from Figure 4.5. The sixth-order coma

aberration values are larger than those of Figure 4.5 and it appears to decrease towards zero as the conjugate factor increases. Even with the larger values, this sixth-order coma aberration curve is not significant when compared to the values of the fourth-order coma aberration curve.

There is a relationship between the values in Figure 4.5 and Figure 4.6. The fourth-order coma aberration values in Figure 4.6 are approximately 3 times the fourth-order coma aberration values in Figure 4.5. Additionally, the sixth-order coma aberration values in Figure 4.6 are approximately 26 times the sixth-order coma aberration values from Figure 4.5.

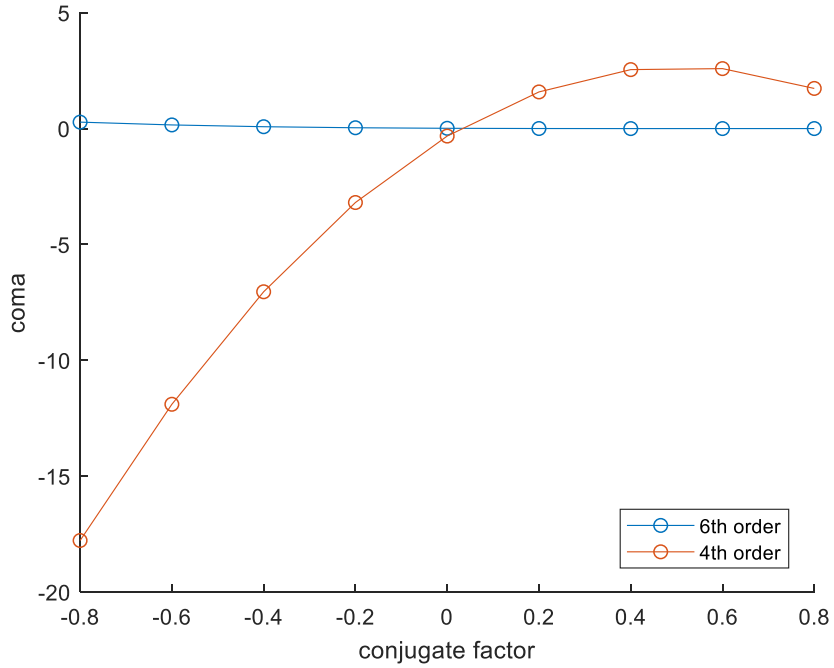

Figure 4.5 Fourth and sixth-order coma aberration for f/4 BK7 thin lens with focal length of 100 mm and object height of 10 mm as a function of the conjugate factor.

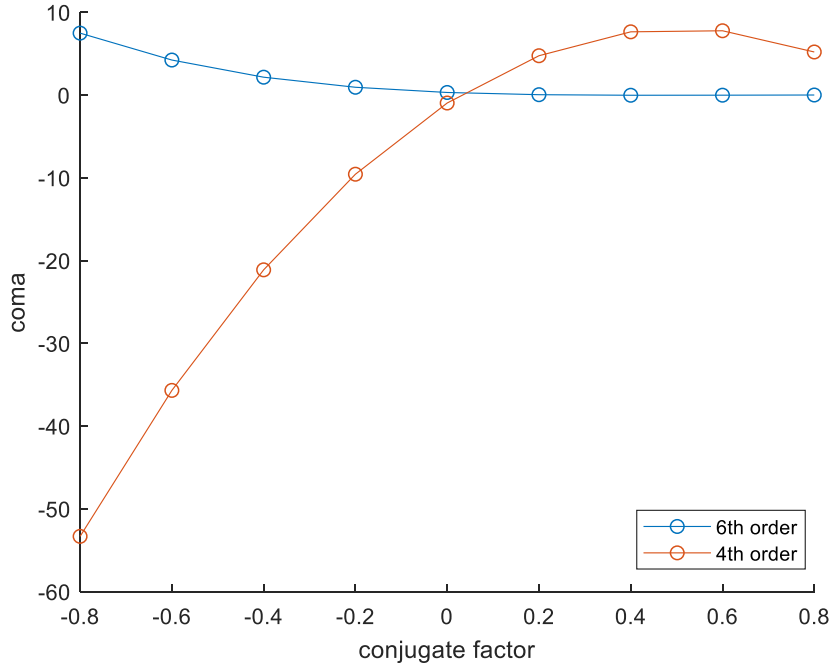

Figure 4.6 Fourth and sixth-order coma aberration for f/4 BK7 thin lens with focal length of 100 mm and object height of 30 mm as a function of the conjugate factor.

4.2.3 Astigmatism as a Function of the Conjugate Factor

Figure 4.7 and Figure 4.8 show the fourth and sixth-order astigmatism aberration for the lens system defined in Section 4.1.1. The object heights used are 10 mm and 30 mm respectively.

For a system of surfaces, at the equation defined in Section 3.2.3 for the fourth-order astigmatism aberration is given by,

$$W_{222} = \frac{1}{2}\not{K}^2\Phi\left[-\frac{1}{2}\left(\frac{n'^2 - n^2}{n^2 n'^2}\cdot Y - \frac{n'^2 + n^2}{n^2}n'^2\right)\right] \tag{2.12}$$

and the thin lens equation for fourth-order astigmatism is given by,

$$W_{222,thin} = \frac{1}{2}\not{K}^2\Phi. \tag{2.13}$$

Equation (2.12) has a linear dependence on the conjugate factor, while the dependence on the conjugate factor disappears for the thin lens equation (2.13).

In Figure 4.7 the fourth-order astigmatism values decrease towards zero as the conjugate factor increases. The sixth-order astigmatism curve appears to hover around zero, however there is a slight increase in astigmatism as the conjugate factor increases. The sixth-order astigmatism is quite small and is negligible when compared to the fourth-order astigmatism.

In Figure 4.8 the same decrease in the fourth-order astigmatism occurs as that from Figure 4.7, but with much higher fourth-order astigmatism. The sixth-order astigmatism curve now approaches zero from negative sixth-order astigmatism values. The magnitude of the sixth-order astigmatism is still a small percentage of the magnitude of the fourth-order astigmatism.

The astigmatism curves in Figure 4.7 and Figure 4.8 appear to have the same shape. In fact, the fourth-order values in Figure 4.8 are approximately 9 times larger than those Figure 4.7, and the sixth-order values in Figure 4.8 are approximately 62 times larger than those in Figure 4.7.

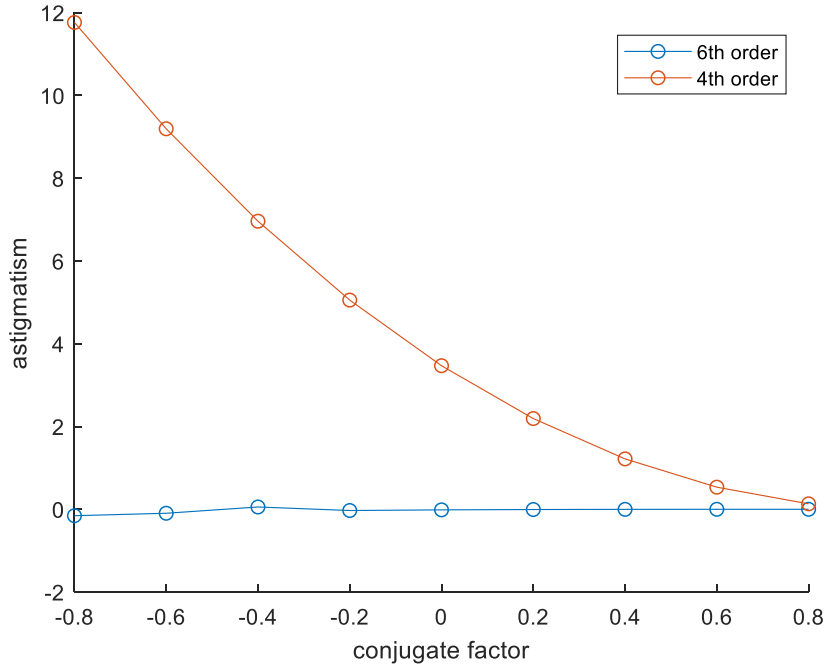

Figure 4.7 Fourth and sixth-order astigmatism for f/4 BK7 thin lens with focal length of 100 mm and object height of 10 mm as a function of the conjugate factor.

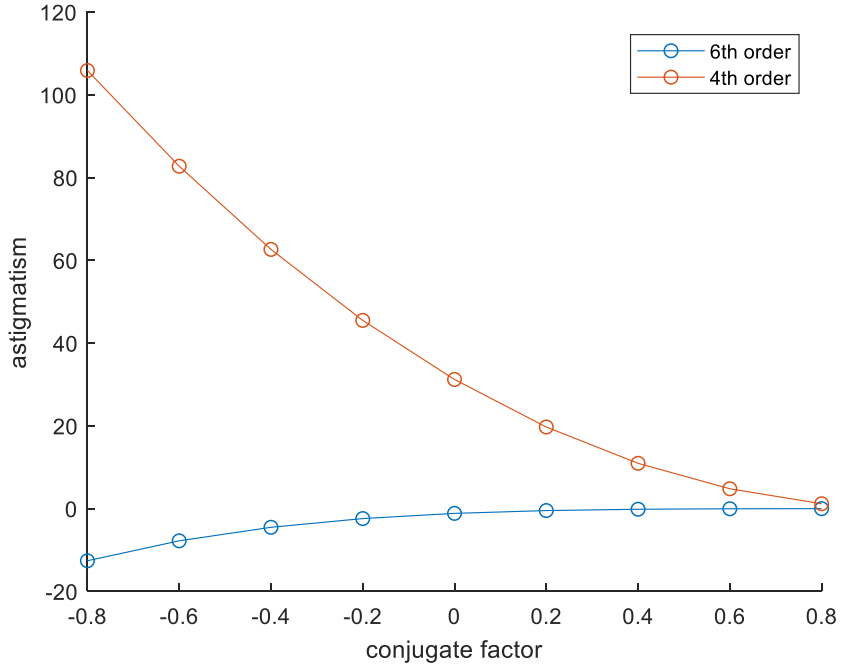

Figure 4.8 Fourth and sixth-order astigmatism for f/4 BK7 thin lens with focal length of 100 mm and object height of 30 mm as a function of the conjugate factor.

4.2.4 Field Curvature as a Function of the Conjugate Factor

Figure 4.9 and Figure 4.10 show the fourth and sixth-order field curvature for the lens system defined in Section 4.1.1. The object heights used are 10 mm and 30 mm respectively.

For a system of surfaces, the equation defined in Section 3.2.4 for the fourth-order field curvature is given by,

$$W_{220} = \frac{1}{2}\mathcal{H}^2\Phi\left(\frac{1}{n'n}\right), \tag{2.14}$$

where equation (2.14) must be applied to every surface. The fourth-order thin lens field curvature equation is given by,

$$W_{220,thin} = \frac{1}{2}\mathcal{H}^2\Phi\left(\frac{1}{n}\right). \tag{2.15}$$

Equations (2.14) and (2.15) have no visible dependence on the conjugate factor. Unfortunately, Figure 4.9 and Figure 4.10 demonstrate otherwise.

The fourth-order field curvature curve in Figure 4.9 appears to be decreasing, approaching zero as the conjugate factor increases. The sixth-order field curvature curve hovers around zero but appears to have a slight increase as the conjugate factor increases. However, the sixth-order field curvature is negligible when compared to the fourth-order field curvature.

The fourth-order field curvature curve in Figure 4.10 appear to have the same decrease as the curve from Figure 4.9, however the fourth-order field curvature is much higher in Figure 4.10. The sixth-order field curvature curve also approaches zero, but from negative field

curvature values. Additionally, the sixth-order field curvature is small when compared to the fourth-order field curvature.

Figure 4.9 and Figure 4.10 have the following relationship: the fourth and sixth-order field curvature curves of Figure 4.10 are 9 and 81 times the fourth and sixth-order field curvature plots of Figure 4.9 respectively.

It's crucial to state that the results of Figure 4.9 and Figure 4.10 are incorrect. Equations (2.14) and (2.15) state that there should be no dependence on the conjugate factor for fourth-order field curvature, and that is what the results should have shown. These incorrect results could potentially stem from the thickness of the lens being too large, or large fields that result in rays no longer being paraxial. Regardless, Figure 4.9 and Figure 4.10 do not obey equations (2.14) and (2.15) and are therefore not correct.

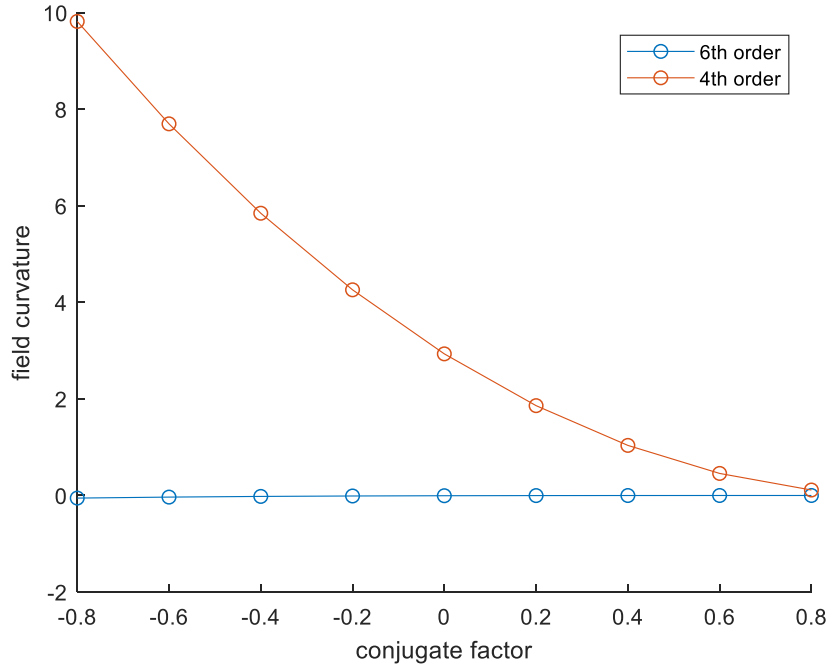

Figure 4.9 Fourth and sixth-order field curvature for f/4 BK7 thin lens with focal length of 100 mm and object height of 10 mm as a function of the conjugate factor.

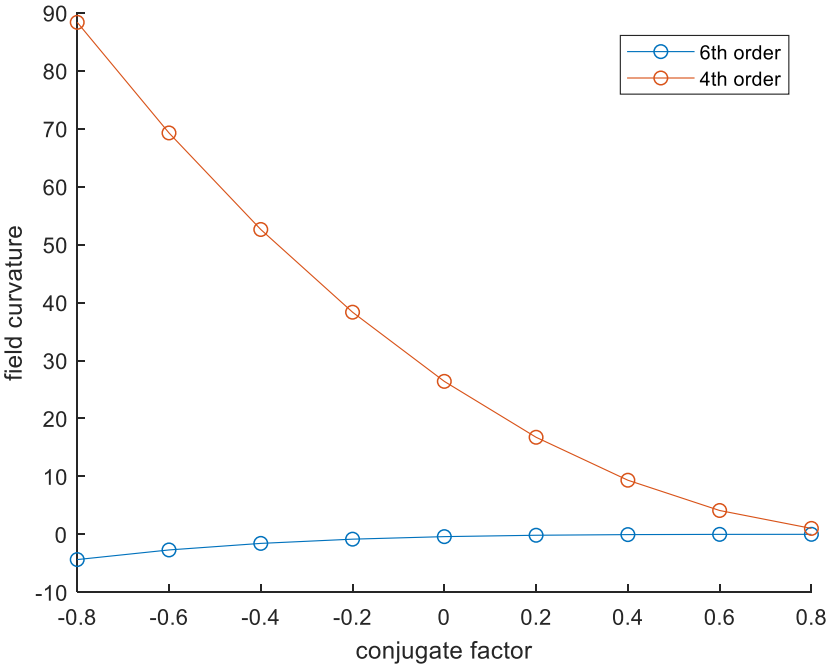

Figure 4.10 Fourth and sixth-order field curvature for f/4 BK7 thin lens with focal length of 100 mm and object height of 30 mm as a function of the conjugate factor

4.2.5 Distortion as a Function of the Conjugate Factor

Figure 4.11 and Figure 4.12 show the fourth and sixth-order distortion for the lens system defined in Section 4.1.1. The object heights used are 10 mm and 30 mm respectively.

For a system of surfaces, the equation defined in Section 3.2.5 for the fourth-order distortion is given by,

$$W_{311} = \frac{\mathcal{H}^3}{y_p^2}\left(\frac{n'^2 - n^2}{n^2 n'^2}\right), \tag{2.16}$$

which must be applied to each surface. The thin lens fourth-order distortion equation is given by,

$$W_{311,thin} = 0. \tag{2.17}$$

Equations (2.16) and (2.17) have no dependence on the conjugate factor. Figure 4.11 and Figure 4.12 show a small dependence, unfortunately.

In Figure 4.11 the fourth-order distortion curve appears to quadratically approach zero from negative distortion values, as the conjugate factor increases. The sixth-order distortion curve appears to approach small negative distortion values from zero, as the conjugate factor increases. Sixth-order distortion is negligible when compared to fourth-order distortion, however the highest value of fourth-order distortion is still relatively small at around -0.45.

In Figure 4.12 the fourth-order distortion curve again approaches zero from negative distortion values as the conjugate factor increases. The sixth-order distortion curve also approaches zero from positive distortion values, and sixth-order distortion is again small when compared to fourth-order distortion.

It's important to note that the results of Figure 4.11 and Figure 4.12 are incorrect. Equations (2.16) and (2.17) state that there should be no dependence on the conjugate factor for fourth-order distortion, and that is what the results should have shown. In fact, the fourth-order distortion curve should just be zero. These incorrect results could potentially stem from the thickness of the lens being too large, or large fields that result in rays no longer being paraxial. Regardless, Figure 4.10 and Figure 4.12 do not obey equations (2.16) and (2.17) and are therefore not correct.

By equation (2.17), Figure 4.20 and Figure 4.21 should have no distortion for the fourth-order curve. Luckily, this result can be shown by setting the setting to just be a simple paraxial lens with no thickness. Table 4.1 shows the design of the lens, and Figure 4.13 shows the lens layout. With this paraxial lens of no thickness, the results predicted in equation (2.17) are achieved.

Figure 4.14 and Figure 4.15 are the plots for the paraxial thin lens with no thickness. As can be seen in these plots, the fourth-order distortion is *actually* zero. Sixth-order distortion is behaving as expected, with the sixth-order distortion curves matching each other at different object heights.

So, equation (2.17) is correct after all for thin lenses. Interestingly, adding any thickness at all to this paraxial lens immediately caused fourth-order distortion in the paraxial system.

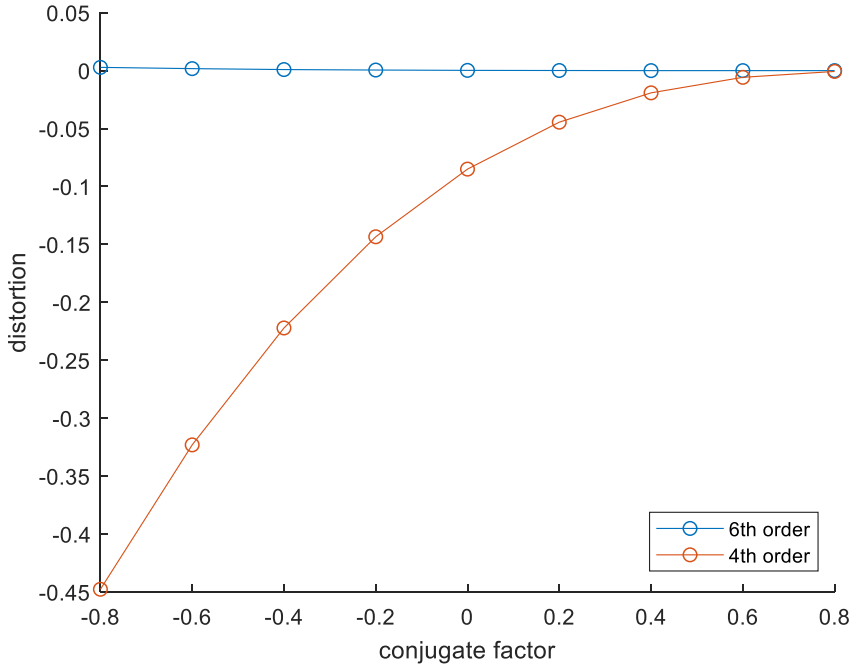

Figure 4.11 Fourth and sixth-order distortion for f/4 BK7 thin lens with focal length of 100 mm and object height of 10 mm as a function of the conjugate factor.

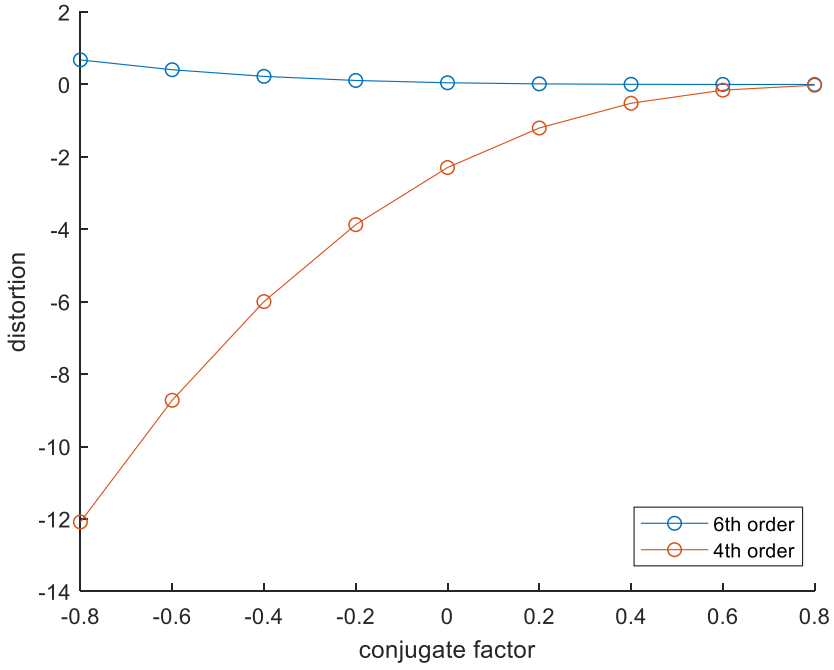

Figure 4.12 Fourth and sixth-order distortion for f/4 BK7 thin lens with focal length of 100 mm and object height of 30 mm as a function of the conjugate factor.

	Surface Type		Coı	Radius	Thickness		Materia	Coı	Clear Semi-Dia		Chi	Me	Coı	TCI	Par 1(unuse	Par 2(unused)
0	OBJEC	Standard		Infinity	200.000	V			10.000		0.0..	10..	0.0..	0.0..		
1	STOP	Standard		Infinity	0.000				12.500	U	0.0..	12..	0.0..	0.0..		
2	(aper)	Paraxial			0.000		BK7		12.500	U					100.000	1
3		Standard		Infinity	200.000	M			12.500		0.0..	12..	0.0..	0.0..		
4	IMAGE	Standard		Infinity	-				10.081		0.0..	10..	0.0..	0.0..		

Table 4.1 Prescription for f/4 BK7 thin lens system with stop at the lens and a focal length of 100 mm. The object height is 10 mm, and the distance from the object to the lens results in a magnification of -1.0. This system uses a paraxial surface type as the lens.

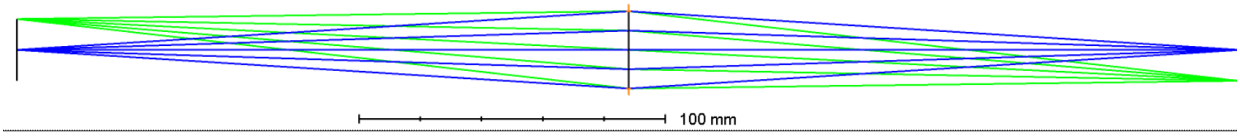

Figure 4.13 Lens layout for f/4 BK7 thin lens system with stop at the lens and a focal length of 100 mm. The object height is 10 mm and the distance from the object to the lens results in a magnification of -1.0. The lens in this system is paraxial.

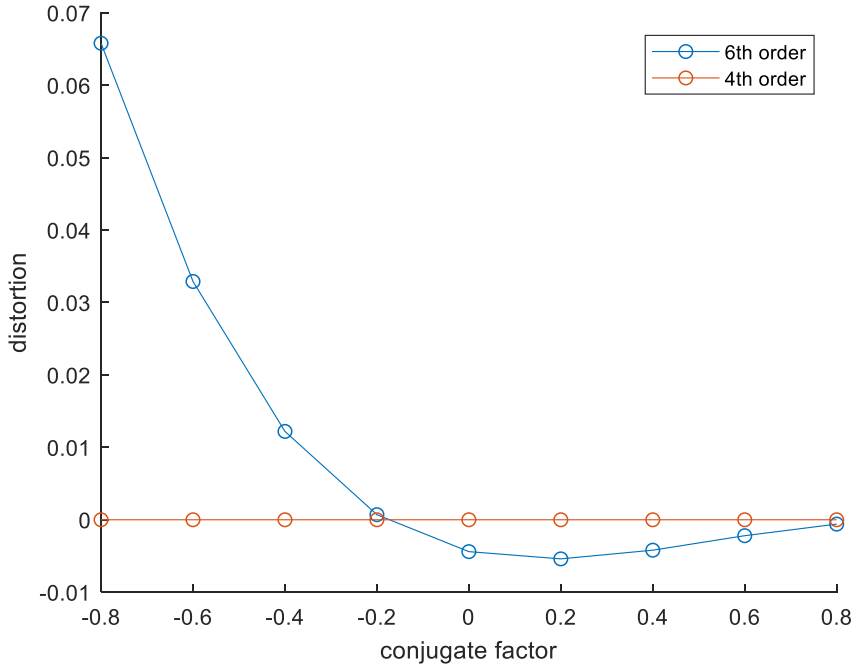

Figure 4.14 Fourth and sixth-order distortion for f/4 BK7 thin paraxial lens with focal length of 100 mm, an object height of 10 mm, and no lens thickness as a function of the conjugate factor.

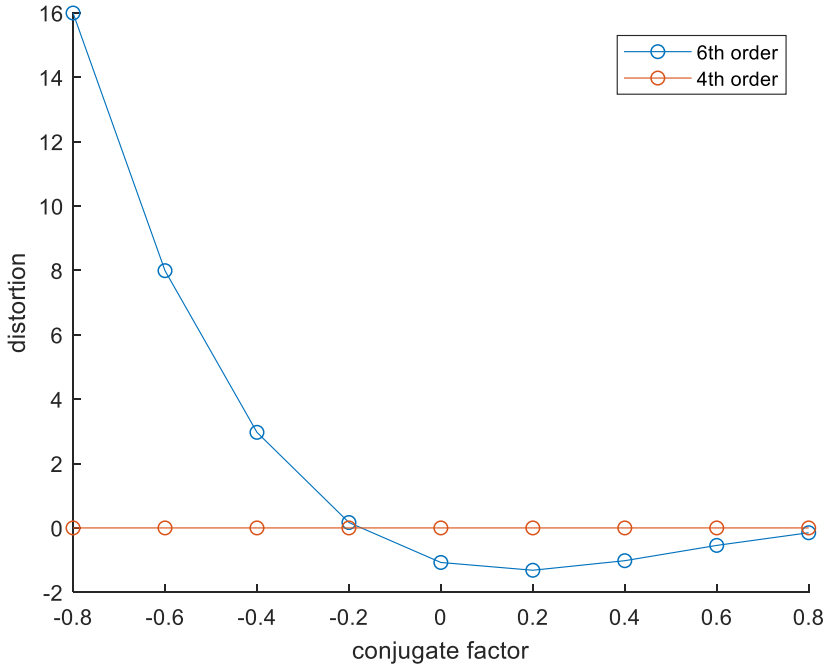

Figure 4.15 Fourth and sixth-order distortion for f/4 BK7 thin paraxial lens with focal length of 100 mm, an object height of 30 mm, and no lens thickness as a function of the conjugate factor.

4.3 *OpticStudio* Analysis of the Conjugate Factor

4.3.1 Lens Layouts and Wave Fans

Figure 4.16, Figure 4.18, Figure 4.20, and Figure 4.22 show the thin lens layouts with conjugate factors of $Y = -0.8, -0.4, 0.4$, and $Y = 0.8$, respectively. These thin lens layouts are also plotted with object heights of 0, 10, and 30 mm. As the conjugate factor increases, the magnification decreases, leading the object to lens distance to increase. As the distance between the object and the thin lens increases, the incident ray angles decrease. This results in less extreme ray angles of exitance, and thus less aberrations.

Figure 4.17, Figure 4.19, Figure 4.21, and Figure 4.23 show the wave fans of the respective lenses from Figure 4.16, Figure 4.18, Figure 4.20, and Figure 4.22. These wave fans include the 0, 10, and 30 mm object heights. As mentioned in the previous paragraph, as the conjugate factor increases across these lenses, the scale on the wave fan plots decreases, which means less total aberration. Across these wave fan plots, the 30 mm object height contributes the highest value to the total aberration value.

As expected, across all the wave fans, at an object height of 0 mm there is only spherical aberration.

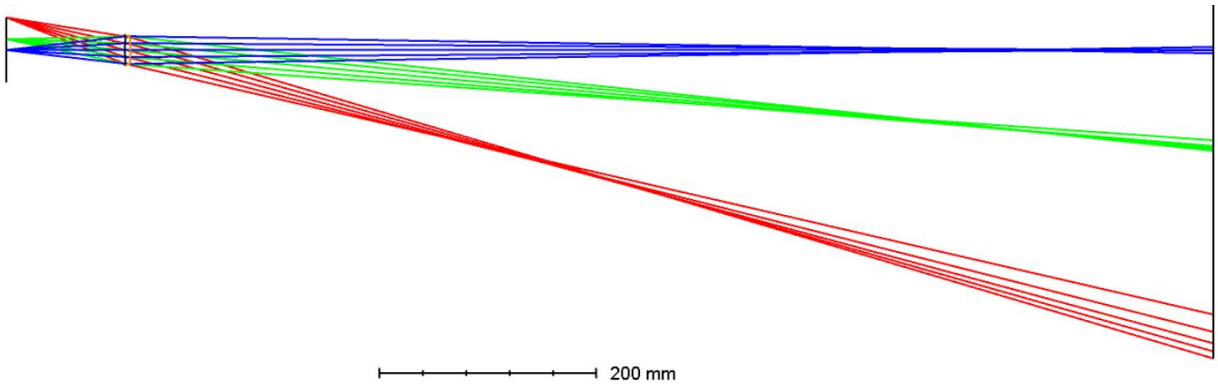

Figure 4.16 Lens layout for f/4 BK7 thin lens with focal length of 100 mm at object heights of 0, 10, and 30 mm, a magnification of $m = -9.0$ and a conjugate factor of $Y = -0.8$.

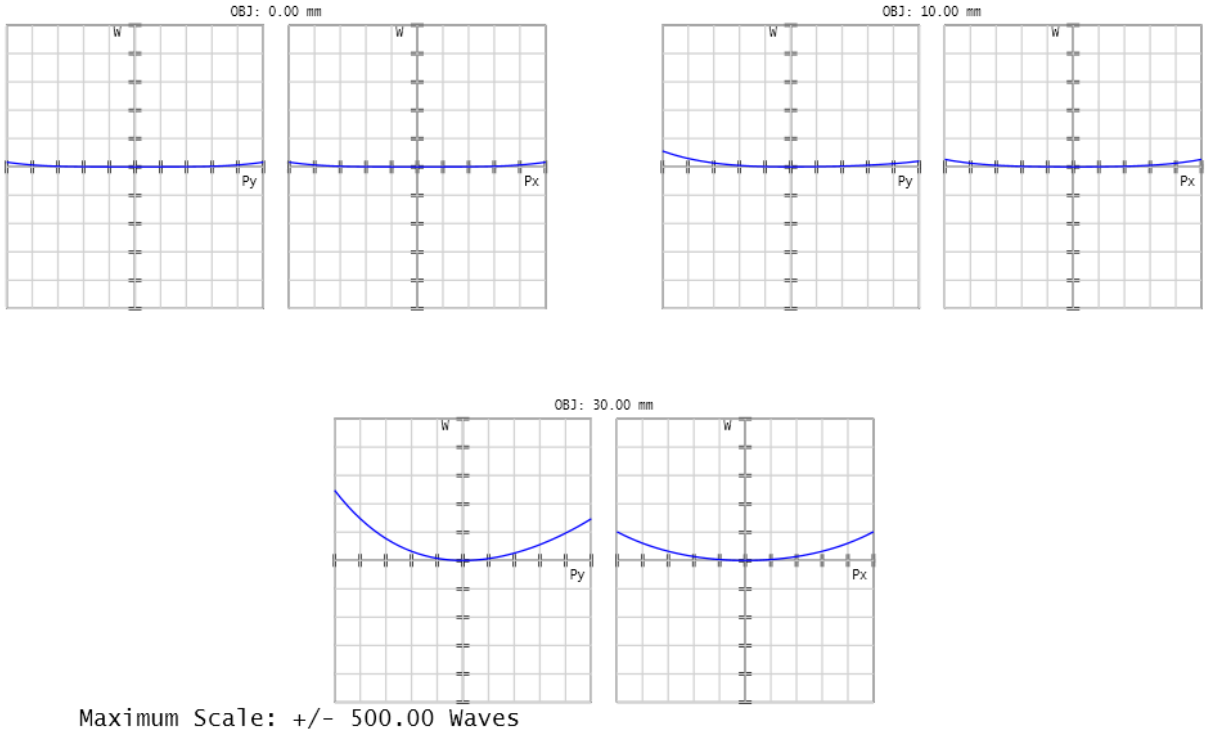

Figure 4.17 Wave fans for f/4 BK7 thin lens with focal length of 100 mm at object heights of 0, 10, and 30 mm, a magnification of $m = -9.0$ and a conjugate factor of $Y = -0.8$.

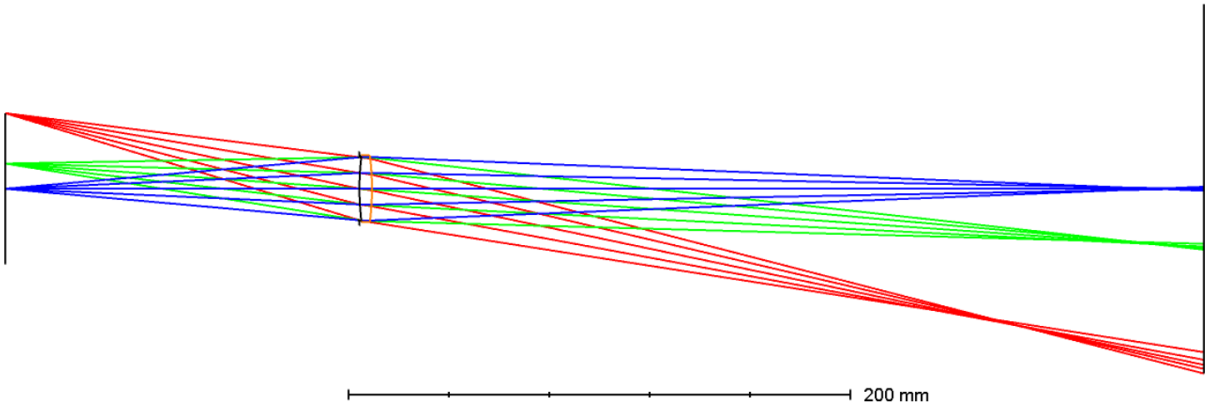

Figure 4.18 Lens layout for f/4 BK7 thin lens with focal length of 100 mm at object heights of 0, 10, and 30 mm, a magnification of $m = -2.33$ and a conjugate factor of $Y = -0.4$.

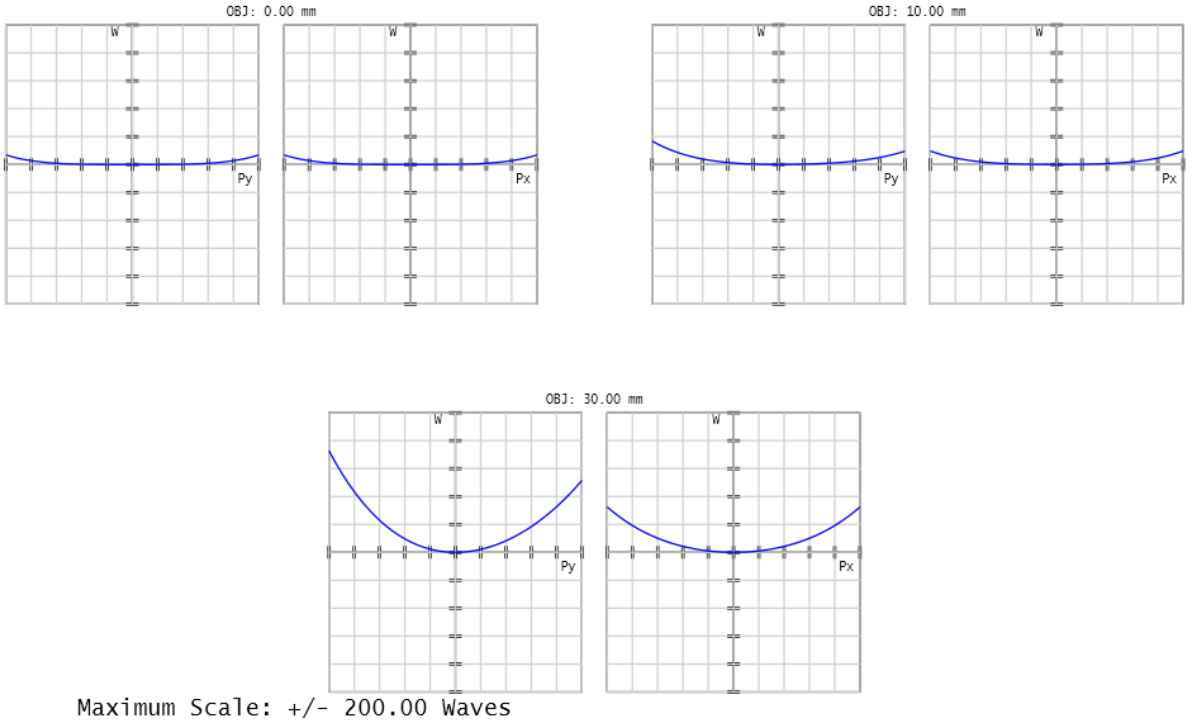

Figure 4.19 Wave fans for f/4 BK7 thin lens with focal length of 100 mm at object heights of 0, 10, and 30 mm, a magnification of $m = -2.33$ and a conjugate factor of $Y = -0.4$.

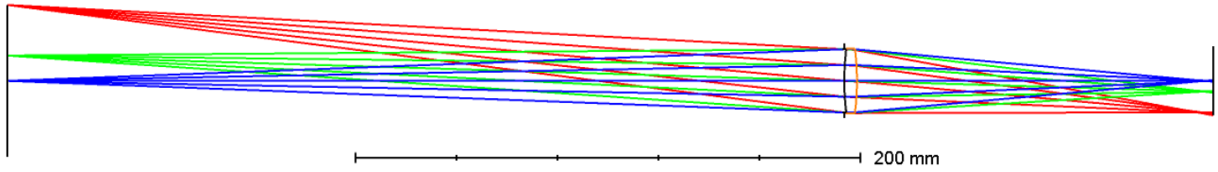

Figure 4.20 Lens layout for f/4 BK7 thin lens with focal length of 100 mm at object heights of 0, 10, and 30 mm, a magnification of $m = -0.43$ and a conjugate factor of $Y = 0.4$.

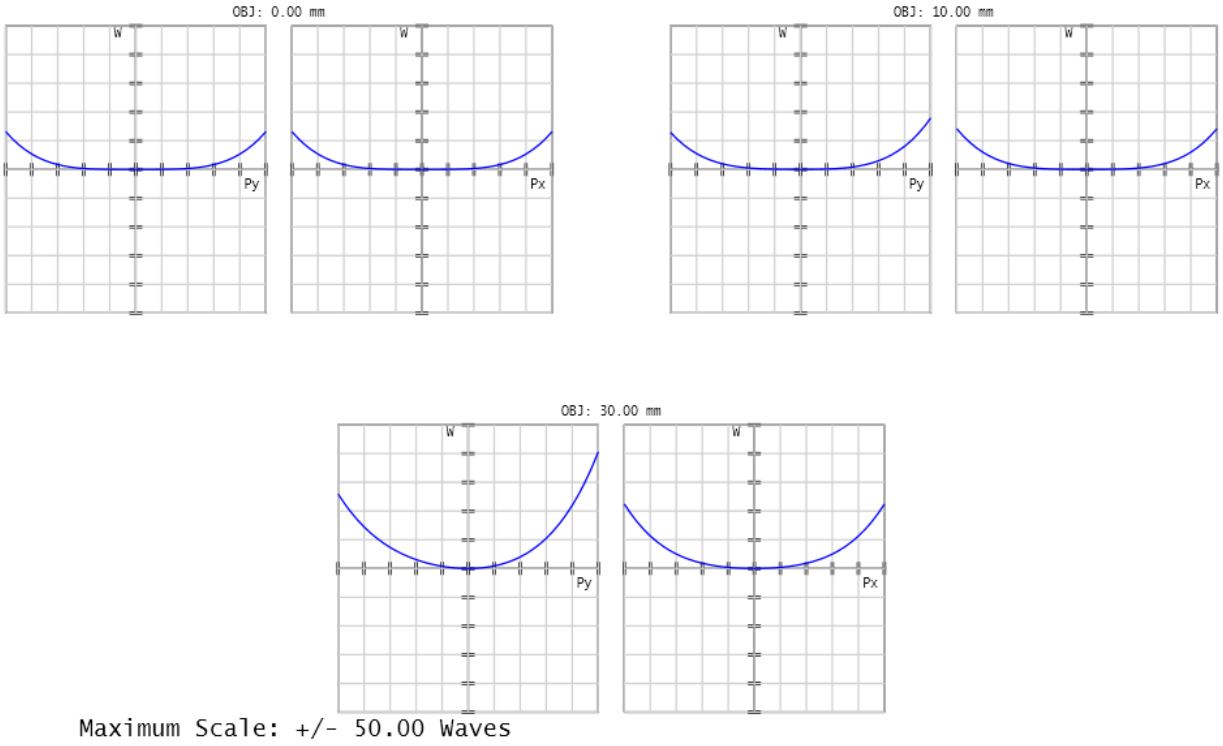

Figure 4.21 Wave fans for f/4 BK7 thin lens with focal length of 100 mm at object heights of 0, 10, and 30 mm, a magnification of $m = -0.43$ and a conjugate factor of $Y = 0.4$.

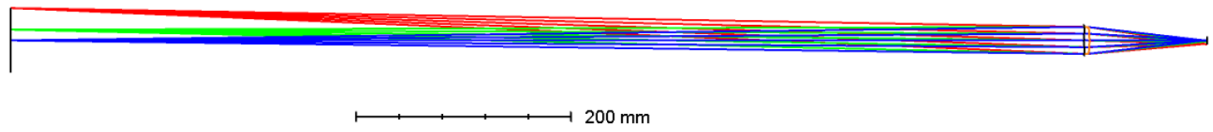

Figure 4.22 Lens layout for f/4 BK7 thin lens with focal length of 100 mm at object heights of 0, 10, and 30 mm, a magnification of $m = -.0.11$ and a conjugate factor of $Y = 0.8$.

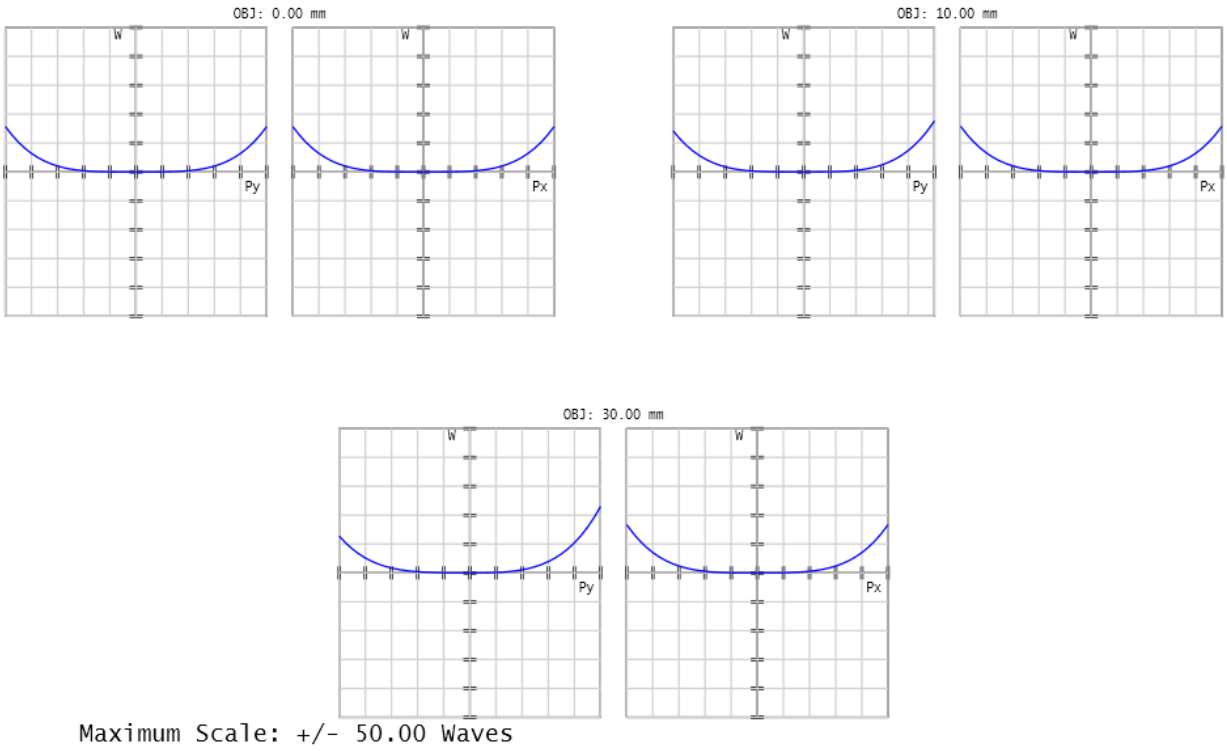

Figure 4.23 Wave fans for f/4 BK7 thin lens with focal length of 100 mm at object heights of 0, 10, and 30 mm, a magnification of $m = -0.11$ and a conjugate factor of $Y = 0.8$.

Chapter 5

This chapter focuses on the fourth and sixth-order monochromatic aberrations as functions of the index of refraction.

The first section describes the f/4 thin lens used in this report. This section also describes the methods used in changing the index of material of the thin lens. The fourth and sixth-order monochromatic aberrations are calculated by the methods outlined in Section 3.1. Again, the lens design and aberration calculation are all done within *OpticStudio,* as well as the index of refraction manipulation.

In the second section, plots of the fourth and sixth-order aberrations as functions of the index of refraction are shows. These plots are analyzed with respect to three different fields: 0, 10, and 30-degrees. These plots are compared against Seidel aberration equations written in terms of structural aberration coefficients. And, the fourth and sixth-order aberrations are compared with each other.

In the last section, certain indices of refraction have been chosen and their respective thin lens layouts and wave fans have been plotted using *OpticStudio*. The reason for this is to understand the deviation of the rays from the nominal image plane by comparing the wave fans and the lens layouts, as was done in Section 3.3.

5.1 Introduction to the Thin Lens System for a Changing Index of Refraction

5.1.1 Description of the System and its Dependence on the Index of Refraction

This chapter uses a similar thin lens system that was described in Section 3.1.1 However, instead of using BK7 as the material for the thin lens, the index of refraction is adjusted, and the aberrations are measured. The thin lens system will continue to consist of the following:

- Stop at the lens.
- Lens made of BK7 with a thickness of 5 mm.
- f/4 lens with an effective focal length of 100 mm.
- Wavelength of 0.58 μm and fields of view of 0, 10, and 30 degrees.

Once again, it must be clarified that although the lens is called a "thin" lens, this is because its thickness is small compared to its focal length. When designed this lens in *OpticStudio,* the lens is not thin.

As in Chapter 3, the lens system will have an object placed at infinity so that they rays coming in are parallel to the optical axis. However, unlike Chapter 3, the shape of the lens will not be changing. All that will be changing in this chapter in the index of refraction of the material.

The lens system will have the prescription listed in Table 5.1, with its respective layout seen in Figure 5.1. The index of refraction is changed simply by altering the index of refraction value under the "Material" section of *OpticStudio*'s lens prescription. It's important to note that

	Surface Type		Coı	Radius		Thickness		Material		Coı		Clear Semi-I	
0	OBJECT	Standard		Infinity		Infinity						Infinity	
1	STOP	Standard		Infinity		0.000						12.500	U
2		Standard		102.844		5.000		1.52,0.0	M			12.500	P
3		Standard		-102.844		98.669	M					12.881	
4	IMAGE	Standard		Infinity		-						19.292	

Table 5.1 Prescription for f/4 thin lens system with stop at the lens and a focal length of 100 mm. The index of refraction of the lens is defined to be n=1.5168 with a dispersion of $\upsilon = 0$.

the Abbe value ν must always be set to zero since this report is not analyzing how the dispersive properties of a material affects aberrations. Figure 5.2 demonstrates how the expanded "Material" section is altered to obtain the desired values.

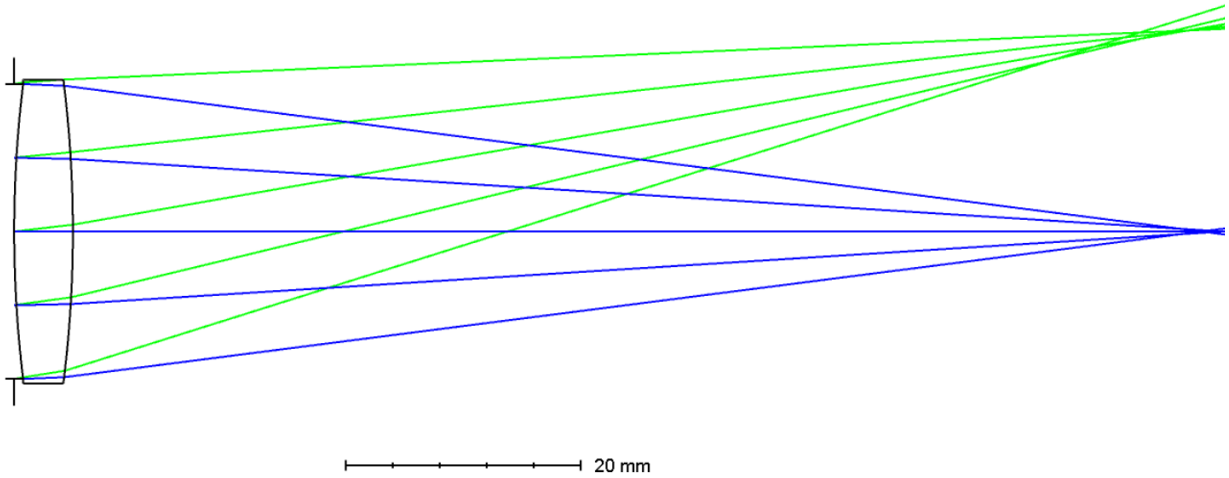

Figure 5.1 Lens layout for f/4 thin lens system with stop at the lens and a focal length of 100 mm. The index of refraction of the lens is defined to be n=1.5168 with a dispersion of $\upsilon = 0$.

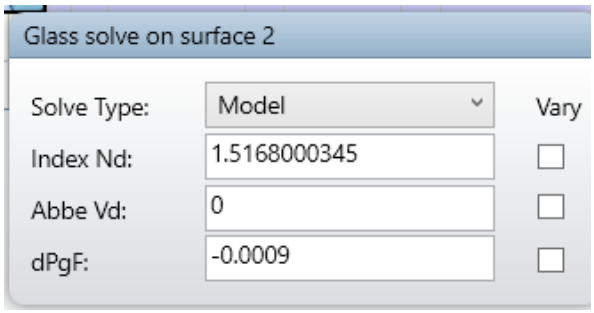

Figure 5.2 Material model used for f/4 thin lens with stop at the lens and a focal length of 100 mm. The index is altered, and the Abbe number is set to zero.

5.2 Aberrations as Functions of the Index of Refraction

5.2.1 Spherical Aberration as a Function of the Index of Refraction

Figure 5.3 shows fourth and sixth-order spherical aberration as a function of the index of refraction. This is for a field of 0 degrees – as spherical aberration has no field dependence changing the field will not change the amount of spherical aberration.

Once again, fourth-order spherical aberration is given by two sets of equations: the first applies to each surface and the second is a simplification for a thin lens model. These are given below,

$$W_{040} = \frac{1}{32} y_p^2 \Phi^3 \left[-\frac{1}{2}\left(\frac{n' + n}{n' - n} - Y \right)^2 \left(\frac{n'^2 - n^2}{n^2 n'^2} \cdot Y - \frac{n'^2 + n^2}{n^2 n'^2} \right) \right], \tag{2.8}$$

$$W_{040,thin} = \frac{1}{32} y_p^4 \Phi^3 \left(AX^2 - BXY + CY^2 + D \right). \tag{2.9}$$

It's easily seen that equation (2.8) heavily relies on the index of refraction of each surface. The same can be said for equation (2.9) by looking at the following values:

$$A = \frac{n+2}{n(n-1)^2},$$

$$B = \frac{4(n+1)}{n(n-1)},$$

$$C = \frac{3n+2}{n},$$

$$D = \frac{n^2}{(n-1)^2}$$

which clearly also depend on the index of refraction. It's important to realize that the power of the thin lens, Φ also has an index of refraction term that its dependent on.

In Figure 5.3 the fourth-order spherical aberration appears to be increasing exponentially as the index of refraction increases. The sixth-order spherical aberration appears to be increasing

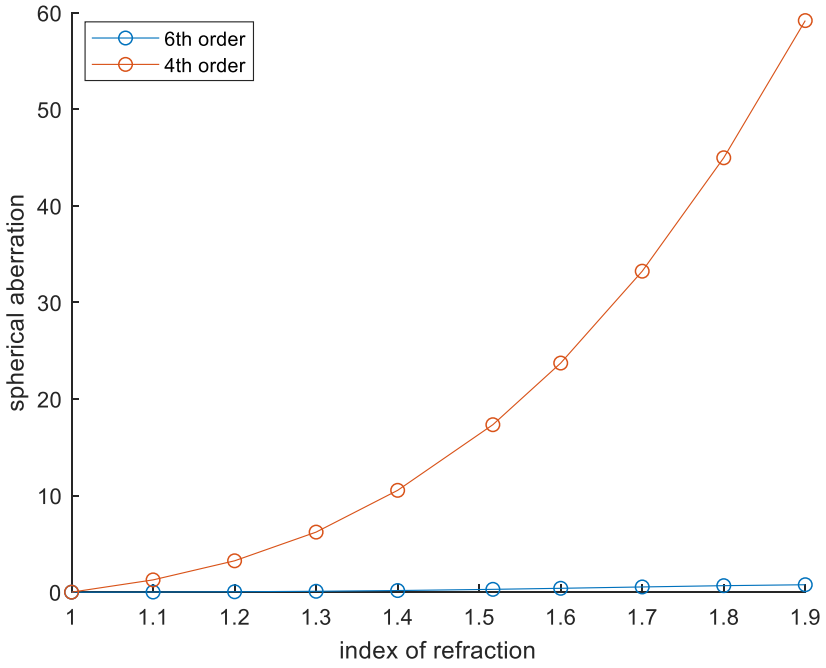

Figure 5.3 Fourth and sixth-order spherical aberration for f/4 thin lens with focal length of 100 mm at 10 degrees as a function of the index of refraction.

linearly with the increase in index of refraction, however sixth-order spherical aberration is negligible when compared to fourth-order spherical aberration.

5.2.2 Coma Aberration as a Function of the Index of Refraction

Figure 5.4 and Figure 5.5 show fourth and sixth-order coma aberration as a function of the index of refraction and at fields of 10 and 30 degrees respectively. Recall that coma is also a function of the field of view.

Again, this report gives two equations for fourth-order coma aberration; the first is an equation applied to each surface and the second is a thin lens simplification of the first. These equations are given below,

$$W_{131} = \frac{1}{4}\mathcal{H}y_p^2\Phi^2\left[-\frac{1}{2}\left(\frac{n'+n}{n'-n}-Y\right)\left(\frac{n'^2-n^2}{n^2n'^2}\cdot Y-\frac{n'^2+n^2}{n^2n'^2}\right)\right], \tag{2.10}$$

$$W_{131,thin} = \frac{1}{4}\mathcal{H}y_p^2\Phi^2\left(EX-FY\right). \tag{2.11}$$

Equation (2.10) relies strongly on the index of refraction. So does equation (2.11) when variables E and F are defined:

$$E = \frac{n+1}{n(n-1)},$$

$$F = \frac{2n+1}{n}.$$

Like with spherical aberration, the power term, Φ is dependent on the index of refraction. But in addition to the power term, the Lagrange invariant term, $\mathcal{H}$ is also dependent on the index of refraction. With this it's clear that both equations rely on the index of refraction.

In Figure 5.4 the magnitude of the fourth-order coma aberration curve is growing exponentially as the index of refraction increases. The sixth-order coma aberration is also increasing as the index of refraction increases, although it appears to be increasing linearly. When compared to fourth-order coma aberration, sixth-order coma aberration is negligible.

In Figure 5.5 the magnitude of the fourth-order coma aberration curve is growing exponentially as the index of refraction increases. The sixth-order coma aberration curve is no longer linear and is also increasing as the index of refraction increases. However, at a field of 30 degrees sixth-order coma aberration can no longer be considered negligible especially as the index of refraction grows.

Fourth and sixth-order coma aberration in Figure 5.4 and Figure 5.5 share a relationship; fourth and sixth-order coma aberration in Figure 5.5 are approximately 3.27 and 35.10 times respectively larger than fourth and sixth-order coma aberration in Figure 5.4.

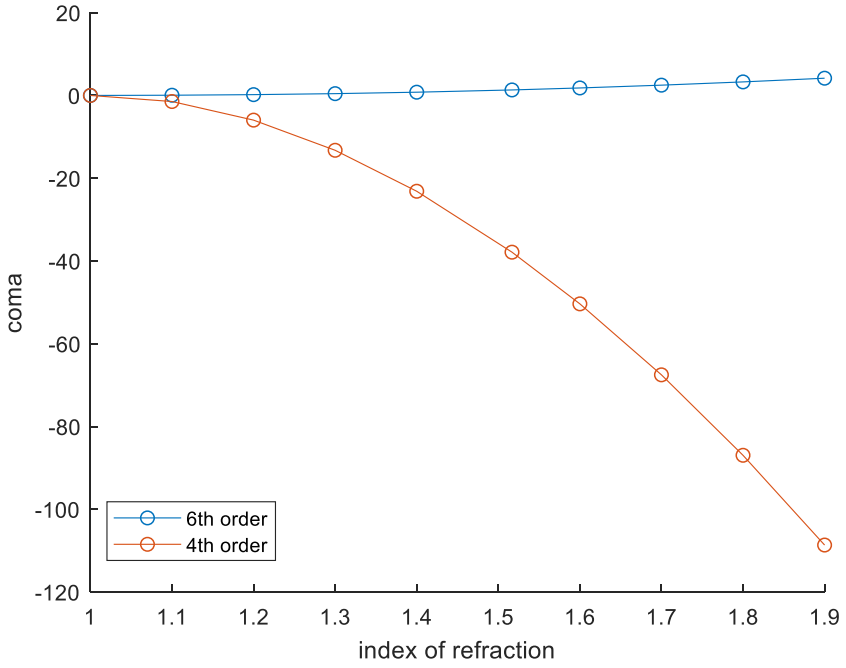

Figure 5.4 Fourth and sixth-order coma aberration for f/4 thin lens with focal length of 100 mm at 10 degrees as a function of the index of refraction.

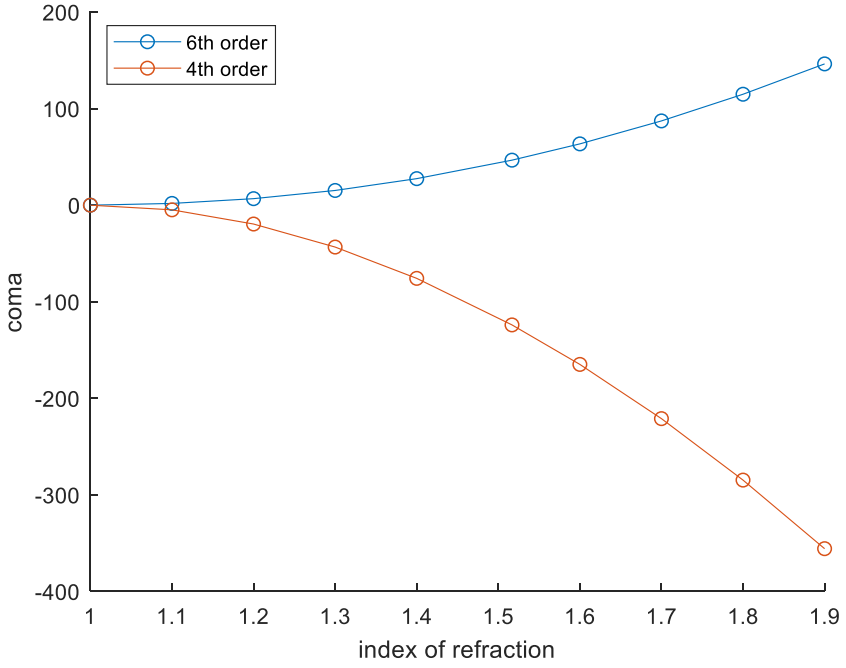

Figure 5.5 Fourth and sixth-order coma aberration for f/4 thin lens with focal length of 100 mm at 30 degrees as a function of the index of refraction.

5.2.3 Astigmatism as a Function of the Index of Refraction

Figure 5.6 and Figure 5.7 show fourth and sixth-order astigmatism aberration as a function of the index of refraction and at fields of 10 and 30 degrees respectively. Recall that more than one field is needed for a full understanding of astigmatism, since astigmatism is also a function of the field of view.

It's once again necessary to write out the two fourth-order astigmatism aberration equations; the first being an equation applied to each surface of the system and the second being a simplification to a thin lens. These equations are given below,

$$W_{222} = \frac{1}{2} \mathcal{K}^2 \Phi \left[-\frac{1}{2} \left(\frac{n'^2 - n^2}{n^2 n'^2} \cdot Y - \frac{n'^2 + n^2}{n^2} n'^2 \right) \right], \tag{2.12}$$

$$W_{222,thin} = \frac{1}{2} \mathcal{K}^2 \Phi. \tag{2.13}$$

Equation (2.12) is clearly dependent on the index of refraction, while in equation (2.13) the index of refraction is buried in the Lagrange invariant and power terms. In breaking down equation (2.13) the equation now states,

$$W_{222,thin} = \frac{1}{2} \left(n\bar{u}y - nu\bar{y} \right)^2 (n-1) \left(\frac{1}{r_1} - \frac{1}{r_2} \right)$$

where the dependence on the index of refraction is clear.

In Figure 5.6 the fourth-order astigmatism curve appears to be increasing linearly as the index of refraction increases. The sixth-order astigmatism curve appears to be decreasing linearly, while its magnitude is increasing. This sixth-order astigmatism is not negligible at higher indices of refraction, although it is small compared to the magnitude of the fourth-order astigmatism.

In Figure 5.7 the fourth and sixth-order astigmatism curves have the same shape as those from Figure 5.6, however their magnitudes are larger and sixth-order astigmatism is large throughout all values of the index of refraction. The fourth and sixth-order astigmatism values in Figure 5.7 are 10.72 and 114.94 times respectively larger than the fourth and sixth-order astigmatism values from Figure 5.6.

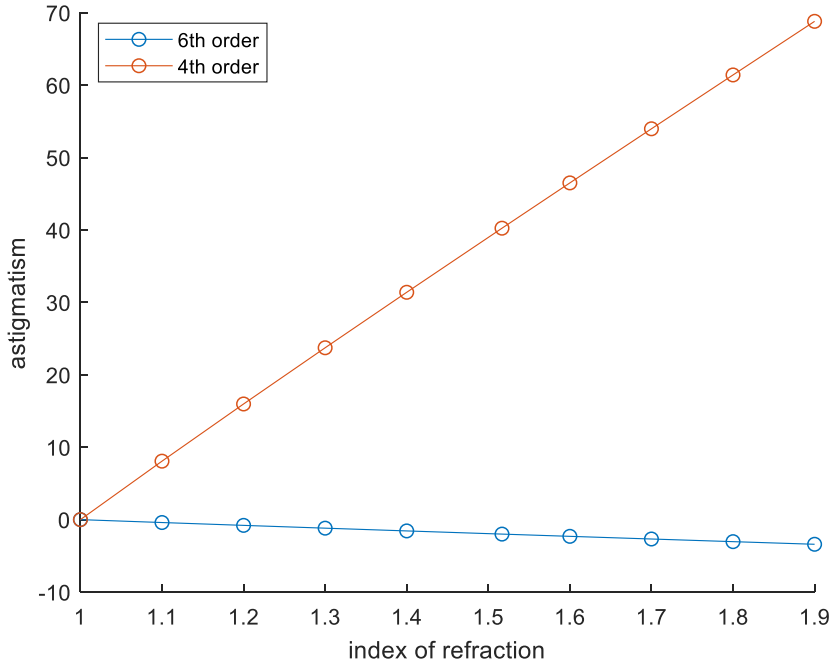

Figure 5.6 Fourth and sixth-order astigmatism aberration for f/4 thin lens with focal length of 100 mm at 10 degrees as a function of the index of refraction.

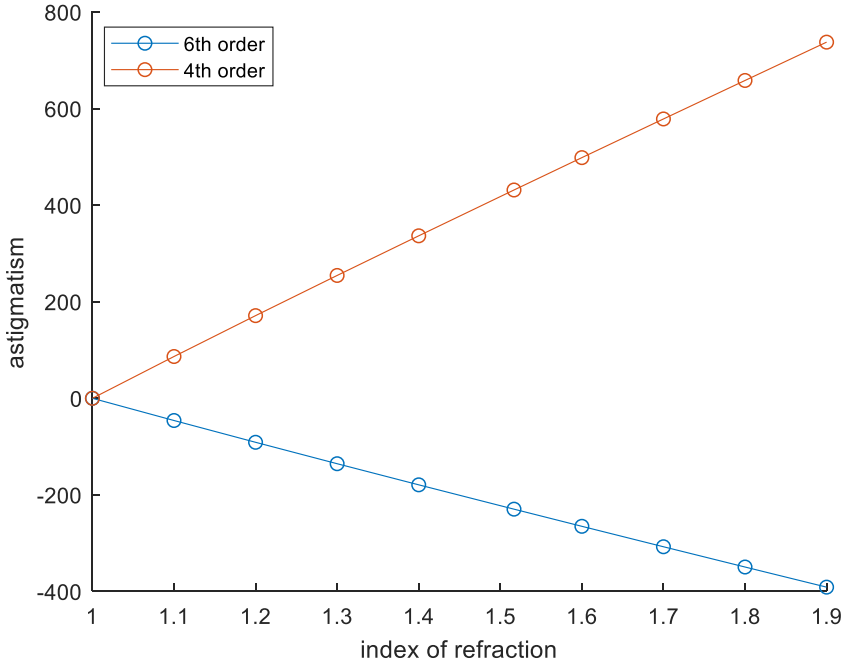

Figure 5.7 Fourth and sixth-order astigmatism aberration for f/4 thin lens with focal length of 100 mm at 30 degrees as a function of the index of refraction.

5.2.4 Field Curvature as a Function of the Index of Refraction

Figure 5.8 and Figure 5.9 show fourth and sixth-order field curvature as a function of the index of refraction and at fields of 10 and 30 degrees respectively. Recall that multiple fields are needed to fully understand field curvature, since it is also dependent on the field of view.

Written again below are the fourth-order field curvature equations, the first being an equation applied to each surface and the second being a simplified version for thin lenses. These equations are,

$$\begin{aligned} W_{220} &= \frac{1}{2}\not{K}^2\Phi\left(\frac{1}{n'n}\right) \\ &= \frac{1}{2}(n\bar{u}y - nu\bar{y})^2(n-1)\left(\frac{1}{r_1}-\frac{1}{r_2}\right)\left(\frac{1}{n'n}\right), \end{aligned} \tag{2.14}$$

$$\begin{aligned} W_{220,thin} &= \frac{1}{2}\not{K}^2\Phi\left(\frac{1}{n}\right) \\ &= \frac{1}{2}(n\bar{u}y - nu\bar{y})^2(n-1)\left(\frac{1}{r_1}-\frac{1}{r_2}\right)\left(\frac{1}{n}\right). \end{aligned} \tag{2.15}$$

These equations have been expanded so that all the terms are written in terms of the index of refraction.

In Figure 5.8 the fourth-order field curvature curve appears to be linearly increasing as the index of refraction increases. The sixth-order field curvature curve is decreasing slowly away from zero as the index of refraction increases and is negligible when compared to the fourth-order field curvature.

In Figure 5.9 the fourth and sixth-order field curvature curves have the same shape as those from Figure 5.8, however their magnitudes are much larger. To that point, sixth-order field curvature is no longer negligible. The fourth and sixth-order field curvature values in Figure 5.9 are 10.72 and 114.94 times respectively more than those in Figure 5.8. Interestingly, this is the same relationship for between the fourth and sixth-order astigmatism aberration values in Section 5.2.3.

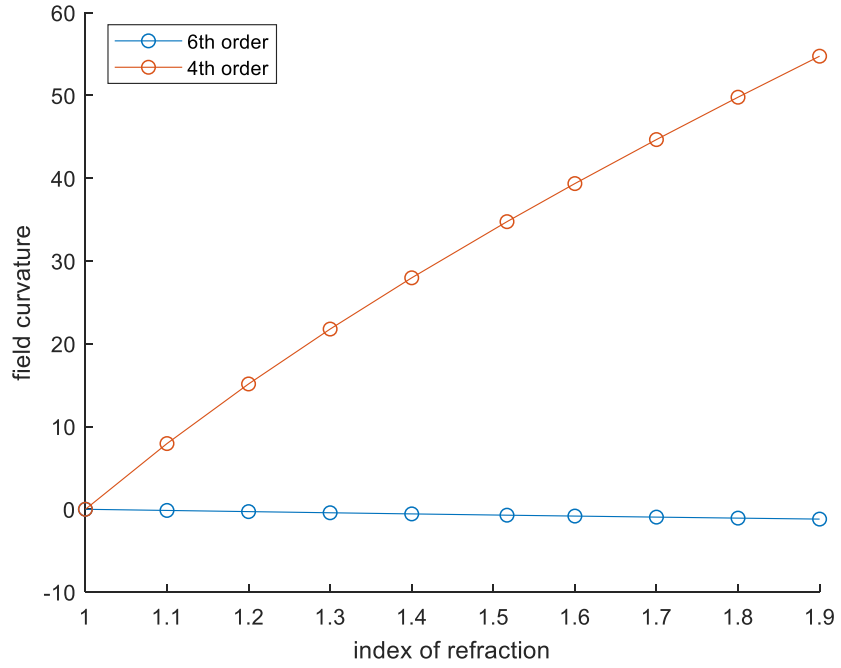

Figure 5.8 Fourth and sixth-order field curvature for f/4 thin lens with focal length of 100 mm at 10 degrees as a function of the index of refraction.

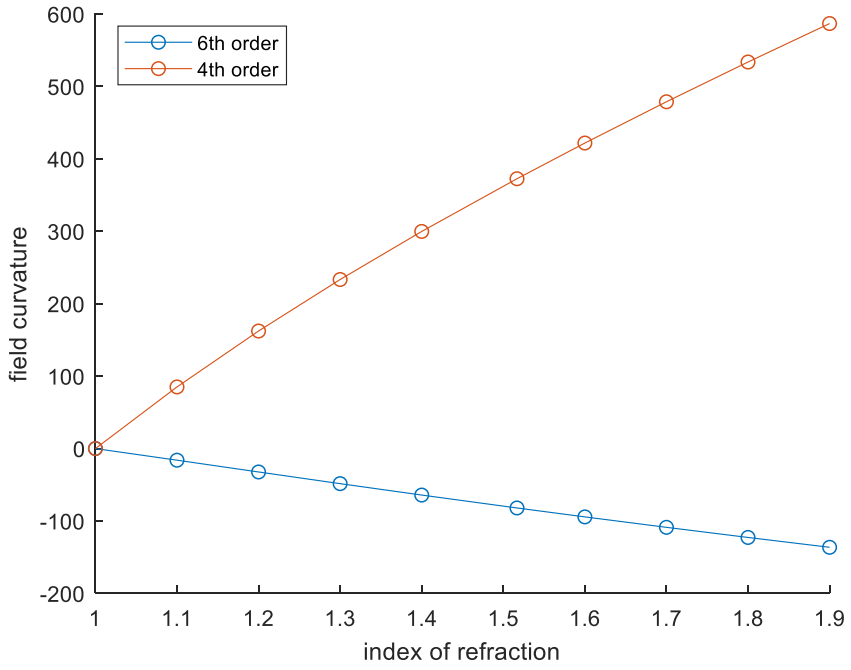

Figure 5.9 Fourth and sixth-order field curvature for f/4 thin lens with focal length of 100 mm at 30 degrees as a function of the index of refraction.

5.2.5 Distortion as a Function of the Index of Refraction

Figure 5.10 and Figure 5.11 show fourth and sixth-order distortion as a function of the index of refraction and at fields of 10 and 30 degrees respectively. Recall that distortion is also a function of the field of view, so it's crucial to look at multiple fields.

Below are the fourth-order distortion equations for both a system of surfaces and a thin lens:

$$\begin{aligned} W_{311} &= \frac{\not{K}^3}{y_p^2}\left(\frac{n'^2 - n^2}{n^2 n'^2}\right) \\ &= \frac{(n\bar{u}y - nu\bar{y})^3}{y_p^2}\left(\frac{n'^2 - n^2}{n^2 n'^2}\right), \end{aligned} \tag{2.16}$$

$$W_{311,thin} = 0. \tag{2.17}$$

Equation (2.16) has been expanded so that all terms are written with their dependence on the index of refraction.

In Figure 5.10 the fourth-order distortion curve increases rapidly from away from zero but begins to approach some limit as the index of refraction increases. The sixth-order distortion curve hovers around zero and is therefore negligible.

In Figure 5.11 the fourth-order distortion curve behaves similarly to that of Figure 5.10, although the magnitude of the distortion is larger in Figure 5.11. However, the sixth-order distortion curve moves away from zero rapidly, giving negative distortion values. The sixth-order distortion is not negligible.

The fourth and sixth-order distortion of Figure 5.11 are 35.10 and 376.28 times respectively larger than those from Figure 5.10.

Despite equation (2.16) stating that fourth-order distortion is not a function of the index of refraction, equation (2.17), Figure 5.10, and Figure 5.11 show otherwise. Looking back to Section 4.2.5, where a new paraxial thin lens system with zero thickness was set up, the fourth-order distortion was zero. However, since the thin lens system set up in this section is not thin, by *OpticStudio's* consideration of thin, equation (2.15) may describe the lens since the equation does rely on the index of refraction. Regardless, equation (2.15) is not a particularly great model for this situation, but it cannot be cast aside.

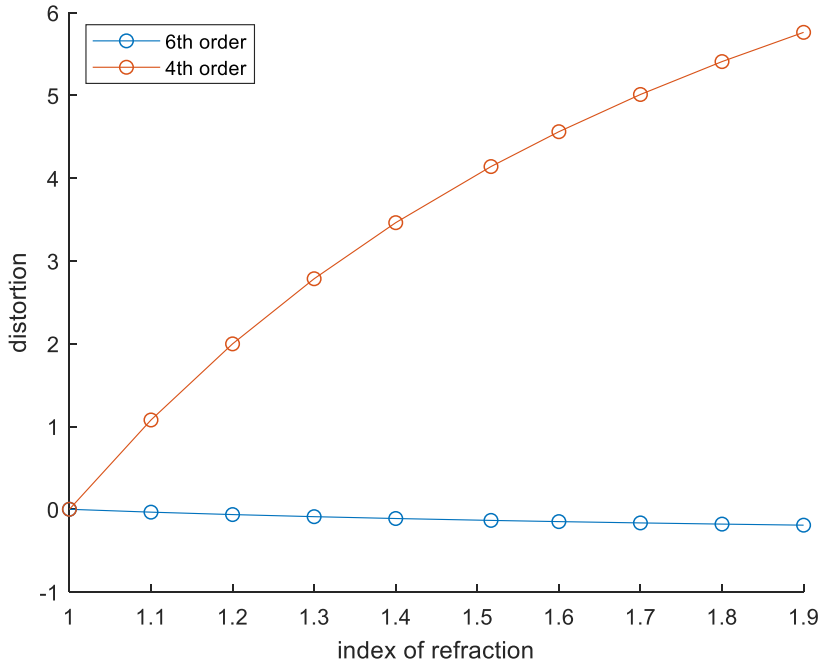

Figure 5.10 Fourth and sixth-order distortion for f/4 thin lens with focal length of 100 mm at 10 degrees as a function of the index of refraction.

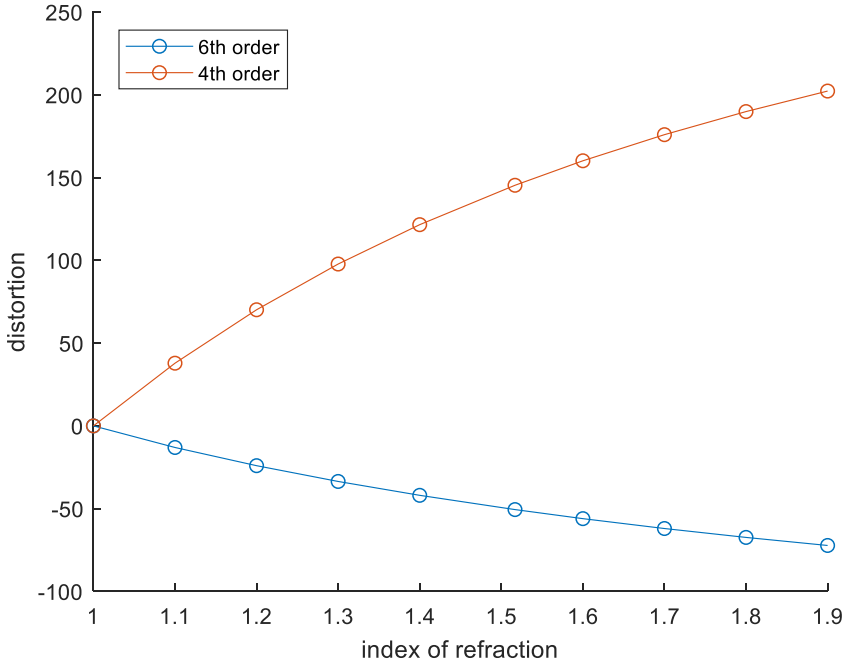

Figure 5.11 Fourth and sixth-order distortion for f/4 thin lens with focal length of 100 mm at 30 degrees as a function of the index of refraction.

5.3 *OpticStudio* Analysis of the Index of Refraction

5.3.1 Lens Layouts and Wave Fans

Figure 5.12, Figure 5.14, Figure 5.16, and Figure 5.18 show the thin lens layouts with indices of refraction of $n = 1.3, 1.5, 1.7$ and $n = 1.9$ and for fields of 0, 10, and 30 degrees. As the index of refraction increase, the exiting rays have more extreme angles. As a result, the rays appear to spread out further from their ideal points. This is also true as the field of view is increased.

Figure 5.13, Figure 5.15, Figure 5.17, and Figure 5.19 show the wave fans of the respective lenses from Figure 5.12, Figure 5.14, Figure 5.16, and Figure 5.18. These wave fans include the 0, 10, and 30-degree fields. As the index of refraction increases across these lenses, the scale of the wave fan plots also increases. As predicted, the 30-degree fields contribute the most to the total aberration. Additionally, the 0-degree field only has spherical aberration.

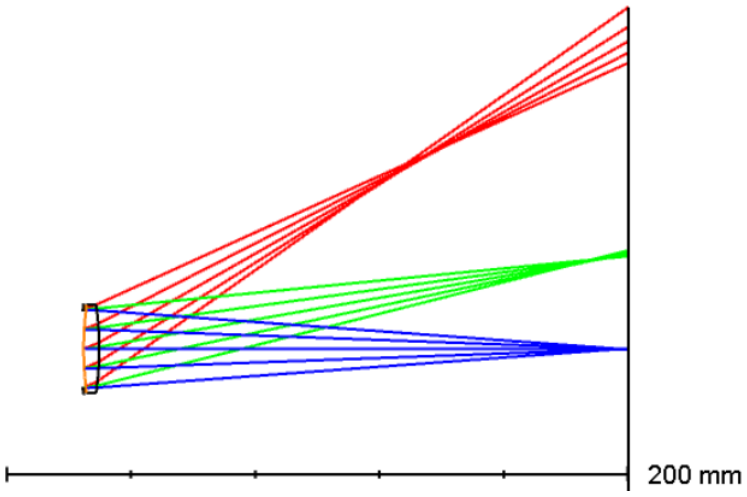

Figure 5.12 Lens layout for f/4 thin lens with focal length of 100 mm at 0, 10, and 30 degree fields and an index of refraction of $n = 1.3$.

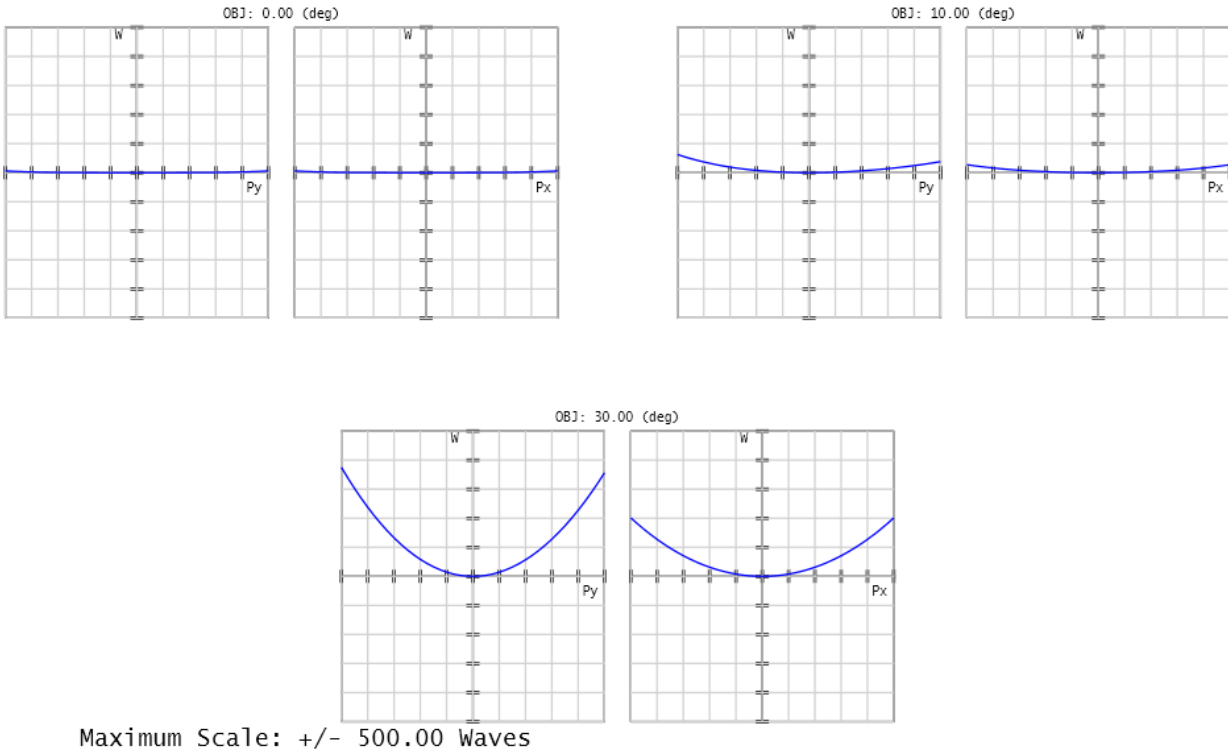

Figure 5.13 Wave fans for f/4 thin lens with focal length of 100 mm at 0, 10, and 30 degrees fields and an index of refraction of $n = 1.3$.

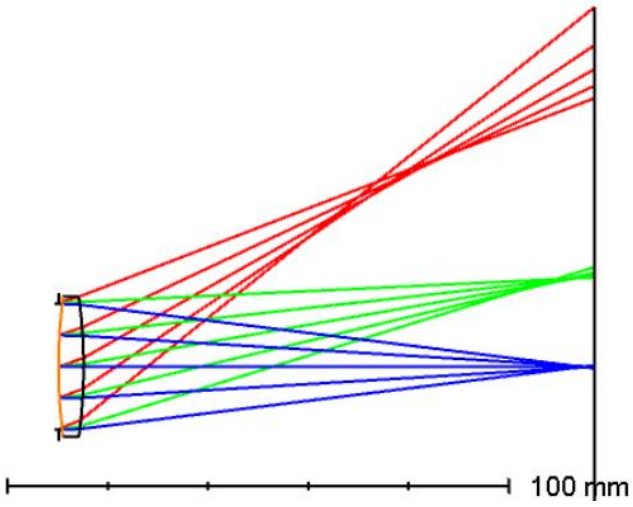

Figure 5.14 Lens layout for f/4 thin lens with focal length of 100 mm at 0, 10, and 30 degree fields and an index of refraction of $n = 1.5$.

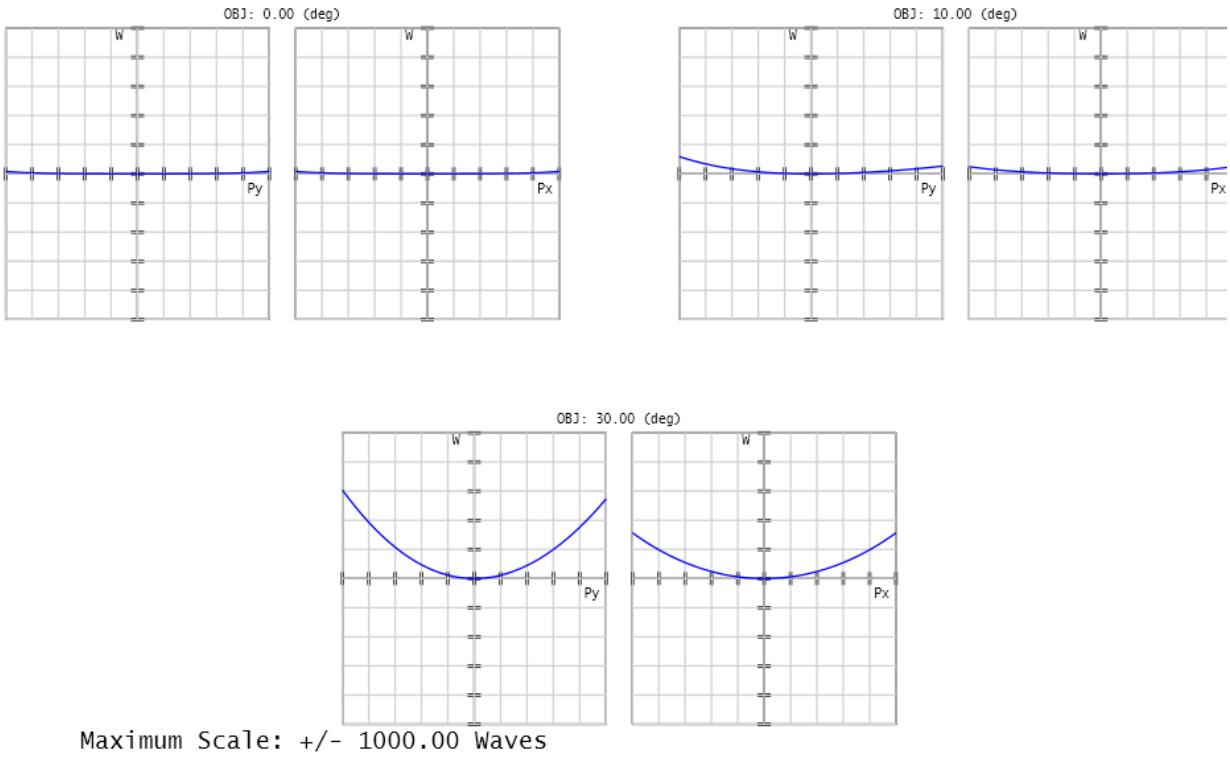

Figure 5.15 Wave fans for f/4 thin lens with focal length of 100 mm at 0, 10, and 30 degrees fields and an index of refraction of $n = 1.5$.

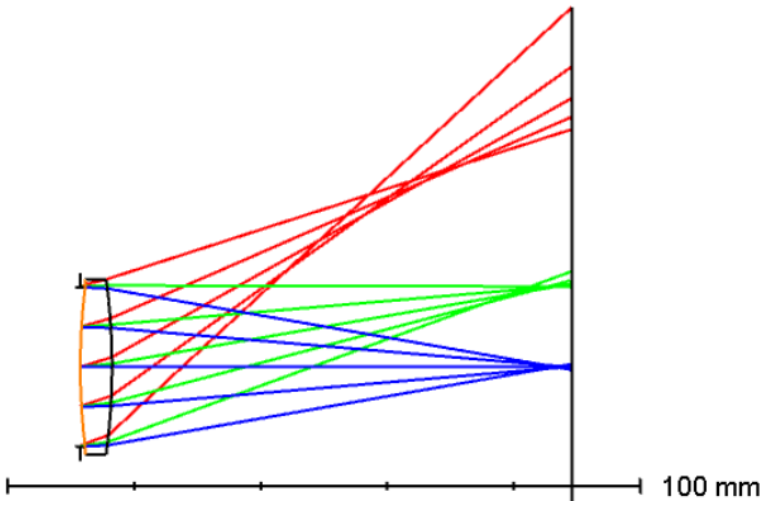

Figure 5.16 Lens layout for f/4 thin lens with focal length of 100 mm at 0, 10, and 30 degree fields and an index of refraction of $n = 1.7$.

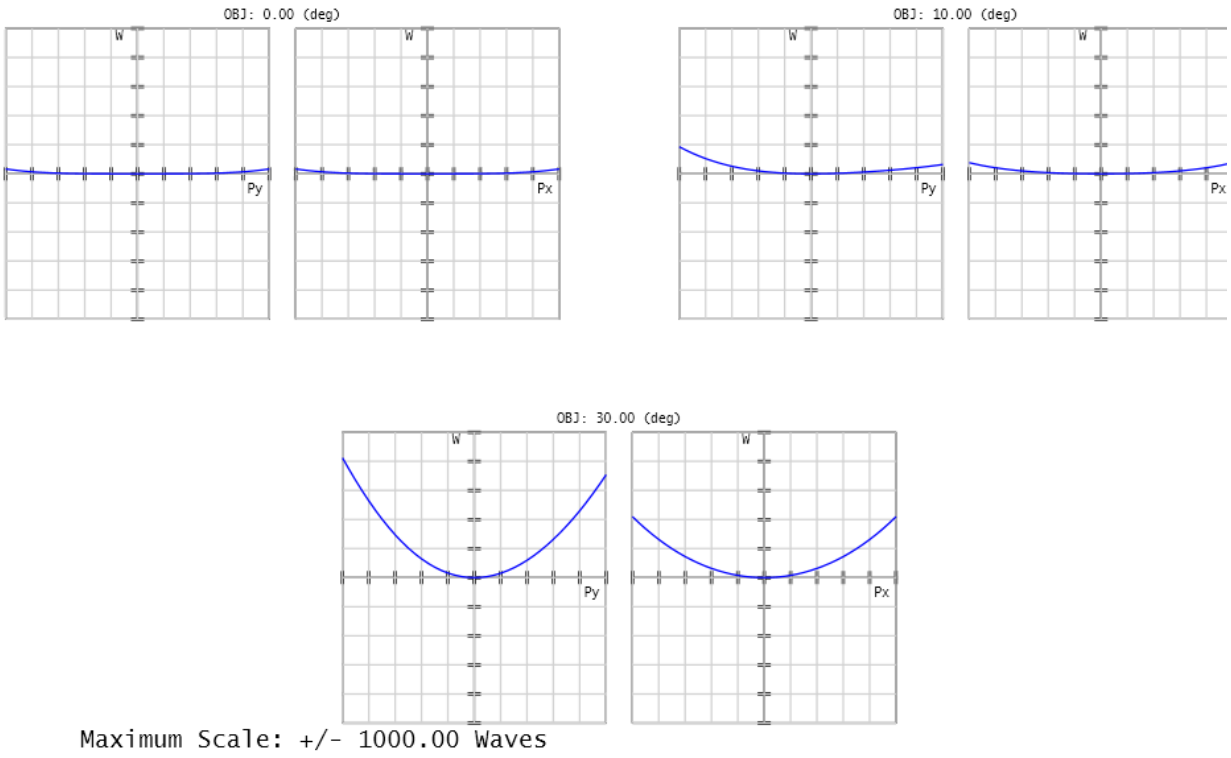

Figure 5.17 Wave fans for f/4 thin lens with focal length of 100 mm at 0, 10, and 30 degrees fields and an index of refraction of $n = 1.7$.

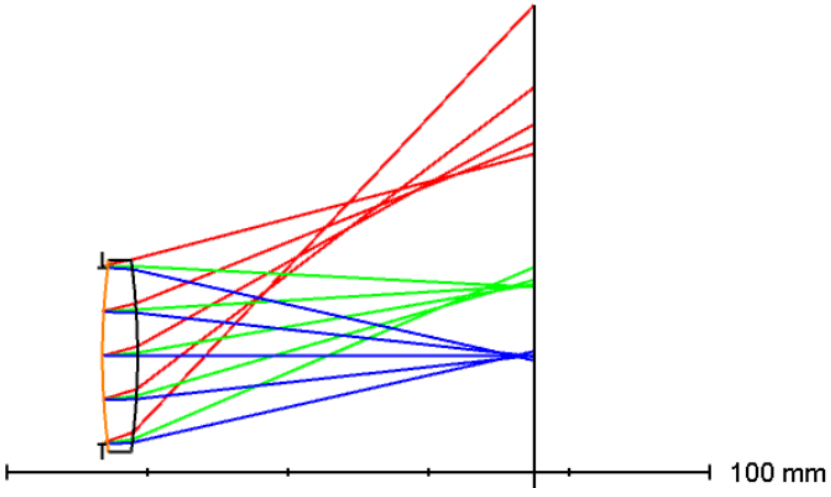

Figure 5.18 Lens layout for f/4 thin lens with focal length of 100 mm at 0, 10, and 30 degree fields and an index of refraction of $n = 1.9$.

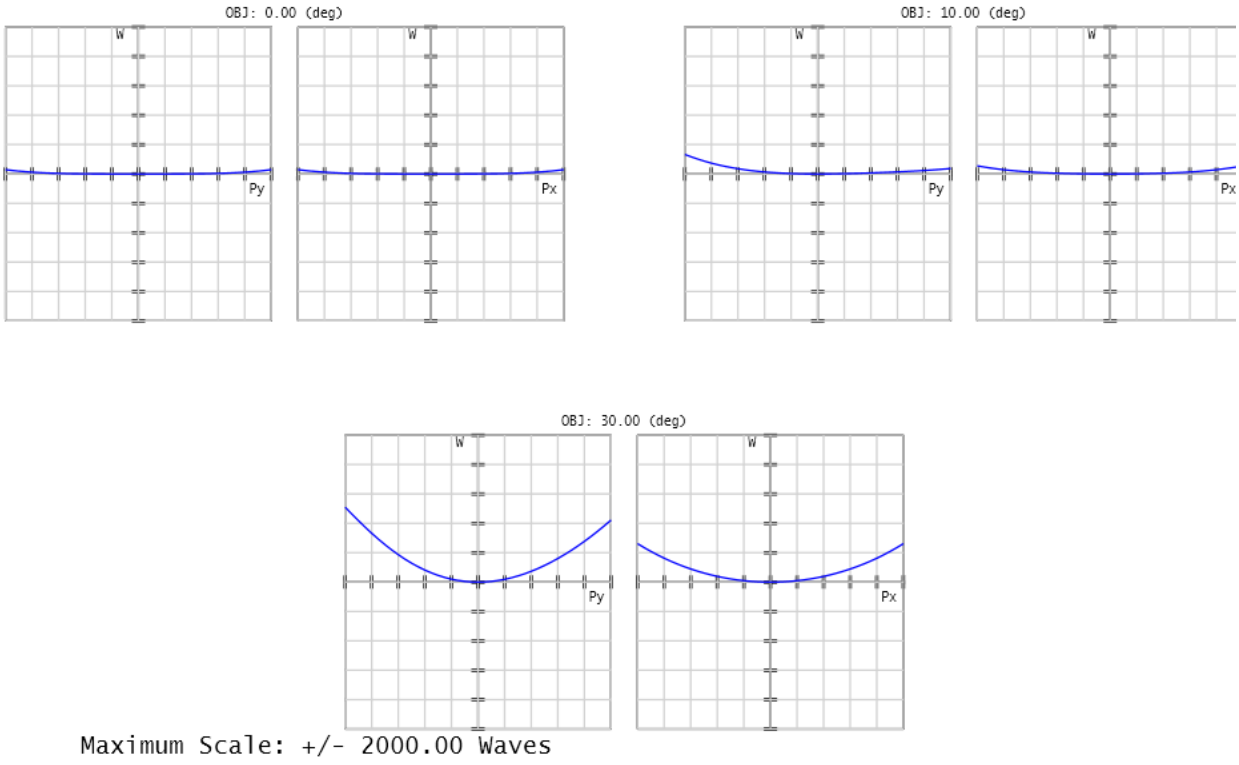

Figure 5.19 Wave fans for f/4 thin lens with focal length of 100 mm at 0, 10, and 30 degrees fields and an index of refraction of $n = 1.9$.

Conclusions

In this report, fourth and sixth-order monochromatic aberrations are analyzed against the shape factor, conjugate factor and index of refraction. In addition, these aberrations are also measured at different fields of view and object heights in order to obtain a comprehensive understanding of the behavior of these aberrations.

The Seidel aberration coefficients were written using structural coefficients in order to obtain expressions for the wave aberration coefficients in terms of the shape factor, conjugate factor, and index of refraction. In addition to these general formulas for fourth-order aberrations, the equations could be simplified further for a thin lens system. However, the equations for a system of surfaces and the equation for a thin lens system both did not always describe the resulting aberration plots completely.

As changing shape factors, conjugate factors, and indices of refraction resulted in greater angles of exitance of the rays, the total amount of aberration was higher. Smaller angles of exitance resulted in lower amounts of total aberration. Additionally, large fields and large object heights also resulted in higher amounts of total aberration.

Fourth-order monochromatic aberrations were always greater than their sixth-order monochromatic counterparts. However, at larger fields and larger object heights, the sixth-order aberrations often were not small enough to completely ignore. To conclude, sixth-order aberrations cannot be ignored without full understanding of the optical system, even if the system is as simple as a thin lens.

References

[1] Kidger, M.J., (2002). *Fundamental Optical Design.* Bellingham, Washington: The International Society for Optical Engineering.

[2] Sasián, J., 'Introduction to aberrations' [PowerPoint presentation]. (p. 30). *OPTI 518: Introduction to aberrations.* Available at: https://wp.optics.arizona.edu/jsasian/courses/opti-518/

[3] Sasián, J., (2013). *Introduction to aberrations in optical imaging systems*. New York: Cambridge University Press.

[4] Sasián, J., 'Sixth-order aberrations' [PowerPoint presentation]. (p. 13). *OPTI 508: Introduction to aberrations*. Available at: https://wp.optics.arizona.edu/jsasian/courses/opti-518/

[5] Sasián, J. (2010). *Theory of sixth-order wave aberrations.* Optical Society of America.

[6] Thompson, K.P., (2005). "Description of the third-order optical aberrations of near-circular pupil optical systems without symmetry," *J. Opt. Soc. Am* Ab**22**, 1389-1401

[7] Hopkins, H. H., (1950). *The Wave Theory of Aberrations,* Oxford University Press.